

**REACTIONS OF PHENOXY RADICALS
UNDER COAL LIQUEFACTION CONDITIONS**

**Thesis by
Puvin Pichaichanarong**

**In Partial Fulfillment of the Requirements
for the Degree of
Doctor of Philosophy**

**California Institute of Technology
Pasadena, California**

1985

(Submitted December 6, 1984)

© 1985

Puvin Pichaichanarong

All Rights Reserved

**With deepest gratitude and love, this thesis is dedicated
to my mother and father, who instilled in me a love of learning,
and to my wife, who loves me for my learning.**

*Well, I left my happy home to see what I could find out.
I left my folks and friends with the aim to clear my mind out.
Well I hit the rowdy road, and many kinds I met there,
Many stories told me of the way to get there....
So on and on I go, the seconds tick the time out,
There's so much left to know, and I'm on the road to findout.*

Cat Stevens, 1970

v
ACKNOWLEDGEMENTS

I would like to express my gratitude to my former advisor, the late Professor William Corcoran, for his love and care for all of us. His sudden departure was a tragic loss, but the personal and professional benefits of his teaching will always remain with me.

I wish to thank my current advisor, Professor George Gavalas, who patiently guided me through the difficult transition period. He provided much-needed direction to my research, while allowing me latitude to explore those areas in which I felt most comfortable. His invaluable support and insight into the many facets of this investigation are greatly appreciated. Dr. Mitsuo Oka of the California State Polytechnic University was very helpful with the organic chemistry aspect of this work. I am also indebted to Mr. David Lawson of the Jet Propulsion Laboratory for his kind advice and for the use of his laboratory equipment.

I gratefully acknowledge the financial support of the Department of Energy and the California Institute of Technology.

I was most fortunate to have had the gracious support of His Royal Highness King Bhumipol of Thailand through his high school, and throughout my undergraduate years in the form of the King's Scholarship. In a very real sense, most of my academic achievements would not have been possible without his generosity and kindness.

Difficult chores in the Chemical Engineering Department could not have been accomplished without the help of several staff members. I am grateful to Donna Johnson for always offering a helping hand, not only in the preparation of this thesis, but in numerous other tasks. Betty Benjamin has been kind with

office supplies. Henry Smith has kept things running smoothly, and George Griffith has been more than helpful with machinery. I am also thankful to Larry Henling of the Analytical Laboratory for his expertise in sample analysis.

Many fine friends have made the difficult times at Caltech bearable and the rest pleasant. In particular, it was not only my pleasure, but my privilege to have been associated with Dave Allen. His advice was instrumental to the progress of this work, and his friendship has been true. Among other friends all of whose names I regrettably cannot list in this limited space, Brian, Teri, Phil, Karl, Murray, and Saran have shared with me numerous happy moments that will always be remembered.

I wish to acknowledge my adorable wife, Kathy. For the past seven years, she has been a constant provider of inspiration, a sure refuge from depression, a sound source of advice, but most of all an equal partner in all my undertakings. I thank her for being there and for accepting me for what I am.

Finally, words can hardly express my love and gratitude towards my father and mother. Their love alone would have catapulted me far, but their unfailing support in every possible way is really the reason this thesis has been completed. I am forever thankful to them for being the best parents I could ever have.

ABSTRACT

This thesis presents the results of model compound studies that address the rate parameters for hydrogen abstraction involving phenoxy radicals, and the products, pathways, and kinetics of phenoxy radical recombination, under coal liquefaction conditions. Thermolysis of selected mixtures of model compounds containing functionalities found in coal-related materials were conducted in a batch reactor at temperatures between 250 and 450°C. The reaction products were analyzed by GC, HPLC, GCMS, and NMR, with emphasis on the identification of radical recombination products. Reactions were modeled by free radical mechanisms and rate parameters at liquefaction temperatures for hydrogen abstraction and recombination reactions involving phenoxy radicals were determined.

Phenoxy radicals were found to be more reactive than benzyl radicals, rapidly abstracting hydrogen atoms to form stable molecules. Hydrogen abstraction by a phenoxy radical from a phenol was faster than from a hydrocarbon. Application of the rate parameters determined for one model compound mixture to other systems of compounds indicated good match with experimental data.

Analysis of the recombination products revealed that, when no good hydrogen donor solvents were available, phenoxy-phenoxy radical recombination products were more abundant than phenoxy-benzyl recombination products. Certain differences and similarities were observed between the behavior of single-ring aromatics and their condensed-ring counterparts. Whereas phenol was quite stable at 400°C, 1-naphthol was found to undergo considerable conversion. A mechanistic scheme for 1-naphthol decomposition was proposed which accounted for

the major reaction products. Thermolysis of various model compound mixtures indicated similar patterns exhibited by single-ring and double-ring aromatics with respect to the pathways of oxygen-oxygen and oxygen-carbon free radical recombination.

Bimolecular reverse disproportionation was demonstrated to be satisfactory in explaining naphthol conversion. Furthermore, dehydration accounted for furan formation and concerted reactions could possibly be involved in naphthalene formation. Thus, in addition to unimolecular dissociation reactions, several pathways exist for the thermal reactions of oxygen compounds.

These model compound studies indicated that the results of a simple model compound mixture could give insight into the understanding of a more complex reaction network. This insight will ultimately provide the link between model compound results and the reactions of coal-related materials.

ix
TABLE OF CONTENTS

Dedication	iii
Acknowledgements	v
Abstract	vii
Table of Contents	ix
List of Figures	xiii
List of Tables	xv

1. Introduction

1.1 Overview of Coal Utilization	1
1.2 Coal Structure and Coal Liquefaction	2
1.3 Model Compound Study	4
1.4 Literature Review	6
1.5 Research Goals	12
References	14

2. Modeling Coal Pyrolysis

2.1 Introduction	20
2.2 Rate Calculations from Thermochemical Quantities	21
2.3 Thermochemical Kinetics	23
2.3.1 The Additivity Rules	24
2.3.2 Free Radicals	25
2.4 Formulation of a Kinetic Mechanism	26
2.4.1 Bond Dissociation Reactions	27

2.4.2	Dissociation of Free Radicals	28
2.4.3	Hydrogen Abstraction Reactions	30
2.4.4	Recombination of Radicals	32
2.4.5	Mechanistic Scheme	32
2.5	Computer Modeling with CHEMR	33
2.5.1	CHEMR Input	34
2.5.2	CHEMR Output	36
2.5.3	Summary	37
	References	38

3. Experimental

3.1	Introduction	44
3.2	The Reactor	44
3.3	Sample Preparation	46
3.3.1	Recrystallization of Benzyl Phenyl Ether	46
3.3.2	Deuteration of 1-Naphthol	47
3.3.3	Product Purification for Further Analysis	48
3.3.4	Chemical Separation	48
3.3.5	Column Chromatography	50
3.4	Analytical Tools	51
3.4.1	Gas Chromatography	51
3.4.2	High Performance Liquid Chromatography	53
3.4.2.1	Solvent Preparation	54
3.4.2.2	HPLC Startup Procedure	54
3.4.2.3	HPLC Operation Procedure	56
3.4.2.4	HPLC Shutdown Procedure	57

3.4.2.5 Fraction Collection	57
3.4.2.6 Parameters Used in Analysis	58
3.4.3 Gas Chromatography-Mass Spectrometry	60
3.4.4 Nuclear Magnetic Resonance Spectroscopy	62
References	64

4. Hydrogen Abstraction Experiments

4.1 Introduction	71
4.2 Thermolysis of Benzyl Phenyl Ether + Phenol-OD + 1-Methylnaphthalene	72
4.2.1 Rate Parameters of Interest	72
4.2.2 Kinetic Modeling	73
4.3 Thermolysis of Benzyl Phenyl Ether + 1-Naphthol-OD + 1,2,3,4-Tetrahydronaphthalene	82
4.3.1 Rate Parameters of Interest	82
4.3.2 Kinetic Modeling	83
4.4 Summary	86
References	89

5. Recombination Experiments Part I. Reactions of Benzyl Phenyl Ether

5.1 Introduction	103
5.2 Thermolysis of Benzyl Phenyl Ether + Toluene	104
5.2.1 Product Identification	106
5.2.2 Kinetic Modeling	111
5.3 Thermolysis of Benzyl Phenyl Ether + Phenol	114

5.3.1 Product Identification	115
5.3.2 Kinetic Modeling	118
5.4 Summary	119
References	122
 6. Recombination Experiments Part II. Reactions of 1-Naphthol	
6.1 Introduction	145
6.2 Thermolysis of 1-Naphthol	146
6.2.1 Product Identification	148
6.2.2 Kinetic Modeling	149
6.2.2.1 Binaphthol and Dinaphthofuran Formation	151
6.2.2.2 Naphthalene and Tetralone Formation	152
6.2.2.3 Kinetic Experiments	154
6.3 Thermolysis of 1-Naphthol + Bibenzyl	158
6.3.1 Product Identification	158
6.3.2 Kinetic Modeling	160
6.4 Thermolysis of 1-Naphthol + 1-Methylnaphthalene	160
6.4.1 Product Identification	161
6.4.2 Kinetic Modeling	162
6.5 Summary	163
References	166
 7. Conclusions and Recommendations for Future Work	
7.1 Conclusions	184
7.2 Recommendations for Future Work	189
References	193

LIST OF FIGURES

Figure 1.1	A Representation of a Coal Molecule	18
Figure 1.2	Chemistry involved in Coal Conversion	19
Figure 3.1	^1H NMR of 1-Naphthol-OH vs. 1-Naphthol-OD	66
Figure 3.2	HPLC of BPE + TO Thermolysis Products	67
Figure 3.3	GC of BB + PD + MN Thermolysis Products vs. GC of Authentic Mixture of TO + PD + MN + BP + BB	68
Figure 3.4	Schematic of Liquid Chromatography System	69
Figure 3.5	GCMS Intensity Scan of BB + PD + MN Thermolysis Products Showing the Toluene Signals	70
Figure 4.1	Model Results vs. Experimental Data Thermolysis of BB + PD + MN, 1 Hour	91
Figure 4.2	Model Results vs. Experimental Data Thermolysis of BPE + NOD + TE, 10 Minutes	92
Figure 5.1	HPLC of BPE + TO Thermolysis Products	124
Figure 5.2	HPLC of BPE + TO Thermolysis Products Phenolic and Neutral Fractions	125
Figure 5.3	GCMS of BPE + TO Thermolysis Products: Fraction F2	126
Figure 5.4	^1H NMR of BPE + TO Thermolysis Products: Fraction F2 .	127
Figure 5.5	GCMS of BPE + TO Thermolysis Products: Fraction F6	128
Figure 5.6	^1H NMR of BPE + TO Thermolysis Products: Fraction F6 .	129
Figure 5.7	GCMS of BPE + TO Thermolysis Products: Fraction F7	130

Figure 5.8	^1H NMR of BPE + TO Thermolysis Products: Fraction F7 .	131
Figure 5.9	Model Results vs. Experimental Data	
	Thermolysis of BPE + TO, 15 Minutes	132
Figure 5.10	HPLC of BPE + PH Thermolysis Products	133
Figure 5.11	GCMS of BPE + PH Thermolysis Products: Fraction F1 ...	134
Figure 5.12	^1H NMR of BPE + PH Thermolysis Products: Fraction F1	135
Figure 5.13	^{13}C NMR of BPE + PH Thermolysis Products: Fraction F1	136
Figure 5.14	Model Results vs. Experimental Data	
	Thermolysis of BPE + PH, 15 Minutes	137
Figure 6.1	HPLC of 1-NOH Thermolysis Products: 425°C, 15 Minutes ..	167
Figure 6.2	Product Concentrations as a Function of 1-NOH Distribution	168
Figure 6.3	Mechanistic Scheme for 1-Naphthol Dissociation	169
Figure 6.4	Model Results vs. Poutsma's Experimental Data:	
	1-NOH Thermolysis, 400°C	170
Figure 6.5	HPLC of 1-NOH + BB Thermolysis Products:	
	425°C, 15 Minutes	171
Figure 6.6	HPLC of 1-NOH + MN Thermolysis Products:	
	425°C, 15 Minutes	172

LIST OF TABLES

Table 2.1	Input Data: Mechanism and Rate Constants	
	Thermolysis of BB + PD + MN	41
Table 2.2	Model Output: Thermolysis of BB + PD + MN	42
Table 4.1	Reactant Mixtures for the Hydrogen Abstraction Experiments .	93
Table 4.2	Thermolysis Mechanism for BB + PD + MN	94
Table 4.3	k_{diff} and Reactant Concentrations as a Function of Temperature	
	Thermolysis of BB + PD + MN	96
Table 4.4	Model Results vs. Experimental Data	
	Thermolysis of BB + PD + MN	97
Table 4.5	Thermolysis Mechanism for BPE + NOD + TE	98
Table 4.6	k_{diff} and Reactant Concentrations as a Function of Temperature	
	Thermolysis of BPE + NOD + TE	101
Table 4.7	Model Results vs. Experimental Data	
	Thermolysis of BPE + NOD + TE	102
Table 5.1	Reactant Mixtures for the Recombination Experiments	
	Part I. Reactions of Benzyl Phenyl Ether	138
Table 5.2	Thermolysis Mechanism of BPE + TO	130
Table 5.3	Model Results vs. Experimental Data	
	Thermolysis of BPE + TO	141
Table 5.4	Thermolysis Mechanism of BPE + PH	142
Table 5.5	Model Results vs. Experimental Data	
	Thermolysis of BPE + PH	144

Table 6.1	Reactant Mixtures for the Recombination Experiments	
	Part II. Reactions of 1-Naphthol	173
Table 6.2	Thermolysis Mechanism for 1-Naphthol	175
Table 6.3	Model Results vs. Poutsma's Experimental Data	
	Thermolysis of 1-Naphthol at 400° C	177
Table 6.4	Thermolysis Mechanism for 1-NOH + BB	178
Table 6.5	Model Results vs. Experimental Data	
	Thermolysis of 1-NOH + BB, 15 Minutes	180
Table 6.6	Thermolysis Mechanism for 1-NOH + MN	181
Table 6.7	Model Results vs. Experimental Data	
	Thermolysis of 1-NOH + MN, 15 Minutes	183

CHAPTER 1

INTRODUCTION

1.1 Overview of Coal Utilization

Coal has been a source of energy since the dawn of the industrial revolution in the early 1840's (1). It dominated the world's energy supply up until the beginning of this century, when petroleum rapidly became the preferred energy source. Since then, coal research has attracted varying levels of interest, depending upon the accessibility of petroleum. For example, fear of depletion of oil supplies, coupled with the expanding automobile industry, ignited coal liquefaction research in the early 1920's. Subsequent discovery of oil in Texas in the mid-1920's, however, discouraged further work in this field. The end of World War II saw petroleum shortages in the United States, and coal research once again flourished, only to be halted by the discovery of massive petroleum reserves in the Middle East in the mid-1940's. Political unrest in the Middle East in 1973 renewed research efforts in coal utilization, and pointed out the vulnerability of overdependence on oil. With today's increasing energy demands, rapid depletion of petroleum reserves, and uncertainties in oil and natural gas supplies, coal is being reconsidered as a potential solution to the current energy problems.

Coal represents 80 percent of the world's proven energy reserve (2). The economically recoverable coal reserve would last over 150 years at the 1973 - 1985 production growth rates (3). Yet coal production today represents only 18 percent of our primary energy supply (4). Even though several alternative

means of energy production, such as solar power and thermonuclear fusion, are being developed to offset the gradual decline of crude oil production, they appear to be in their early stages, and their full potential will not be realized in the near future. Other processes, such as conversion of geothermal and hydroelectric energy, have well established technologies but are limited by natural resources. Finally, shale oil and tar sand conversions to fuels have encountered numerous environmental problems (5). It becomes apparent, therefore, that coal as a source of synthetic liquid fuels will satisfy a significant part of our energy needs during the 'transition period' of the next few decades, until other technologies have had time to mature. With this objective in mind, a thorough understanding of the reactions of coal liquefaction will be key to unleashing the total usefulness of coal.

1.2 Coal Structure and Coal Liquefaction

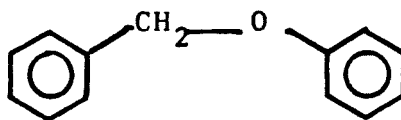
Organic substances in coal consist primarily of fused aromatic clusters connected together by various types of nonaromatic linkages such as methylene, ethylene, and ether bridges (6). From the available data on the composition of coal, several researchers have attempted to derive a representative structure for bituminous coal that is consistent with the observed chemistry. A recent, sophisticated model of a 'coal molecule' was proposed by Wiser (7) and is given in Figure 1.1. The model shows a number of fused aromatic rings joined by relatively weak bonds. Each aromatic cluster, or modular unit, consists of a nucleus, the majority of which is estimated by a procedure known as 'structural analysis' to contain two to three condensed, saturated and unsaturated rings (8).

Examples of such nuclei include naphthalene, tetralone, biphenyl, furan, and phenanthrene. These modular units are relatively stable at liquefaction temperatures, typically between 350 and 450° C. A typical coal molecule contains between 5 and 20 such modular units (9).

Figure 1.2 is a schematic diagram of the chemistry involved in the process of coal liquefaction (1). At elevated temperatures, weak linkages such ethylene and ether bridges dissociate, and the crosslinked structure of coal fragments into radicals. In the presence of a hydrogen donor, the radicals rapidly abstract hydrogens, 'capping' the active sites, and becoming stable species. Each species consists of a modular unit or groups of units roughly of molecular weights 300 to 1000. In the absence of a hydrogen donor, the radicals recondense to form larger, more complex molecules that are undesirable. Such termination reactions of these radicals are not well understood, and their mechanisms deserve a detailed study, so that solvents and reaction conditions may be chosen to minimize the formation of undesirable recombination products. The presence of free radicals in liquefaction processes has in fact been confirmed by electron-spin-resonance spectroscopy (esr) studies (10). This work will therefore apply free-radical mechanisms in studying the abstraction and recombination reactions. This admittedly is a simplified description of the reaction pathways that occur during coal liquefaction processes. Effects such as catalysis by mineral matters and transport limitations due to irregular coal's pore structures have been neglected. The above approach, however, should be valid for the systems of pure compounds of small molecular weights under study.

1.3 Model Compound Study

Coal has an extremely complex chemical structure, consisting of highly substituted aromatic clusters. Further, the composition of coal varies greatly even among coals of the same rank. Studying the kinetics of coal itself would yield a global picture resulting from a multitude of intertwined reactions, from which individual types of reactions could not be isolated. The use of model compounds to concentrate on particular classes of reactions minimizes confusing side reactions. A model compound is a pure compound of low molecular weight that contains the same types of functionalities as in coal-related materials. For example, benzyl phenyl ether has the following structure:



It simulates coal in the sense that it contains aromatic rings, connected together by an ether bridge. Model compound experiments allow us to isolate and examine classes of reactions important in coal processing (11). Qualitative and quantitative results can be readily obtained on elementary reaction mechanisms, rate parameters, and product structures and distributions. The thermal reactions of model compounds containing the representative functional groups found in coal have been extensively studied (12 - 20).

Even as model compounds are used to approximate the chemistry of coal, it would still be impossible to investigate all of the thousands of mixtures of model compounds potentially relevant to coal liquefaction. Instead, mechanistic

models are developed for the reactions of a few significant model compounds, and then these mechanisms are combined to predict the reactions of mixtures of compounds. Eventually, the ability to predict the reactions of a complex mixture from the results of experiments involving one, two, or three model compounds will allow the transition from model compound studies to the reactions of coal-related materials.

A major disadvantage of this approach is the large number of elementary reactions required to model even a simple system of two or three model compounds. In order to study the kinetics of a complex mixture, simplifications of the mechanism will have to be made. In the following chapters, attention will be paid to the ways in which the number of reactions in a mechanism can be reduced without significant penalty in the accuracy of model results. Eliminating unimportant reactions will also reduce the number of rate parameters that must be estimated, although for coal-related systems, each mechanism consists of only a few rate-limiting reactions. The model is generally insensitive to perturbations in the values of most other rate parameters (20).

The aforementioned disadvantages are more than offset by the insight into the nature of the chemical processes that the mechanisms offer. Rate-limiting steps can be identified, rate parameters can be calculated, and the extent of interaction between groups of functionalities in mixtures can be estimated by combining mechanisms (11). Therefore the model compound approach will be adopted in our work.

1.4 Literature Review

The abundance of hydroxyl groups, ether bridges, and other oxygen-containing groups in coal, as shown in Figure 1.1, indicates that oxygen constitutes a significant fraction of a typical coal molecule. Sub-bituminous and bituminous coals have been known to contain up to 20 weight percent oxygen, mainly in the form of phenols and ethers (1). In this thesis, we focus our attention on such oxygen groups.

Phenolic and other oxygen functional groups exercise profound and multifaceted influence on the physical and chemical processes of coal liquefaction. Phenolic groups in coal increase the polarity and thereby decrease the solubility of coal molecules and their fragments, resulting in higher yields of preasphaltenes and insoluble residues. Phenolic compounds in the recycle solvent, on the other hand, increase the solubility of the initial products of liquefaction (1).

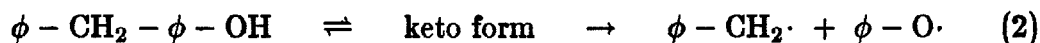
The chemical role of phenolic hydroxyls on liquefaction is multifaceted. Carbon-centered radicals can abstract phenolic hydrogen to form phenoxy radicals, which in turn can abstract hydrogen or form products of recombination. Recombination results in the incorporation of light or heavy phenols from the recycle solvent into coal liquids. Heavy phenols are active in char forming reactions. Hydroaromatic molecules carrying phenolic groups are known to be very effective hydrogen donors (1). The formation and removal of oxygen-carrying groups in coal liquid fractions during liquefaction has been measured for several coals (21).

Model compound studies have provided considerable information about thermal reactions of oxygen functional groups that are thought to be important in coal liquefaction. It has been found, for example, that phenolic groups

dramatically enhance the rate of dissociation of methylene bridges (22). The direct dissociation



where ϕ is the phenyl group or a condensed aromatic unit, does not proceed at liquefaction temperatures because of the high activation energy ($E_a \cong 80$ kcal/mol, which corresponds to a half life of about 9000 hours at 400°C). In contrast, the presence of phenolic hydroxyl in the ortho or para position induces a phenol-enol tautomerism, with the keto form amenable to dissociation:



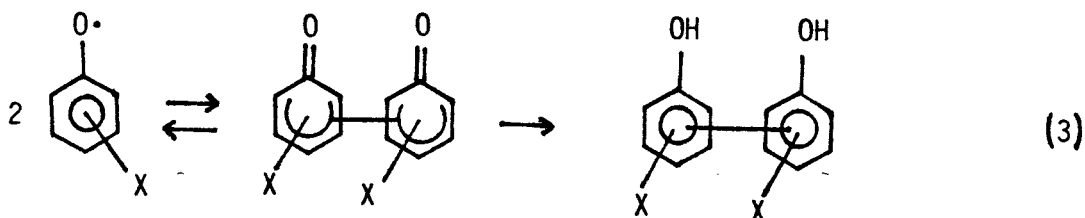
Several studies have dealt with the dissociation of ether bridges connecting aromatic units. Bridges of the diaryl type ($\phi - \text{O} - \phi$) or aryl benzyl type ($\phi - \text{O} - \text{CH}_2 - \phi$) have been examined. Along with methylene and possibly ethylene bridges, ether bridges are believed to constitute the predominant links among aromatic units. Ether bridge dissociation, therefore, has been regarded as an important step in liquefaction. The thermolysis of certain complex aryl methyl ethers at 425°C in the absence of any solvent yielded the decomposition products $\phi - \text{OH}$, $\phi - \text{CH}_3$, plus higher molecular weight compounds and char (23). The thermolysis of benzyl phenyl ether by itself and in the presence of tetralin or tetrahydroquinoline at 375°C yielded mainly phenol, toluene, and phenyl tolyl ether (24). Some higher molecular weight material was also obtained and was found to be heavier in the absence of the hydrogen donor. The products were qualitatively explained by a free radical mechanism and certain comparisons were made between phenoxy and benzyl radicals relative to hydrogen abstraction and recombination reactions.

Results from the thermolysis of several compounds containing an ether bridge at 450°C in the presence of tetralin were reported by Kamiya *et al.* (25). Diphenyl ether underwent no conversion while phenyl naphthyl ether and dinaphthyl ether underwent about 25 percent conversion in two hours. Benzyl phenyl ether was totally converted in 30 minutes. This study also revealed that the presence of phenolic compounds in the solvent enhances the rate of dissociation of benzyl phenyl ether considerably but does not influence the dissociation of bibenzyl. Evidently, phenolic hydroxyl groups stabilize the phenoxy radical or the transition state. Rearrangements of aryl aryl ethers containing alkyl chains in the ortho or para position have been reported by Factor *et al.* (26).

The reactions of phenoxy radicals, unsubstituted and substituted, have been studied quite extensively at temperatures up to 60°C largely in connection with the use of phenols as inhibitors of hydrocarbon oxidation (29, 30, 31, 32). A review of this work including detailed thermodynamic and kinetic analysis of experimental data is provided by Mahoney and DaRooge (33). Of particular relevance to coal liquefaction are the results concerning hydrogen abstraction and recombination reactions of phenoxy radicals. Unlike carbon-centered radicals, phenoxy radicals are very selective in hydrogen abstraction reactions with the rate constants varying considerably with changes in the substituents of the radical or the substrate. One striking result is that the rate constants for hydrogen abstraction by phenoxy radicals from phenol substrates are higher by two to four orders of magnitude than the corresponding constants for abstraction from hydrocarbon substrates. This difference was attributed to the formation of a hydrogen bonded complex in the former but not in the latter case.

Recombination reactions among unsubstituted and substituted phenoxy radicals lead to dimers via keto intermediates (31, 33, 34), as illustrated by

the following scheme:



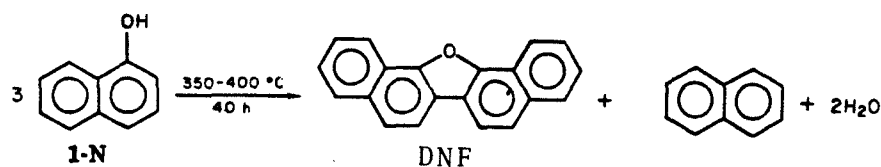
with the coupling at the ortho or para position with respect to OH. When all these positions are occupied, termination follows a different route (30). Depending on the presence and location of substituents, the rate of recombination could essentially be at the diffusion limit, or much lower because of unfavorable equilibrium in the first reversible step.

Under liquefaction conditions phenoxy radicals produced from ether and phenolic groups participate in hydrogen abstraction and recombination reactions to form more stable products. The nature and relative amount of such products depends quite sensitively on the detailed mechanism and kinetics of hydrogen abstraction and recombination reactions involving phenoxy radicals as well as carbon-centered radicals (mostly α radicals).

The literature on the reactions of phenoxy radicals under liquefaction conditions is relatively scarce. In the few cases where the thermolysis of phenols were studied, no detailed kinetic mechanisms were proposed and no rate parameters were elucidated. Briner (35) studied the conversion of phenol at 450° C at various pressures and reaction times. The products were assumed to be diphenyl ether and water, but they were not experimentally verified. Bahr (36) reported the formation of diphenyl ether and dibenzofuran in flow thermolysis of gaseous phenol diluted with nitrogen over activated charcoal at 300 - 350° C. Merz and Weith

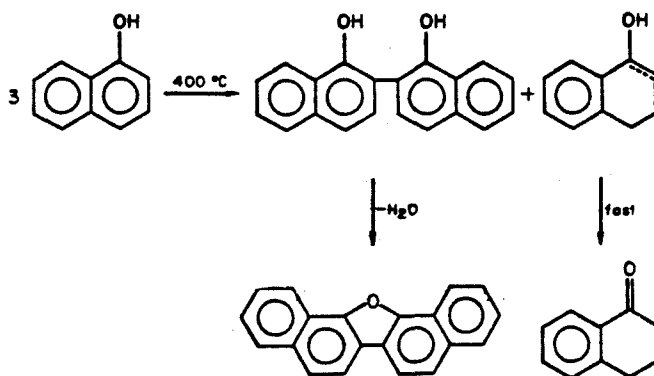
(37) heated 1-naphthol to 350 - 400°C for 40 hours under largely liquid-phase conditions and isolated water, naphthalene, and a compound $C_{20}H_{12}O$, from the crude product. The product $C_{20}H_{12}O$ had subsequently been formed by heating 1-naphthol at lower temperatures with various oxidizing or dehydrogenating agents (38 - 44). This compound was ultimately identified as dinaphthofuran (45). Hall (46) found dinaphthofuran to be the major product of the reactions of 1-naphthol under hydrogen pressure at 400°C for two hours. Higher temperatures promoted formation of naphthalene and tetrahydronaphthalene. He proposed that furan formation was preceded by ether formation.

Merz and Weith (37) assigned the following partial stoichiometry to the thermolysis of 1-naphthol:



where DNF is dinaphthofuran.

In a recent study of 1-naphthol thermolysis at 400°C for up to 16 hours, Poutsma and Dyer (47) identified binaphthol and tetralone as the predominant initial products, as well as a host of minor products. He suggested that binaphthol further underwent condensation to form dinaphthofuran, and proposed the following global scheme for the formation of these products:



Apparently, tetralone was very slowly dehydroxylated to yield naphthalene, although no detailed chemistry of this conversion was provided. The initial rate for ring coupling and hydrogen transfer was estimated to have an apparent kinetic order of about 2.5. The nonintegral order indicated that this was a global initial rate, consisting of a number of elementary reactions as yet unexplained. In other words, none of the aforementioned researchers investigated the detailed mechanistic pathways for the thermolysis of phenols, and reported no rate data at liquefaction temperatures for the associated elementary reactions. Moreover, these experiments employed very long reaction times, allowing extensive reactions of the original recombination products. The complex structure of the resulting crude product eluded identification and obscured mechanistic studies.

Yet other studies of phenol thermolysis (48 - 56) were done at temperatures from 650°C up to 865°C. At such high temperatures, however, dissociation and product formation followed different reaction pathways. For example, at these temperatures, phenol were found to undergo decarbonylation to form cyclopentadiene, dehydroxylation to form benzene, and dehydroxylation to form

benzene (50). As will be discussed in a future chapter, our experimental results showed that these compounds were only minor products of phenol thermolysis at 400°C. Clearly, these high temperature reactions would not be relevant to coal liquefaction processes.

1.5 Research Goals

The aforementioned studies (27 - 34) contain a wealth of information about the reactivity of phenoxy radicals at room temperature. Other workers (35 - 47) reported on the thermolysis products of phenols at liquefaction temperatures, but failed to provide rate parameters or mechanistic models. From the standpoint of coal liquefaction it is essential to extend previous work in several directions. One is to determine rate parameters for certain reactions that have not been investigated in previous studies. Examples of such reactions are the abstraction of phenolic hydrogen by α radicals and the recombination between phenoxy radicals and α radicals. A second direction is to determine rate parameters at liquefaction temperatures. In the case of recombination reactions (reaction 3) above, the second step may be sufficiently rapid at temperatures above 400°C, such that the rate of the overall reaction reaches the diffusion limit. A third direction is to isolate and identify the molecular structures of the major products of recombination between the phenoxy radical and the α radical. Mechanistic pathways for their formation can then be proposed and computer model can be used to check their validity. A final and important direction is to determine the effect of condensed aromatic nuclei on the phenoxy radicals in view of the fact that most coal units contain condensed rings rather than ben-

zene rings. Along the way, emphasis will be placed upon the successful use of model and experimental results for a simple model compound system to predict the behavior of a more complex mixture of compounds. It is this insight that is required to make the ultimate transition from model compound results to the reactions of coal-related materials.

This thesis presents the results of model compound studies that address the rates of hydrogen abstraction from phenolic groups and the rates and products of recombination between phenoxy-phenoxy and phenoxy-benzyl radicals. These model compounds include single and double ring aromatics. Chapter 2 outlines the thermochemical estimates of rate parameters of the elementary reactions associated with the thermal reactions of coal. It also presents a brief discussion on how these rate values are utilized in CHEMR, the computer model used in simulating the free-radical mechanisms. The experimental techniques and analytical tools, mainly gas chromatography, liquid chromatography, gas chromatography-mass spectrometry, and nuclear magnetic resonance spectroscopy, are described in Chapter 3. Chapter 4 describes the hydrogen abstraction experiments and explains how rate parameters associated with the reactions of the phenoxy radicals were determined. Chapter 5 focuses upon the recombination reactions involving the phenoxy radical, while Chapter 6 centers on the thermolysis of naphthol. Chapter 7 summarizes the results of rate and product determination, the advantages and disadvantages of the model compound study, and recommendations for future work.

REFERENCES

- [1] Whitehurst, D. D., Mitchell, T. O. and Farcasiu, M., 'Coal Liquefaction,' Chapters 1 and 2, Academic Press, New York, 1980
- [2] Probst, R. F. and Hicks, R. E., 'Synthetic Fuels,' Chapter 1, McGraw-Hill Book Company, New York, 1982
- [3] United Nations Economic Commissions for Europe, 'Coal: 1985 and Beyond,' Pergamon Press, Great Britain, 1978
- [4] Balzhiser, R. E., *Chemical Engineering*, 1977, **84**, 72
- [5] Kralik, J. G., Ph.D. Thesis, California Institute of Technology, Pasadena, California, 1982.
- [6] Dreyden, I. G. G., 'Chemistry of Coal Utilization,' Suppl. Vol., (Ed. H.H. Lowry), John Wiley, New York, 1963, Chapter 6
- [7] Wiser, W., *Am. Chem. Soc. Fuel Div. Preprints*, 1975, **20**(2), 122
- [8] Gavalas, G. R. and Oka, M., *Fuel*, 1978, **57**, 285
- [9] Gavalas, G. R., 'Coal Pyrolysis,' *Coal Science and Technology*; 4, Elsevier Scientific Publishing Co., Amsterdam, The Netherlands, 1982
- [10] Petrakis, L., Grandy, D. W. and Jones, G. L., *Fuel*, 1983, **62**, 1066
- [11] Allen, D. T., 'Modeling the Reactions of Coal Liquids,' Ph.D. Thesis, Department of Chemical Engineering, California Institute of Technology, Pasadena, California, 1983
- [12] Benjamin, B. M., Raaen, V. F., Maupin, P. H., Brown, L. L. and Collins, C. J., *Fuel*, 1978, **57**, 269
- [13] Cronauer, D. C., Jewell, D. M., Shah, Y. T. and Kueser, K. A., *Ind. Eng. Chem. Fund.*, 1978, **17**, 291

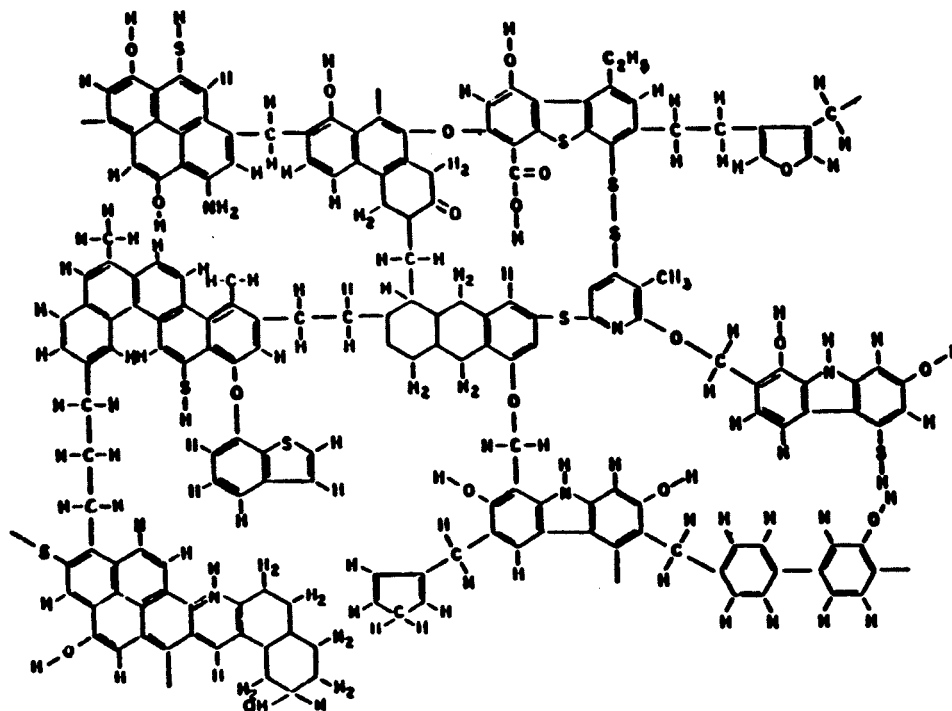
- [14] Cronauer, D. C., Jewell, D. M., Shah, Y. T. and Modi, R. J., *Ind. Eng. Chem. Fund.*, 1979, **18**, 153
- [15] Cronauer, D. C., Jewell, D. M., Modi, R. J. and Sashadri, R. J., *Ind. Eng. Chem. Fund.*, 1979, **18**, 368
- [16] Yao, T. and Kamiya, Y., *Bull. Chem. Soc. Jpn.*, 1979, **52**, 492
- [17] Miller, R. E. and Stein, S. E., *J. Phys. Chem.*, 1981, **85**, 580
- [18] Krishnamurthy, S., Panvelker, S. and Shah, Y. T., *Am. Inst. Chem. Eng. J.*, 1981, **27**, 994
- [19] Houalla, M., Nag, N. K., Sapre, A. V., Broderick, D. H. and Gates, B. C., *Am. Inst. Chem. Eng. J.*, 1978, **24**, 1015
- [20] Allen, D. T. and Gavalas, G. R., *Int. J. Chem. Kinet.*, 1983, **15**, 219
- [21] Cronauer, D. C. and Ruberto, R. G., 'Investigation of Mechanism of Reactions Involving Oxygen-Containing Compounds in Coal Hydrogenation,' EPRI AF-913, Project 713-1, Final Report, 1979
- [22] McMillen, D. F., Ogier, W. C. and Ross, D. S., *Am. Chem. Soc. Preprints*, 1981, **26**(2), 181
- [23] Depp, E. A. and Neuworth, M. B., *Sonderdruck aus 'Brennstoff-Chemie'*, 1958, 2
- [24] Schlosberg, R. H., Davis, Jr., W. H. and Ashe, T. R., *Fuel*, 1981, **60**, 201
- [25] Kamiya, Y., Yao, T. and Oikawa, S., *Am. Chem. Soc., Div. Fuel Chem. Preprints*, 1979, **24**(2), 116
- [26] Factor, A., Finkbeiner, H., Jerussi, R. A. and White, D. M., *J. Am. Chem. Soc.*, 1959, **81**, 57
- [27] Mahoney, L. R., *J. Am. Chem. Soc.*, 1967, **89**, 1895
- [28] Mahoney, L. R. and DaRooge, M. A., *J. Am. Chem. Soc.*, 1967, **89**, 5619
- [29] Mahoney, L. R. and DaRooge, M. A., *J. Am. Chem. Soc.*, 1970, **92**, 890

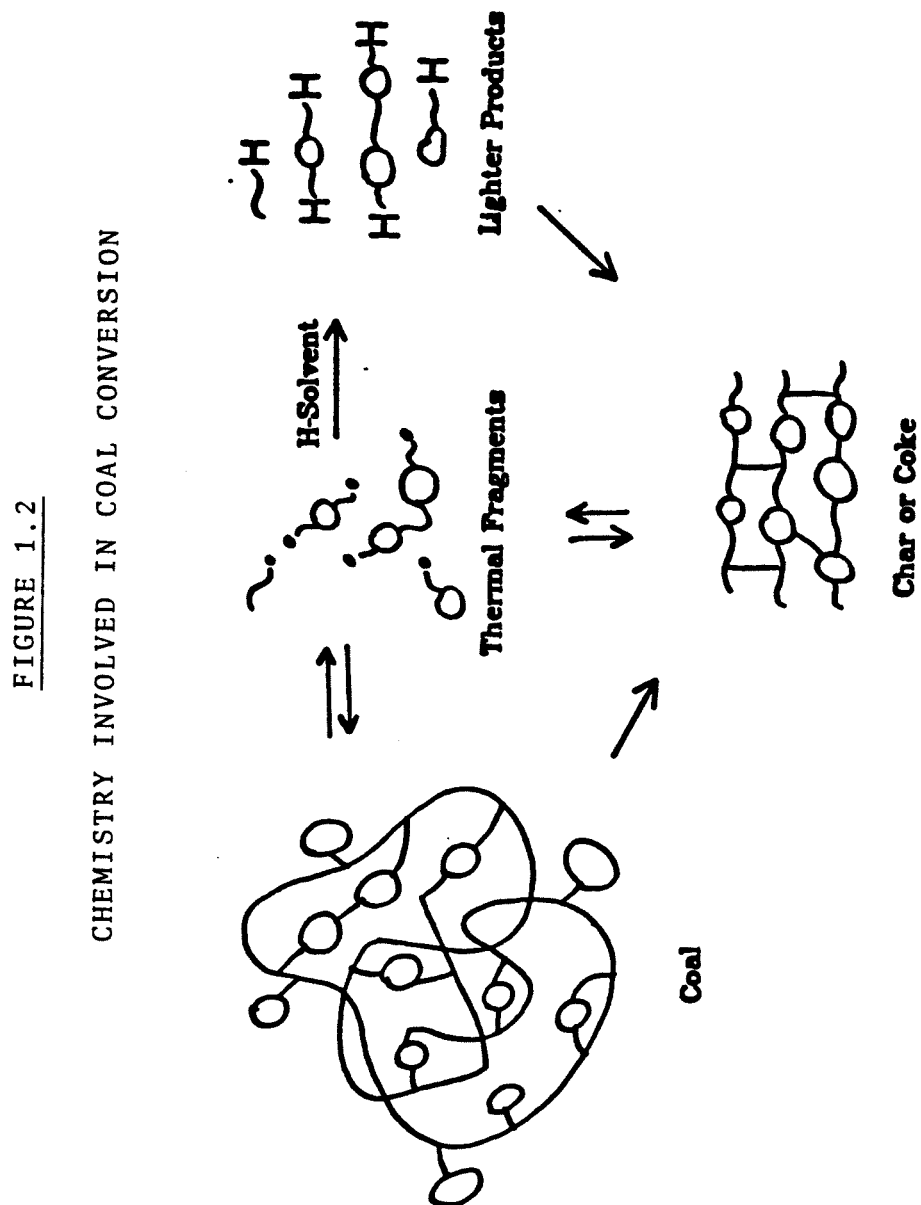
- [30] Weiner, S. A. and Mahoney, L.R., *J. Am. Chem. Soc.*, 1972, **94**, 5029
- [31] Mahoney, L. R. and Weiner, S. A., *J. Am. Chem. Soc.*, 1972, **94**, 585
- [32] Mahoney, L. R. and Weiner, S. A., *J. Am. Chem. Soc.*, 1972, **94**, 1412
- [33] Mahoney, L. R. and DaRooge, M. A., *J. Am. Chem. Soc.*, 1975, **97**, 4722
- [34] Joschek, H. I. and Miller, S. I., *J. Am. Chem. Soc.*, 1966, **88**, 3273
- [35] Briner, E., Bron-Stalet, J., and Paillard, H., *Helv. Chim. Acta*, 1932, **15**, 619
- [36] Bahr, T., *Dtsch. Chem. Ges.*, 1931, **64**, 2258
- [37] Merz, V. and Weith, W., *Ber. Dtsch. Chem. Ges.*, 1881, **14**, 187
- [38] Graebe, C., Knecht, W. and Unzeitig, J., *Justus Liebigs Ann. Chem.*, 1881, **209**, 132.
- [39] Knecht, W. and Unzeitig, J., *J. Ber. Dtsch. Chem. Ges.*, 1880, **13**, 1724
- [40] Clemo, G. R. and Spence, R., *J. Chem. Soc.*, 1928, 2811
- [41] Wichelhaus, H., *Ber. Dtsch. Chem. Ges.*, 1903, **36**, 2942
- [42] Cocker, W., Cross, B. E., Edward, J. T., Jenkinson, D.S. and McCormick, J., *J. Chem. Soc.*, 1953, 2355.
- [43] Vorozhtsov, N. N. Jr. and Koptug, V. A., *J. Gen. Chem. USSR*, 1958, **28**, 3010
- [44] Raaen, V. F. and Roark, W. H., *Fuel*, 1978, **57**, 650
- [45] Clemo, G. R., Cockburn, J. G. and Spence, R., *J. Chem. Soc.*, 1931, 1265
- [46] Hall, C. C., *Fuel*, 1933, **12**, 419
- [47] Poutsma, M. L. and Dyer, C. W., *J. Org. Chem.*, 1982, **47**(18), 3367
- [48] Hagemann, A., *A. Angew. Chem.*, 1929, **42**, 355
- [49] Braekman-Danheux, C. and Heyvaert, A., *Ann. Mines Belg.*, 1972, **37**; *Chem. Abstr.*, 1972, **77**, 4666
- [50] Cypres, R. and Bettens, B., *Tetrahedron*, 1974, **30**, 1253; 1975, **31**, 359

- [51] Spielman, R. and Cramers, C. A., *Chromatographia*, 1972, 5, 295
- [52] Voronkov, M. G., Deryagina, E. N., Sukhomazova, E. N. and Klochkova, L. J., *J. Org. Chem. USSR*, 1975, 11, 1116
- [53] Schaden, G., *Justus Liebigs Ann. Chem.*, 1978, 559
- [54] Raudsepp, H. T. and Raudsepp, H. E., *Tr. Tallin. Politekh. Inst., Ser. A*, 1967, No. 254, 35
- [55] Braedel, P. and Vinh, T. H., *Proc. Int. Conf. Coal. Sci.*, Dusseldorf, Verlag Gluckauf GmbH, Essen, 1981, p. 509.
- [56] Cypres, R. *Am. Chem. Soc. Div. Fuel Chem. Preprints*, 1981, 26(3), 44

FIGURE 1.1

A REPRESENTATION OF A COAL MOLECULE





CHAPTER 2

MODELING COAL PYROLYSIS

2.1 Introduction

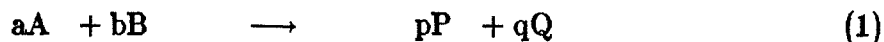
The thermal reactions of coal are generally believed to proceed via free radical mechanisms (1). Several researchers (2, 3, 4) have postulated the involvement of free radicals in the processes of coal liquefaction. Two studies (5, 6) have utilized coal liquefaction models in which free radicals were explicitly included as intermediates. Other investigators have measured free radicals in coals and treated coals (7), in coal liquid fractions (8, 9), and in slurries after liquefaction (10, 11). Recently, Petrakis *et al.* (12), using conventional electron paramagnetic resonance (ESR), have measured pre-existing and transient free radicals under hydroliquefaction conditions.

This chapter discusses the principal elementary reactions of model compounds that contain certain representative structures found in coal liquids. In particular the oxygen-containing compounds will be of interest. Due to the information provided by the aforementioned studies, these elementary reactions will be treated as free-radical reactions. Section 2.2 provides a brief review of the thermochemical quantities necessary for rate calculations. The rate parameters of several reactions can be obtained by analogy with similar reactions in the literature. In most cases, however, the rate parameters must be estimated by techniques such as transition-state theory and, more importantly, group additivity method, also known as thermochemical kinetics (13). Benson and coworkers (14, 15) were largely responsible for the development of thermochemical kinetics,

the essence of which will be summarized in Section 2.3. Section 2.4 then applies thermochemical estimates to the major elementary reactions that are pertinent to the study, and explains the arrangement of these elementary reactions into a sound kinetic mechanism. Finally Section 2.5 briefly describes the computer program CHEMR, which utilizes the formulated mechanistic schemes to model the thermolysis of the model compound systems under study.

2.2 Rate Calculations from Thermochemical Quantities

Consider the elementary reaction



The equilibrium constant K_1 can be written in terms of the rate constants of the forward and reverse reactions:

$$K_1 = \frac{[P]^p [Q]^q}{[A]^a [B]^b} = \frac{k_1}{k_{-1}} \quad (2)$$

For the majority of chemical reactions, the rate constant can be expressed in the Arrhenius form:

$$k = A \exp \left(- \frac{E_a}{RT} \right) \quad (3)$$

where A is the preexponential factor, popularly termed the Arrhenius factor, and E_a is the activation energy of the reaction. Thus,

$$K_1 = \frac{A_1}{A_{-1}} \exp \left[- \frac{E_{a_1} - E_{a_{-1}}}{RT} \right] \quad (4)$$

K_1 can also be related to the standard free-energy change ΔG_1^0 as follows:

$$\Delta G_1^0 = -RT \ln K_1 \quad (5)$$

By definition,

$$\Delta G_1^0 \equiv \Delta H_1^0 - \Delta S_1^0 \quad (6)$$

where ΔH_1^0 is the standard enthalpy change and ΔS_1^0 is the standard entropy change in the reaction, both at reaction temperature. Thus,

$$\ln K_1 = -\frac{\Delta H_1^0}{RT} + \frac{\Delta S_1^0}{R} \quad (7)$$

If equation (4) is rewritten as

$$\ln K_1 = \ln \frac{A_1}{A_{-1}} + \left[-\frac{E_{a_1} - E_{a_{-1}}}{RT} \right] \quad (8)$$

Comparison of equations (7) and (8) thus yields

$$\Delta S_1^0 = R \ln \left(\frac{A_1}{A_{-1}} \right) \quad (9)$$

and

$$\Delta H_1^0 = E_{a_1} - E_{a_{-1}} \quad (10)$$

Alternatively, the A factor can be derived from transition state theory. For a first-order decomposition reaction, the expression is:

$$A = \frac{ek_B T}{h} \exp \left[\frac{\Delta S^{0+}}{R} \right] \quad (11)$$

where k_B is the Boltzmann's constant, h is the Planck's constant, and ΔS^{0+} is the entropy difference between the transition-state activated complex and the reactants. Calculation of ΔS^{0+} , however, is subject to a great deal of uncertainty due to lack of reliable information on the structure of the activated complex.

The standard enthalpy change is related to the standard heats of formation ΔH_f^0 by:

$$\Delta H^0 = p\Delta H_f^0(P) + q\Delta H_f^0(Q) + \dots - a\Delta H_f^0(A) - b\Delta H_f^0(B) - \dots \quad (12)$$

Finally, the variations of ΔH_0 and ΔS_0 with temperature are given by the thermodynamic relations:

$$\left[\frac{\partial \Delta H^0}{\partial T} \right] = \Delta C_p^0 \quad (13)$$

$$\left[\frac{\partial \Delta S^0}{\partial T} \right] = \frac{\Delta C_p^0}{T} \quad (14)$$

The value ΔC_p^0 tends to change very little over temperature intervals as great as 500°K so that, given $\Delta H_{T_0}^0$ and $\Delta S_{T_0}^0$, ΔH_T^0 and ΔS_T^0 can be calculated from an average value $\Delta C_p^0_{T_m}$ as follows:

$$\Delta H_T^0 = \Delta H_{T_0}^0 + \Delta C_p^0_{T_m} (T - T_0) \quad (15)$$

$$\Delta S_T^0 = \Delta S_{T_0}^0 + \Delta C_p^0_{T_m} \left(\ln \frac{T}{T_0} \right) \quad (16)$$

Therefore, calculations of a rate constant, via the Arrhenius expression in terms of A and E_a , can be performed if the thermochemical quantities ΔS^0 , ΔH_f^0 , and ΔC_p^0 are available. The calculated values of A and E_a have been found experimentally to be constant over a temperature range of at least 100°K. This constancy will prove to be advantageous in the succeeding model compound studies where the computer model's ability to predict experimental data will be tested over temperature intervals of up to 100°C.

The following section describes the use of thermochemical kinetics to calculate the quantities ΔS^0 , ΔH_f^0 , and ΔC_p^0 .

2.3 Thermochemical Kinetics

Due to the staggering number of even very low molecular weight compounds, thermochemical data are available for only a limited number of polyatomic species. Fortunately, statistical thermodynamics enabled calculations

of the standard entropies and heat capacities of molecules given their geometrical structures and vibrational frequencies. The values of C_p° , and S° have been tabulated for many simple molecules over ranges of temperature. Even these calculations, however, are not trivial. An extremely rapid and reasonably accurate method of estimation of thermochemical data has been developed by Benson (15), and will now be discussed.

2.3.1 The Additivity Rules

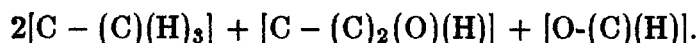
Most molecular properties of larger molecules can roughly be considered as being composed of additive contributions from the individual atoms or bonds in the molecule (15). Because the forces between atoms are very 'short range,' appreciable only over distances on the order of one to three angstroms, individual atoms appear to contribute nearly constant amounts to molar properties, specifically entropy and heat of formation. Benson and Buss (16) suggested a hierarchical system of additivity laws, the simplest of which was the additivity of atom properties. In that scheme, partial values for a property as assigned to each atom, and the molecular property was simply the sum of all the atom contributions. The law is precise for an exceptional property such as molecular weight. An obvious limitation to this law, however, would be any chemical reaction. Since atoms are conserved, this law would predict the same molecular properties for reactants and products. This is definitely not the case for entropy and enthalpy in most reactions.

The next higher-order approximation is the additivity of bond properties. Benson reported that bond additivity reproduced C_p , S° , and ΔH_f° to within ± 2 cal/mol-K on the average, but was poorer for heavily branched compounds.

The bond additivity rules also give the same properties for isomeric species.

The second-order approximation to additivity behavior is the additivity of group properties. A group is defined as a polyvalent atom (ligancy ≥ 2), in a molecule together with all of its ligands. The adopted nomenclature is to identify first the polyvalent atom and then its ligands. Thus $[C - (H_3)(C)]$ represents a carbon atom connected to three hydrogen atoms and another carbon atom, that is, a primary methyl group. The molecules that can be treated are those with two or more polyvalent atoms. Two examples of analysis of molecules into groups are as follows:

1. $CH_3 - CH_3$ contains two identical groups: $[C - (C)(H)_3]$.
2. $CH_3CHOHCH_3$ contains four groups:



A basic limitation on the use of group properties lies in the increase in number of groups as substitution increases. Benson provided the currently available values of group contributions to C_p° , S° , and ΔH_f° . On the average, C_p° , and S° estimated by group additivity are within ± 0.3 cal/mol-K of the observed values, while ΔH_f° estimates are within ± 0.5 kcal/mol.

2.3.2 Free Radicals

With the exception of a few stable free radicals, very few direct thermochemical data on free radicals are available. The best values for heats of formation are invariably deduced from kinetic measurements of bond dissociation energies, whereas entropies and heat capacities are only calculable from statistical formulae. Nonetheless, the laws of group additivity also apply to radicals. Within

the limits of present data, the assumption that groups such as $[C - (C\cdot)(C)_2(H)]$ have the same partial heat of formation as the corresponding nonradical group $[C - (C)_3(H)]$ appears to be valid. This assumption thus allows estimation of ΔH_f° for several radicals. The values of S° for radicals can be calculated from assumed structures and frequency assignments, but the estimated values are perhaps best achieved by analogy with related compounds. Benson again provided the available free-radical group additivities for several important radicals.

The application of group additivity will now be discussed in relation to the major elementary reactions for the model compound systems in this thesis.

2.4 Formulation of a Kinetic Mechanism

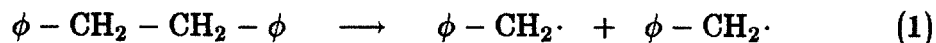
The classes of reactions most important to the model compound studies are the bond dissociation, free-radical dissociation, hydrogen abstraction, and radical recombination reactions. While rate parameters for these reactions can be estimated by the aforementioned technique, it must be realized that such estimations involve a certain amount of uncertainty (13). First of all, group contribution data almost always refer to gas-phase kinetics, while coal pyrolysis occurs in a condensed phase. Allen (17) has shown, however, that group additivity estimates were applicable to condensed-phase reactions of model compounds that were similar in structure to coal-derived products. A second source of uncertainty is the fact that most experimental information is available on single ring aromatics, while coal molecules primarily consist of condensed ring compounds. Despite these difficulties, the estimated rate parameters are still invaluable in the absence of experimentally evaluated rate data. More importantly, these rate

values can be refined by small adjustments through comparison between various sets of model compound studies.

After rate parameters of a few representative reactions are calculated, the principal elementary reactions will be assembled into a kinetic mechanism which simulates the reaction of a certain model compound system.

2.4.1 Bond Dissociation Reactions

The two reactions pertinent to this work are the dissociation of the ethylene bridge in 1,2 diphenyl ethane (bibenzyl) and the dissociation of the ether bridge in benzyl phenyl ether:



To obtain the heat of reaction, it is not necessary to calculate the heats of formations of both the reactants and the products. In reactions (1), for example, the group contributions from both aromatic rings are the same in bibenzyl as in the two benzyl radicals, so that these contributions cancel one another. Indeed, the only two groups that change are those with the aliphatic carbons as the polyvalent atoms. The heat of reaction can thus be written as:

$$\begin{aligned} \Delta H &= 2\Delta H_f(\phi - \text{CH}_2\cdot) - 2\Delta H_f(\phi - \text{CH}_2 - \text{CH}_2 - \phi) \\ &= 2[\cdot\text{C} - (\text{C}_B)(\text{H})_2] + 2[\text{C}_B - (\text{C}\cdot)] - 2[\text{C} - (\text{C}_B)(\text{C})(\text{H})_2] - 2[\text{C}_B - (\text{C})] \end{aligned}$$

where C_B signifies a carbon in a benzene ring.

The tables in Benson (14) gives $[\cdot\text{C} - (\text{C}_B)(\text{H})_2] = 23.0$, $[\text{C} - (\text{C}_B)(\text{C})(\text{H})_2] = -4.86$, and $[\text{C}_B - (\text{C}\cdot)] = [\text{C}_B - (\text{C})] = 5.51$. Thus,

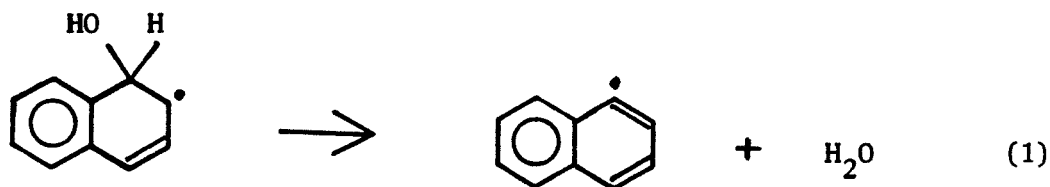
$$\Delta H = 2 \times 23.0 - 2(-4.86) = 55.7 \text{ kcal/mol}$$

The reverse reaction, a free radical recombination, has very small activation energy conventionally taken as zero. Thus for the dissociation of bibenzyl, the activation energy is estimated as $E_a = \Delta H \cong 56$ kcal/mol. This value is roughly 5 kcal/mol below those reported in the literature (18, 19). It turned out that the thermolysis of bibenzyl has been extensively studied and the rate parameters well established, and this work will adopt the rate parameters given in the literature (see Chapter 4). In the absence of such information, however, the estimated rate values would have provided a good starting point from which better estimates could be attained from comparison with results from other model compound systems.

The dissociation of benzyl phenyl ether has also been well studied (20, 21), and the available rate data will be adopted for use in this work.

2.4.2 Dissociation of Free Radicals

Only one particular instance in this study involves the dissociation of a free radical.

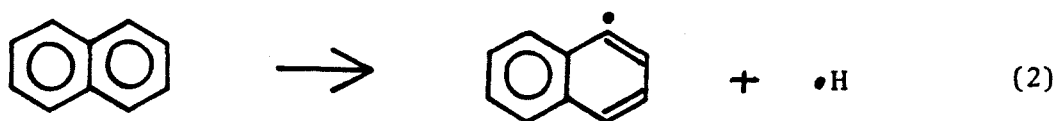


The reaction results in no net gain or loss of free radicals, and thus belongs in the class of propagation reactions. The heat of formation can be written as follows:

$$\Delta H_{(1)}^0 = [\cdot C_B - (C_B)] + [C_B - (C_B\cdot)] + [O - (H)_2]$$

$$- [\cdot C - (C_d)(C)(H)] - [C - (C_B)(C\cdot)(H)(O)]$$

where C_d represents a doubly bonded carbon atom. As discussed previously, $[C_B - (C_B)\cdot]$ and $[C - (C_B)(C\cdot)(H)(O)]$ can be approximated by $[C_B - (C_B)]$ and $[C - (C_B)(C)(H)(O)]$, respectively. The only unknown, the group contribution from $[\cdot C_B - (C_B)]$, must be calculated from the following reaction:



The bond dissociation energy for this reaction was estimated to be the same as that for benzene dissociation to yield the phenyl radical (22), or about 102 kcal/mol. The heat of formation of naphthalene was given by Reid, *et al.* (23) as 36.1 kcal/mol. If naphthalene is represented as NE-H, then the following equation follows, where $D(\text{NE-H}) \equiv$ the bond dissociation energy of the carbon-hydrogen bond in naphthalene:

$$D(\text{NE-H}) = \Delta H_f^\circ(\text{NE}\cdot) + \Delta H_f^\circ(\text{H}\cdot) - \Delta H_f^\circ(\text{NE-H})$$

so that $\Delta H_f^\circ(\text{NE}\cdot) \cong 86$ kcal/mol.

If, as before, the assumptions are made that

$$[C_B - (C_B\cdot)(C_B)(C_B)] \cong [C_B - (C_B)(C_B)(C_B)] \quad \text{and}$$

$$[C_B - (C_B\cdot)(C_B)(H)] \cong [C_B - (C_B)(C_B)(H)],$$

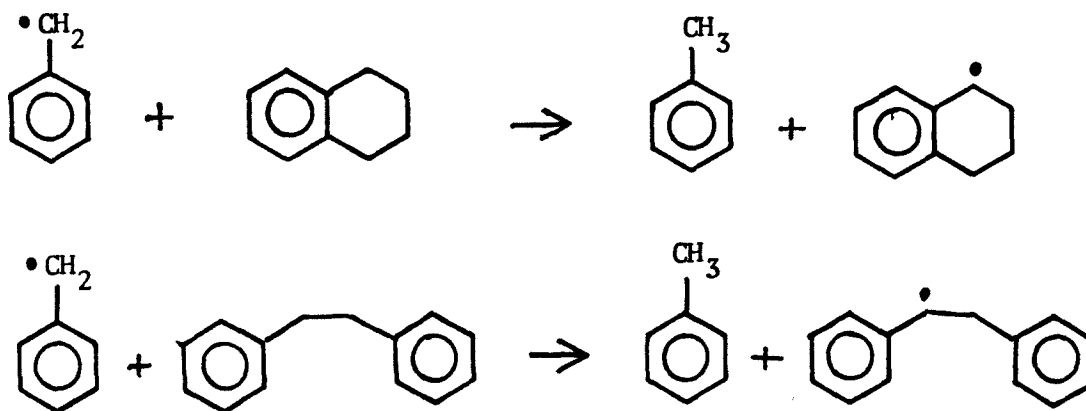
$$\Delta H_f^\circ(\text{NE}\cdot) = 7[C_B - (H)] + 2[C_B - (C_B)] + [\cdot C_B - (C_B)]$$

Thus, $[\cdot C_B - (C_B)(C_B)] = 53 \text{ kcal/mol}$ and finally $\Delta H_{(1)}^\circ = 18.1 \text{ kcal/mol}$.

By analogy with a similar reaction (14), the A factor was estimated to be 10^{13} .

2.4.3 Hydrogen Abstraction Reactions

Obviously a large number of hydrogen abstraction reactions exist even in the relatively small model compound systems under study. Nonetheless, several reactions are quite similar, and in certain cases, two reactions would be identical from the standpoint of thermochemical kinetics. For example, the following two abstraction reactions



would have the same values of A and E_a according to group additivity method because the 'groups' undergoing change in both tetralin and bibenzyl can both be represented as $[C - (C_B)(C)(H)_2]$, and the same groups in the products can

both be expressed as $[\cdot\text{C} - (\text{C}_\text{B})(\text{C})(\text{H})]$. For either reaction,

$$\Delta\text{H}^\circ = [\cdot\text{C} - (\text{C}_\text{B})(\text{C})(\text{H})] + [\text{C} - (\text{C}_\text{B})(\text{H})_3] - [\text{C} - (\text{C}_\text{B})(\text{C})(\text{H})_2] - [\cdot\text{C} - (\text{C}_\text{B})(\text{H})_2]$$

The contribution for $[\text{C} - (\text{C}_\text{B})(\text{H})_3]$ is not listed in the literature. Its value must now be calculated from the present molecule, toluene. For toluene, the heat of formation is found to be 11.95 kcal/mol (24). Thus, from the equation

$$\Delta\text{H}_\text{f}^\circ = 5[\text{C}_\text{B} - (\text{H})] + [\text{C}_\text{B} - (\text{C})] + [\text{C} - (\text{C}_\text{B})(\text{H})_3]$$

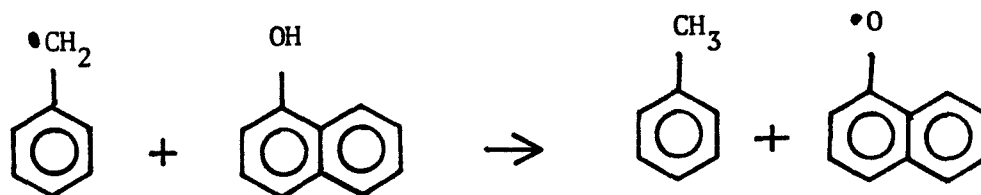
$[\text{C} - (\text{C}_\text{B})(\text{H})_3]$ was calculated to be -10.1 kcal/mol. Finally for reactions (1) and (2), $\Delta\text{H} = -3.5$ kcal/mol.

Gavalas (13) has shown, however, that the reaction

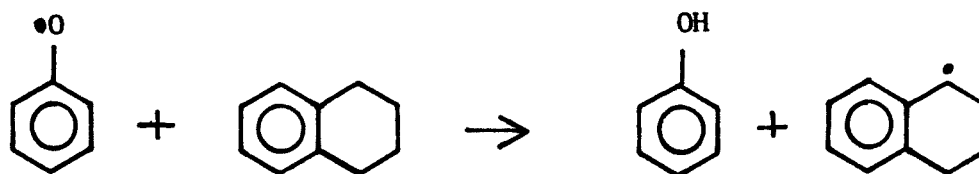


has a minimum activation energy approaching 9 kcal/mol as the number of carbons in X exceeds 1. He also estimated the A factor to be $\log_{10} A = 7.0$. Thus for reactions (1) and (2), as well as other analogous reactions, the activation energies will be taken as 9 kcal/mol and the A factor as 10^7 .

In contrast to carbon-centered radicals, oxygen-centered radicals have not been well studied, and the group additivity values for oxygen radicals have scarcely been reported. In fact, one objective of this thesis is to estimate the rate parameters of hydrogen abstraction reactions involving phenoxy radicals such as



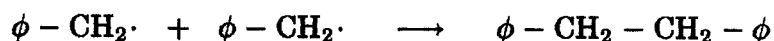
and



The rate parameters associated with these reactions will be established in Chapter 4.

2.4.4 Recombination of Radicals

As mentioned above, the recombination of two radicals to form a stable product is the reverse of the dissociation reaction, for example



These reactions are extremely rapid and in the condensed phase are assumed to proceed with only diffusional limitation. The activation energy for these reactions are conventionally taken to be zero. The rate constants are calculated instead through the mixtures' viscosity using the Stokes-Einstein equation

$$k_{\text{diff}} = \frac{8RT}{3 \times 10^3 \eta}$$

Chapter 4 will explain in detail the procedure for estimation of k_{diff} for various model compound mixtures at reaction temperature.

2.4.5 Mechanistic Scheme

The three classes of elementary reactions mentioned are now arranged into a kinetic mechanism. The dissociation reaction is also termed initiation reaction,

where two free radicals are generated from a stable compound. The hydrogen abstraction reactions are one of many classes of reactions that are called propagation reactions. Here one free radical abstracts a hydrogen atom from a stable molecule, resulting in no net loss or gain of radicals. The recombination reaction is termed termination reaction, where two free radicals combine to form a stable molecule. The selection of the appropriate propagation reactions and the necessary termination reactions for a mechanism will be dealt with on an individual basis as each model compound mixture is discussed, in Chapters 4, 5, and 6. For now, suffice it to say that the bond dissociation, hydrogen abstraction, and radical recombination reactions comprise the necessary reactions in formulating a sound mechanistic scheme that simulates free-radical interactions in a model compound system.

2.5 Computer Modeling with CHEMR

CHEMR is a computer modeling scheme for chemical kinetics, originally developed to describe the formation of photochemical smog. It calculates the time-dependent concentration profiles of the reacting species in a reaction mechanism. Comparison of predicted concentrations with experimental data then allows validation of kinetic schemes and reaction rate constants. The original program, CHEMK, integrates a system of ordinary differential equations associated with a kinetic mechanism, given a set of initial conditions. This fast and efficient computer program was written by Whitten (25) and Overton (26) and utilizes the routines first developed by Gear (27) and modified by Hindmarsh (28). The Gear routine has since been modified to increase the program effi-

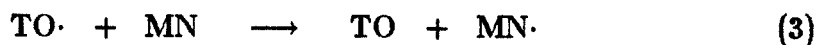
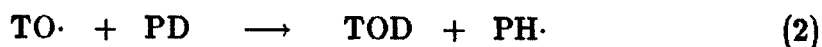
ciency by Spellman and Hindmarsh (29). The resulting version of CHEMK can handle chemical kinetic mechanisms containing up to 89 species and up to 200 reactions. It can also handle time-dependent temperatures and rate constants, and reaction schemes with stoichiometric coefficients. The latest modification was implemented by McRae (30), the major improvement being the ability to take negative coefficients. This final version is called CHEMR. The emphasis of this section is placed on providing a description of program input, and the analysis of the output data. A more detailed account of the computer program appears in the report by Whitten and Hogo (31), and the complete program listing is provided by McRae (30).

2.5.1 CHEMR Input

Table 2.1 contains a typical input data file for CHEMR. In this particular example, the model compound mixture was bibenzyl (BB) + phenol-OD (PD) + methyl naphthalene (MN). This mechanism is slightly simpler than the final form in Chapter 4, but will serve to highlight the major characteristics of an input file.

Each elementary reaction is listed individually and is numbered sequentially. The rate constant at 298°K must be specified, and the activation energy in degrees Kelvin (actually E_a/R , R being the Universal Gas Constant) must also be provided if the reaction is temperature dependent. Alternatively, the rate constant at the reaction temperature can be listed while activation energy is designated as zero. This method of listing has two applications. First, in the case of hydrogen abstraction experiments, the unknown rate constant of the reaction involving a phenoxy radical can be listed at reaction temperature given

an approximate ratio of that rate to the known rate of a well-studied reaction, such as hydrogen abstraction involving a hydrocarbon radical. For example, reactions (2) and (3) are:



The rate parameters for reaction (3) are known from group additivity calculation and also by analogy with similar reactions reported in the literature. Chapter 4 will demonstrate a method for approximating the ratio k_2/k_3 . It is then more convenient to list k_2 at reaction temperature as a multiple (or fraction) of k_3 , and designate E_{a_2} as zero, as is done in Table 2.1. The ratio k_2/k_3 is smoothly adjusted until model prediction of the product distribution agrees with experimental data. Once the rate constant is determined, the activation energy and the A factor can be back-calculated. The other instance where the activation energy is listed as zero occurs in the termination reactions. Here the activation energy is conventionally taken to be zero, and the rate constant is calculated from the viscosity of the reactant mixture at reaction temperature, as outlined above in section 2.3.4.

The title line follows the kinetic mechanism. For this particular input file, the title is 'BB + PD + MN 425C 1HR.' The following line is for output specification. The first number represents the number of reactants with initial nonzero concentrations, which in this case is three. Next is the specific time of initial print, followed by the time interval. Both are 900 seconds or 15 minutes in this case. The next line contains alphanumeric identification of the reactants with nonzero initial concentrations. The corresponding initial concentrations at reaction temperatures are listed below the appropriate reactant species. The

concentrations are calculated from the critical properties of the compounds, as outlined in Chapter 4. The next line is for time specification. The first number is simulation starting time. The second number represents simulation ending time, which in this case is 3600 seconds or one hour. Then comes the temperature, 698°K or 425°C. This temperature is taken to be constant throughout the simulation. This particular input file does not yield any output that is plotted graphically, but plot options could be incorporated if desired.

Chapter 4 will discuss the selection of elementary reactions to be included in the mechanistic scheme for the model compound system 'BB + PD + MN.' Obviously the twenty reactions shown in Table 2.1 do not account for all free-radical reactions in this reactant mixture. The task is to minimize the number of reactions, thus minimizing computing time as well as the number or rate parameters to be determined, without sacrificing a kinetic mechanism to adequately describe the model compound system under study.

2.5.2 CHEMR Output

The computer model yields concentration profiles for all reacting species in the reaction mixture at specified time intervals. From this information, conversion for the reactants and yield for products can be calculated and compared with experimental observation. Table 2.2 shows the model output corresponding to the input data given in Table 2.1. In addition to concentration profiles, the output further provides the reaction rates as well as the net rates, also at specified time intervals. The reaction rate is the transient rate for each elementary reaction, while the net rate for a reacting species represents the combined rate of formation and depletion of the species as a result of all reactions producing

or exhausting that species. The latter becomes useful for tracing the behavior of a certain product over time. In Chapter 5, the concentrations of certain reaction products will be shown to first increase with temperature then decrease as the temperature exceeds a certain value. The sign change in the net rate, from positive to negative, provides a quick clue to this behavior.

2.5.3 Summary

In this thesis the computer program CHEMR will serve two purposes. In the first case, a sound kinetic mechanism is formulated from a set of well-established elementary reactions, and the rate parameters associated with all but one elementary reaction are either known from the literature or estimated through thermochemical techniques. The unknown rate parameters can then be determined if a first approximation can be achieved. Chapter 4 discusses this application of CHEMR to determine hydrogen abstraction rates involving phenoxy radicals. In the second case, a mechanistic scheme is postulated from the knowledge of product structures and concentration profiles, using known rate parameters. The proposed kinetic mechanism is then validated through its success in predicting experimental results. Chapter 5 will demonstrate this aspect of CHEMR in its ability to predict the temperature dependence of certain recombination products. Finally Chapter 6 will employ CHEMR to verify a proposed mechanistic scheme for 1-naphthol dissociation.

REFERENCES

- [1] Whitehurst, D. D., Mitchell, T. O., and Farcasiu, M., 'Coal Liquefaction. The Chemistry and Technology of Thermal Processes,' Academic Press, New York, 1980
- [2] Curran, G. P., Struck, R. T., and Gorin, E., *Ind. Eng. Chem. Proc. Des. Dev.*, 1967, **6**, 166
- [3] Wiser, W. H., *Fuel*, 1968, **47**, 475
- [4] Neavel, R. C., *Fuel*, 1976, **55**, 237
- [5] Attar, A., *Am. Chem. Sol. Div. Fuel Chem., Preprints*, 1978, **23**(4), 169
- [6] Gunn, S. R., Sama, J. K., Chowdhury, P. B., Mukherjee, S. K., and Mukherjee, D. K., *Fuel*, 1979, **58**, 176
- [7] Uebersfeld, J., Etienne, A., and Combrisson, J., *Nature*, 1954, **174**, 614
- [8] Retcofsky, H. L., Hough, M., and Clarkson, R. B., *Am. Chem. Soc. Div. Fuel. Chem., Preprints*, 1979, **24** (1), 83
- [9] Grandy, D. W. and Petrakis, L., *Fuel*, 1979, **58**, 239
- [10] Petrakis, L. and Grandy, D. W., *Fuel*, 1980, **59**, 227
- [11] Petrakis, L. and Grandy, D. W., *Fuel*, 1981, **60**, 120
- [12] Petrakis, L., Grandy, D. W., and Jones, G. L., *Fuel*, 1983, **62**, 1066
- [13] Gavalas, G. R., 'Coal Pyrolysis,' Coal Science and Technology; **4**, Elsevier Scientific Publishing Company, Amsterdam, The Netherlands, 1982
- [14] Benson, S. W., and O'Neal, H. E., Kinetic Data on Gas Phase Unimolecular Reactions, NSRDS-NBS, **21**, 1970
- [15] Benson, S. W., 'Thermochemical Kinetics: Methods for the Estimation of Thermochemical Data and Rate Parameters,' John Wiley & Sons, New

York, Second Edition, 1976

- [16] Benson, S. W., and Buss, J. H., *J.Chem. Phys.*, 1958, **29**, 546
- [17] Allen, D. T., 'Modeling the Reactions of Coal Liquids,' Ph.D. Thesis, Department of Chemical Engineering, California Institute of Technology, Pasadena, California, 1983
- [18] Sato, Y., *Fuel*, 1979, **58**, 318
- [19] Poutsma, M. L., *Fuel*, 1980, **59**, 335
- [20] Schlosberg, R. H., Szajowski, P. F., Dupre, G. D., Danik, J. A., Kurs, A., Ashe, T. R., and Ulmstead, W. N., *Fuel*, 1983, **62**, 690
- [21] Kamiya, Y., Yao, T., and Oikawa, S., *Am. Chem. Soc., Div. Fuel Chem. Preprints*, 1979, **24** (2), 116
- [22] Ladacki, M. and Szwarc, M., *J.Chem. Phys.*, 1952, **20** (11), 1814
- [23] Reid, R. C., Prausnitz, J. M., and Sherwood, T. K., 'The Properties of Gases and Liquids,' McGraw-Hill Book Company, New York, Third Edition, 1977
- [24] Perry, R. H. and Chilton, C. H., *Chemical Engineers' Handbook*, McGraw-Hill Book Company, New York, Fifth Edition, 1973
- [25] Whitten, G. Z., 'Rate Constant Evaluations Using a New Computer Modeling Scheme,' 167th National Meeting, American Chemical Society, 1974
- [26] Overton, J. H., 'Users Guide to EPASIM-A Chemical Kinetics Simulation Program,' TN-262-1643, Northrop Services, Inc., Huntsville, Alabama, 1976
- [27] Gear, C. W., 'Numerical Initial Value Problems in Ordinary Differential Equations,' Prentice-Hall, Englewood Cliffs, New Jersey, 1971
- [28] Hindmarsh, A. C., 'GEAR: Ordinary Differential Equation System Solver,' Report UCID-30001, Rev. 3, Lawrence Livermore Laboratory, Livermore, California, 1974

- [29] Spellman, J. W. and Hindmarsh, A. C., 'GEARS: Solution of Ordinary Differential Equations Having a Sparse Jacobian Matrix,' Report UCID-30116, Lawrence Livermore Laboratory, Livermore, California, 1975
- [30] McRae, G. J., 'A Computer Program for the Numerical Solution of Chemical Kinetic Problems,' Environmental Quality Laboratory, California Institute of Technology, Pasadena, California, 1983
- [31] Whitten, G. Z. and Hogo, H., 'Modeling of Simulated Photochemical Smog with Kinetic Mechanisms. Volume 2. CHEMK: A Computer Modeling Scheme for Chemical kinetics,' EPA-600/3-80-028b, U.S. EPA, Research Triangle Park, North Carolina, 1980

TABLE 2.1

INPUT DATA: MECHANISM AND RATE CONSTANTS
THERMOLYSIS OF BB + PD + MN

	2#	1#yes			k ₂₉₈	E _a /R
bb	1	to.	to.	to.	1.68E-32	32713.
to.	2	pd	to.	ph.	1170.3	0.
to.	3	mn	to	mn.	2.51E0	4529.
to.	4	bb	to	bb.	2.51E0	4529.
ph.	5	mn	ph	mn.	2.51E0	4529.
ph.	6	bb	ph	bb.	2.51E0	4529.
mn.	7	pd	mnd	ph.	1170.3	0.
mn.	8	bb	mn	bb.	2.51E0	4529.
bb.	9	pd	bbd	ph.	93.823	0.
bb.	10	mn	bb	mn.	6.79E-3	6291.
to.	11	to.	bb		1.918E8	
to.	12	ph.	bb		1.918E8	
to.	13	mn.	p2		1.918E8	
to.	14	bb.	p3		1.918E8	
ph.	15	mn.	p4		1.918E8	
ph.	16	ph.	p5		1.918E8	
ph.	17	mn.	p6		1.918E8	
mn.	18	bb.	p7		1.918E8	
mn.	19	mn.	p8		1.918E8	
bb.	20	bb.	p9		1.918E8	
BB + PD + MN	425C 1HR	bb.	p10		1.918E8	
3		900.		900.		
bb	pd					
0.534	2.136	mn				
0.	3600.	2.136				
		698.				
eof						

TABLE 2.2

MODEL OUTPUT: THERMOLYSIS OF BB + PD + MN

BB + PD + MN 425C 1HR									
INITIAL CONCENTRATIONS									
bb	0.534E+00	pd	0.214E+01	mn	0.214E+01				
THE TEMPERATURE OF THE CELL WAS = 6.98E+02 AND THE ERROR TOLERANCE = 1.00E-02									
THE RATE CONSTANTS USED WERE									
1	0.352E-04	2	0.117E+04	3	0.152E+05	4	0.152E+05	5	0.152E+05
7	0.117E+04	8	0.152E+05	9	0.152E+05	10	0.152E+05	11	0.152E+05
13	0.152E+05	14	0.152E+05	15	0.152E+05	16	0.152E+05	17	0.152E+05
19	0.152E+05	20	0.152E+05					18	0.152E+05
TIME = 0.000E+00 STEP (H) = 0.000E+00									
bb	0.534E+00	to.	0.000E+00	pd	0.214E+01	tod	0.000E+00	ph.	0.214E+01
to	0.000E+00	mn.	0.000E+00	bb.	0.000E+00	ph	0.000E+00	mn	0.000E+00
p2	0.000E+00	p3	0.000E+00	p4	0.000E+00	p5	0.000E+00	bbd	0.000E+00
p8	0.000E+00	p9	0.000E+00	p10	0.000E+00	TEMP	0.000E+00	p7	0.000E+00
NET REACTION RATES									
bb	-0.180E-04	to.	0.000E+00	pd	0.000E+00	tod	0.000E+00	mn	0.000E+00
to	0.000E+00	mn.	0.000E+00	bb.	0.000E+00	ph	0.000E+00	bbd	0.000E+00
p2	0.000E+00	p3	0.000E+00	p4	0.000E+00	p5	0.000E+00	p7	0.000E+00
p8	0.000E+00	p9	0.000E+00	p10	0.000E+00	TEMP	0.000E+00		
THE REACTION RATES ARE									
1	0.100E-04	2	0.000E+00	3	0.000E+00	4	0.000E+00	5	0.000E+00
7	0.000E+00	8	0.000E+00	9	0.000E+00	10	0.000E+00	11	0.000E+00
13	0.000E+00	14	0.000E+00	15	0.000E+00	16	0.000E+00	17	0.000E+00
19	0.000E+00	20	0.000E+00					18	0.000E+00
TIME = 0.900E+03 STEP (H) = 0.200E+02									
bb	0.452E+00	to.	0.010E-09	pd	0.191E+01	tod	0.100E-02	ph.	0.620E+00
to	0.293E-01	mn.	0.032E-07	bb.	0.233E-06	ph	0.223E+00	mn	0.179E+01
p2	0.934E-06	p3	0.123E-04	p4	0.357E-04	p5	0.710E-05	bbd	0.179E+01
p8	0.122E-02	p9	0.356E-02	p10	0.104E-01	TEMP	0.690E+03	p7	0.271E-03
NET REACTION RATES									
bb	-0.825E-04	to.	-0.105E-11	pd	-0.230E-03	tod	0.183E-05	ph.	-0.117E-10
to	0.299E-04	mn.	0.332E-10	bb.	-0.273E-10	ph	0.229E+03	mn	0.106E-03
p2	0.985E-09	p3	0.131E-07	p4	0.366E-07	p5	0.756E-08	p6	0.106E-06
p8	0.133E-05	p9	0.372E-05	p10	0.104E-04	TEMP	0.880E+00		
THE REACTION RATES ARE									
1	0.159E-04	2	0.103E-05	3	0.243E-04	4	0.563E-05	5	0.432E-04
7	0.106E-03	8	0.572E-03	9	0.181E-04	10	0.563E-05	11	0.985E-09
13	0.111E-07	14	0.364E-07	15	0.756E-08	16	0.100E-06	17	0.133E-05
19	0.372E-05	20	0.104E-04					18	

TABLE 2.2
MODEL OUTPUT: THERMOLYSIS OF BB + PD + MN (contd.)

[illegible]

CHAPTER 3

EXPERIMENTAL

3.1 Introduction

This chapter discusses the experimental aspects of this thesis. In the next section, the reactor setup and the procedure for a typical experimental run are described. Section 3.3 illustrates the sample preparation techniques. It also explains the procedures for collection of product samples, as well as methods for product isolation and purification for further analysis. A most important part of this work, however, is the identification of reaction products. For this reason, emphasis will be placed upon the four major analytical tools that have been the most helpful, namely the gas chromatograph, the high-performance liquid chromatograph, the gas chromatograph-mass spectrometer, and the proton and carbon-13 nuclear magnetic resonance spectrographs. Section 3.4 outlines the theory and utility of each apparatus. Later, Chapters 5 and 6 will demonstrate how the application of these analytical tools in concert with one another allows identification of relatively complex reaction products.

3.2 The Reactor

All thermolysis experiments were carried out in a $\frac{1}{2}$ in i.d. stainless steel tube reactor. The tube had a swagelok fitting on either end. A valve could be attached so that gas samples could be taken for analysis. The reactor was im-

mersed in a molten tin bath equipped with a rocking mechanism, which agitated the reaction mixture in the tube by a side to side motion. The tin bath was heated by two sets of 600-watt coil heaters connected in parallel, which heated the bath to the desired temperature within two to three hours. The bath temperature was controlled by a thermostat. Once the bath attained the desired temperature, fluctuation in temperature was typically less than $\pm 2^{\circ}\text{C}$. The tin bath afforded uniform and rapid heating of the reactor. A thermocouple sealed inside a second tubing bomb reactor indicated that heatup time was under 45 seconds in all runs.

The procedure for each run is as follows.

1. One and a half to two grams of reactants were charged into the reactor.
2. The reactor was purged with nitrogen and then sealed.
3. The reactor was inserted into the receptacle in the tin bath and the agitator was switched on.
4. After the specified reaction time, the agitator was turned off and the reactor was removed from the tin bath.
5. The reactor was immediately immersed in a water bath. The temperature decreased 100°C within 30 seconds of removal from the tin bath.
6. After cooling, the reactor exterior was cleaned with acetone and then dried.
7. If desired, product gases were metered and analyzed by gas chromatography.
8. Liquid and solid products were washed from the reactor and placed in a vial.

3.3 Sample Preparation

All reactants except benzyl phenyl ether (BPE), 1,2-tetrahydro naphthalene (tetralin), and phenol-OD were obtained from Aldrich Chemical Company. BPE was purchased from Frinton Laboratories, tetralin from K and K Chemicals, and phenol-OD from MSD Isotopes. With the exception of BPE, all compounds were used as received. The purities, as determined by gas chromatography, were better than 97 percent in all cases. Spectrophotometric grade acetonitrile (CH_3CN) and water were obtained through American Scientific Products.

3.3.1 Recrystallization of Benzyl Phenyl Ether

Due to the light purple color of BPE, it was recrystallized before use. The procedure is as follows.

1. BPE was slowly stirred into 10 ml of 95 percent ethanol in a beaker set on a hot plate at a low setting. BPE was added until the solution was supersaturated.
2. A few drops of ethanol absolute was added to dissolve residual BPE.
3. The beaker was immediately placed in an ice bath.
4. After the formation of crystals was complete, the recrystallized BPE was washed with a cold solution of 75 % ethanol over a Buchner funnel connected to an aspirator.
5. The crystals were dried in a desiccator under vacuum overnight.

The resulting BPE was a very lightly pink powder, which was kept under nitrogen.

3.3.2 Deuteration of 1-Naphthol

Phenol-OD was commercially available. 1-Naphthol, however, was not. It was prepared in our laboratory by deuterium exchange with heavy water (D_2O), as described in the following procedure.

1. 30 g D_2O was added to 4.5 g 1-naphthol (100:1 equivalent).
2. A minimum amount of tetrahydrofuran (THF) was added to completely dissolve 1-naphthol.
3. 2-3 drops of concentrated hydrochloric acid (HCL) was added to catalyze the exchange.
4. The solution was heated to $50^\circ C$ and stirred vigorously overnight.
5. THF and the bulk of D_2O were rotovapped off under reduced pressure at $100^\circ C$.
6. Trace amount of D_2O was removed as follows:
 - i. 2-3 ml dichloromethane (CH_2Cl_2) was added to dissolve 1-naphthol-OD.
 - ii. The mixture was stirred with anhydrous magnesium sulfate ($MgSO_4$).
 - iii. $MgSO_4$ was removed by filtration
 - iv. CH_2Cl_2 was rotovapped off.
7. 1-naphthol-OD was dried in a desiccator under vacuum overnight.

The proton NMR (Figure 3.1) indicates that the deuterium exchange in 1-naphthol-OD was essentially complete. The signal corresponding to the hydroxyl proton has virtually disappeared in the 1-naphthol-OD chromatogram.

3.3.3 Product Purification for Further Analysis

At the end of an experimental run, the thermolysis products were washed from the reactor tube using acetonitrile. Acetonitrile was selected because it was a cosolvent for the HPLC. In the case where the products were sparingly soluble in acetonitrile, anhydrous ethyl ether was used instead because its high volatility facilitated removal from the product mixture. For HPLC analysis, a product sample was diluted in acetonitrile and the solution centrifuged to remove small undissolved particles that could obstruct the HPLC columns, the injection valve, or the connecting tubing.

Section 3.4 will describe fractionation by the HPLC. Each fraction that was isolated from the product mixture contained the cosolvents, water and acetonitrile. These solvents, as well as other impurities, must be removed before the sample could be submitted for GCMS and especially NMR analysis. The purification procedure is as follows.

1. To the fraction was added 10 - 15 ml diethyl ether.
2. The mixture was placed in a separation funnel and the bulk of water was removed.
3. Traces of water was removed by addition of anhydrous MgSO_4 , which was subsequently filtered off.
4. The solution was placed in a rotovapor to remove the ether.
5. The resulting compound was dried in a desiccator under vacuum overnight.
6. For high resolution NMR, 1 ml acetone- d_6 was added and the sample was evacuated in a desiccator for an additional 4 hours.

3.3.4 Chemical Separation

The focus of this study was on phenolic compounds. It was thus desirable

to separate the phenolic (acidic) compounds from the neutral compounds in a product mixture. The procedure for the separation process is listed below.

1. A product sample was dissolved in 20 ml anhydrous diethyl ether and the solution was placed in a separation funnel.
2. The solution was extracted three times with 5 ml 3 M NaOH.
3. The ether (neutral) fraction was treated as follows.
 - i. The fraction was washed twice with 2 ml water.
 - ii. The fraction was dried over MgSO_4 and ether was rotovapped off.
 - iii. The neutral products were dried in a desiccator under vacuum overnight.
4. The aqueous (phenolic) fraction was treated as follows.
 - i. Concentrated HCl was added dropwise until the solution turned acidic.
 - ii. The solution was extracted twice with 10 ml ether.
 - iii. The solution was washed twice with 2 ml water.
 - iv. The fraction was dried over MgSO_4 and ether was rotovapped off.
 - v. The product was dried in a desiccator under vacuum overnight.

Figure 3.2 illustrates the HPLC chromatograms of the thermolysis products of toluene and benzyl phenyl ether, comparing the phenolic fraction, the neutral fraction, and the entire products. Prior to detailed analysis of each product species, chemical separation already revealed that the mixture contained only two major phenolic products, corresponding to peaks 1 and 2. Chapter 5 will discuss the process of identification of these products, and illustrate how the knowledge of the phenolic character of peaks 1 and 2 was useful in determining

the structures of the corresponding compounds.

It turned out that peak 1 in Figure 3.2 corresponds to phenol. Note that, due to its solubility in water, a certain amount of phenol was lost in the process of extraction from water. This loss presented no problem because phenol was not one of the unknown products of interest. The other unknown products were not soluble in water and were recoverable from extraction from water.

3.3.5 Column Chromatography

Another method for separation of phenolic (polar) compounds from neutral (nonpolar) compounds should be mentioned. This method, however, did not turn out to be appropriate for this work.

1. A silica gel slurry in hexane was packed into a 30 cm. column to make a 10 cm. layer.
2. A sample to be separated was dissolved in benzene.
3. 0.5 ml of the sample was gently placed above the gel layer.
4. 1 ml hexane was then added and the column was drained until the liquid layer was almost flush with the gel layer. This step was repeated three times.
5. 10 - 15 ml hexane was added and the liquid was drained, each 10 ml collected in a beaker.
6. Hexane was evaporated off by placing the beakers in a fume hood.

The nonpolar compounds should elute first, appearing in the earlier beakers, while the polar compounds should appear in later beakers.

The ineffectiveness of this method was attributed to the fact that the heavy neutral compounds did not elute early enough. Only toluene and few other low-

molecular-weight compounds eluted early. Thus the latter fraction contained not only the phenols but also the high-molecular-weight products such as bibenzyl. This result defeated the purpose of the technique, which was designed to isolate the phenolic compounds from the rest. Column chromatography was thus dropped from consideration.

3.4 Analytical Tools

3.4.1 Gas Chromatography (GC)

Gaseous products were analyzed by a Varian Aerograph Model 142010-00 Gas Chromatograph equipped with a thermal conductivity detector (TCD) and linear temperature programmer. The column was a 7 foot, $\frac{1}{8}$ in. o.d. stainless steel column packed with 5 grams of Carbosphere. Liquid and solid products were dissolved in dichloromethane and analyzed by a Hewlett-Packard Model 5710A Gas Chromatograph equipped with a flame ionization detector (FID). The column was a 30 meter DB-1 capillary column, and the chromatograms were temperature programmed from 60 to 200°C.

The reactants and the major reaction products must first be located on a chromatogram. A method called 'spiking' was employed where a small amount of an authentic sample was added to the mixture to be injected into the GC. The peak in the chromatogram that was intensified, as observed graphically and also in the integration data, was tentatively assigned the structure of that authentic compound. In this manner, major reaction products were located on the chromatogram. For example, Figure 3.3 compares a gas chromatogram of the thermolysis products of bibenzyl + phenol-OD + 1-methylnaphthalene, to

a chromatogram of a mixture of these authentic compounds: toluene, phenol-OD, 1-methylnaphthalene, biphenyl, and bibenzyl. (Biphenyl was added to the reactant mixture as an inert standard for calibration.) In essence, by 'spiking' them with authentic compounds, the species in the product mixture were tentatively identified by matching their retention times with those of the appropriate authentic compounds. Further evidence such as a mass number could then be obtained to validate the identity of the species.

One disadvantage of the method of 'spiking' was that the column might not be sufficiently selective, and two similar but not identical products might elute too closely together to allow separation. In that case, one product could be mistaken for the other. Usually, this was not the problem in this study, because the compounds of interest were sufficiently different. Further, temperature program and/or carrier gas flow rate could be adjusted to improve resolution. Another drawback was the unavailability of some of the compounds under investigation. Compounds such as benzyl phenol was not commercially available, and their identification could not be accomplished by spiking. Overall, however, spiking allowed quick identification of simple compounds that were commercially available.

Gas chromatography was used mainly to obtain the relative concentrations of the major compounds in the product mixture. Each chromatogram yielded integration data, or areas under curves, corresponding to the relative intensities of the various signals. A standard solution containing known concentrations of major product species was injected into the GC. A response factor for converting area under curve to concentration for each compound was determined. These conversion factors were then applied to the integration data for each experimental run to convert them to concentrations of the various product species.

Gas chromatography provided a fast way of obtaining concentration data of low-molecular-weight, volatile compounds. An additional advantage was the very small amount of sample (1 - 5 μL) required for each injection. For more information, the book by McNair & Bonelli (1) provides an excellent introduction to the theory and practice of gas chromatography, while the text by Freeman (2) deals in more detail with the applications of high-resolution gas chromatography, with emphasis on capillary column chromatography. A good part of the book is devoted to qualitative and quantitative analysis of GC spectra.

In this work, gas chromatography was utilized primarily in the hydrogen abstraction experiments, where the identities of the thermolysis products of interest were already known, and only needed to be confirmed by spiking. The conversion data were the major concern in those experiments, and will be discussed in Chapter 4.

3.4.2 High Performance Liquid Chromatography (HPLC)

Complex, low-volatile reaction products were not suitable for analysis by gas chromatography. The high-boiling nature of such compounds made vaporization difficult at temperatures below those associated with the onset of GC column degradation (roughly 250°C) (3). Liquid chromatography offered better resolution of heavy compounds through flow rate and mobile-phase ratio adjustment. The chromatograph was a Spectra-Physics Model 3500B High Performance Liquid Chromatograph equipped with two reciprocating pumps and with solvent gradient programming capability. A Perkin-Elmer LC-55 Spectrophotometer was utilized as an ultraviolet detector. The signal from the spectrophotometer went through a Spectrum 1021 Filter, and then to a Spectra-Physics Systems

I Computing Integrator. The sample exiting the spectrophotometer could be collected by a Pup Model 1200 Fraction Collector. A schematic diagram of the HPLC system appears in Figure 3.4.

The reversed-phase separation mode had been demonstrated to be appropriate for the aromatic compounds being analyzed (3). Two stainless steel columns with i.d. of 7 mm and length of 250 mm custom-packed with 10 μ particles of Spherisorb Octa Decyl Silica (ODS) were used in series to permit large sample injection volumes (up to 500 μ L). The mobile-phase gradient of water and acetonitrile resulted in adequate separation.

3.4.2.1 Solvent Preparation

Only the highest quality, particulate-free solvents should be utilized as mobile phases for the HPLC so that the columns and the 0.01 in. i.d. tubing would not be obstructed and damaged. For this reason, 99+ % spectrophotometric grade acetonitrile and HPLC grade water were employed. All solvents were vacuum filtered through a fine (4 - 5.5 μ) or ultrafine (0.9 - 1.4 μ) Pyrex millipore filter before use. As part of a daily startup procedure, all solvents were degassed by being subjected to a partial vacuum during slow magnetic stirring.

3.4.2.2 HPLC Startup Procedure

The procedure listed in the Spectra-Physics Instruction Manual (4) was somewhat modified for best results. The modified procedure is as follows.

1. The detector, integrator, and recorder were switched on to allow plenty of time of warm up.
2. The solvents were degassed and the reservoirs were put in place, with the

filters completely immersed.

3. All flow rates were set to 00. Flow Feedback was set to Off, Pump Controls to Internal, and Meter to Motor Speed.
4. The HPLC power was turned on and the Pressure Monitor upper limit was set at 3000 psig. This upper limit could be checked by depressing the Pressure Readout button.
5. The Pump Control Power and Solvent Programmer were turned on.
6. The pumps were primed according to the direction in the Instruction Manual.
7. Flow Feedback referencing was achieved as described in the Instruction Manual.
8. The Pump Controls were switched to External.
9. The Solvent Programmer flow rate was set to 60 to flush out the system for 5 - 10 minutes.
10. The flow rate was set to 40 (or the desired flow rate) and the Column Bypass Valve was closed. The pressure should rise to 800 to 1000 psig. The column pressure was allowed to reach an equilibrium value, where fluctuation should be less than 30 psig.
11. Solvent Gradient Program was run by pressing the Start button without injecting a sample, followed by pressing the Run button on the integrator.
12. At the end of the solvent gradient run, initial condition was reestablished by:
 - i. putting the integrator on Standby
 - ii. opening the Column Bypass Valve
 - iii. setting the Solvent Programmer to Initial
 - iv. turning up the flow rate to 60 for 2 - 5 minutes

13. The HPLC was readied for a run by:

- i. reducing the flow rate to the desired value (50 - 60)
- ii. closing the Column Bypass Valve
- iii. allowing the column pressure to stabilize (within 30 psig.)
- iv. allowing the detector response to stabilize (within 0.3 absorbance units).

3.4.2.3 HPLC Operation Procedure

1. A gas-tight syringe was set in the Luer connection on the Injection Valve and the injector handle was put in the Load position.
2. The detector was zeroed and the recorder was put in the Record mode.
3. The sample inlet tube was cleaned with a Kimwipe.
4. While air was being drawn into the syringe, the sample inlet tube was rapidly immersed in a liquid sample and 0.5 ml was drawn into the syringe to thoroughly flush the 100 μ L sample loop.
5. The injector handle was smoothly turned to Inject while the inlet tube was kept immersed. The Solvent Gradient Program was initiated by pressing the Start button, and the integrator by the Run button. The starting column pressure was recorded.
6. After the chromatogram was obtained, initial condition was achieved by:
 - i. putting the integrator and recorder on Standby.
 - ii. opening the column bypass valve.
 - iii. returning the injector handle to Load.

- iv. setting the Solvent Programmer to Initial
 - v. setting the flow rate to 60 for 2 - 5 minutes.
7. The flow rate was returned to the original value, the Column Bypass Valve was closed, and pressure and detector absorbance were allowed to reach equilibrium.
 8. The syringe was emptied and reinserted into the Luer connection for the next run.

3.4.2.4 HPLC Shutdown Procedure

1. The system was flushed with acetonitrile for 5 - 10 minutes at a flow rate setting of 60.
2. The flow rate was turned to 00, and the column bypass valve was opened.
3. The pump controls were switched to Internal, and the flow feedback to Off.
4. The pump power was turned off, and the solvent programmer was turned off.
5. The HPLC, detector, and recorder power was turned off.
6. The integrator was put on Shunt and then switched off.

3.4.2.5 Fraction Collection

The Pup Fraction Collector permitted isolation of various species in a sample. The delay time between the detector and the fraction collector must be determined so that a particular peak could be correlated with a specific fraction. A sample containing phenolphthalein was injected into the HPLC. As soon as the signal was registered on the chart recorder, the fraction collector was switched on, and a sample was taken every 10 seconds. Later, NOH was added to the

presence in a particular timed fraction. The delay time between detection by the spectrophotometer and collection by the fraction collector was thus determined. As a check, this delay time was also calculated from the mobile-phase flow rate and the tubing dimensions.

3.4.2.6 Parameters Used in Analysis

The following operational parameters for the high performance liquid chromatograph were used in the analyses of the products of recombination experiments.

Sample Loop Size:	100 μ L
Nominal Flow Rate:	1.6 - 2.4 ml/min
Solvent Program	
Initial Concentration:	50 - 60 %
Final Concentration:	99 % (100 % CH ₃ CN)
Delay Time:	20 minutes
Sweep Time:	10 minutes
Gradient:	Linear
UV Wavelength:	254 nm
Integrator Attenuation:	$\times 16$
Chart Speed:	0.1 in./min
Integration Parameters:	Peak width = 50.

All others at default values.


The UV wavelength was chosen to maximize sensitivity to the oxygen-substituted benzene rings encountered in this study (5).

The HPLC was used in both the analytical and the preparative modes. In the analytical mode, the HPLC served much the same function as the GC – it provided concentration data for the product species. A dilute sample was injected and a chromatogram yielded separation of the major compounds in the sample, including the associated integration data. Identification of simple products were achieved by 'spiking' or comparing the elution times with those of authentic compounds. In the preparative mode, the HPLC enabled isolation of a compound from a product mixture. A concentrated sample was injected and the peaks of interest were isolated. These fractions were purified by the method described in Section 3.3.3, and were subjected to GCMS and/or NMR analysis to determine their molecular structures.

In summary, HPLC was a powerful tool for quantitative analysis of thermolysis products. Low-volatile compounds unsuitable for GC analysis were analyzed by HPLC. Besides determining relative concentrations of compounds in a mixture, HPLC also allowed fractionation of various species for further analysis by GCMS or NMR. HPLC was utilized mostly in the recombination experiments, where identification of relatively complex thermolysis products were the primary goal of the study. These experiments will be discussed in Chapters 5 and 6.

Excellent reviews on the theory and practice of HPLC can be found in references 6 - 8. Johnson and Stevenson (6) provided groundwork for the beginner, while Simpson (7) and Snyder and Kirkland (8) gave detailed accounts of the more sophisticated aspects of the HPLC.

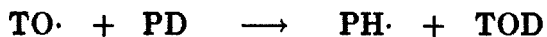
3.4.3 Gas Chromatography Mass Spectrometry (GCMS)

Knowledge of the molecular weight of an unknown product of recombination  proved to be very important in identifying the product's chemical structure. Because the free-radical species were known by careful selection of the reactant mixture, compounds resulting from recombination of these species could only have a limited number of molecular weights. For example, when the benzyl radical ($\phi - \text{CH}_2\cdot$, mass 91) and the phenoxy radical ($\phi - \text{O}\cdot$, mass 93) were present, recombination products could only have masses 182, 184, or 186. If the mass was determined to be 182, then it must contain two benzyl groups. Experience then dictated that this compound would most likely be 1,2-diphenyl ethane (or bibenzyl, $\phi - \text{CH}_2 - \text{CH}_2 - \phi$). If a mass 272 was detected by GCMS, the corresponding compound would result from a bibenzyl radical (mass 181) and a benzyl radical, and it most likely would not contain the phenoxy radical. By designing experiments to yield few free-radical species and by using analogy with literature results, we could determine the constitutive functional groups and assign a possible structure to a compound given its molecular weight.

Mass spectra were obtained on a Kratos MS25 Gas Chromatograph-Mass Spectrometer. An SC-30 packed column was used in a Perkin-Elmer Sigma 3 Gas Chromatograph. A typical chromatogram was temperature programmed from 100 to 280°C, and a typical mass range scanned was 28 to 600. The data were collected on a Data General Nova 3 Minicomputer.

GCMS was also important for another reason. In the hydrogen abstraction experiments (Chapter 4), deuterated compounds were used to distinguish between two different hydrogen donors. For example, deuterated phenol was utilized in the system bibenzyl + phenol-OD (PD) + 1-methylnaphthalene (MN).

The benzyl radical ($\text{TO}\cdot$) underwent the following reactions:



where TOD is deuterated toluene ($\text{C}_7\text{H}_7\text{D}$) and TO is toluene (C_7H_8). GCMS allowed distinction between TOD (mass 93) and TO (mass 92). The natural abundance of C-13 must, however, be taken into consideration. Figure 3.5 shows a GCMS mass intensity scan containing the signals for TO, TOD, and other ions. Let M denote the molecular ion, $d_0 = \text{TO}$, and $d_1 = \text{TOD}$. Then the signals represent:

$$\text{Signal intensity at mass 92} \equiv \text{M} - \text{H}(d_1) + \text{M}(d_0)$$

$$\text{Signal intensity at mass 93} \equiv \text{M}(d_1) + \text{M} + 1(d_0)$$

That is, $\text{M} - \text{H}(d_1)$ was the contribution from the $\text{C}_7\text{H}_6\text{D}\cdot$ ion, $\text{M} + 1(d_0)$ from $^{13}\text{CC}_6\text{H}_8$, $\text{M}(d_1)$ from $\text{C}_7\text{H}_7\text{D}$, and $\text{M}(d_0)$ from C_7H_8 .

From a GCMS of an authentic sample of toluene, the ratios

$$\frac{\text{M} + 1(d_0)}{\text{M}(d_0)} \quad \text{and} \quad \frac{\text{M}(d_0)}{\text{M} - \text{H}(d_0)}$$

were calculated. It was next assumed that

$$\frac{\text{M}(d_0)}{\text{M} - \text{H}(d_0)} = \frac{\text{M}(d_1)}{\text{M} - \text{H}(d_1)}$$

Thus, given 4 equations and 4 unknowns, the desired ratio

$$\frac{\text{M}(d_1)}{\text{M}(d_0)} = \frac{[\text{TOD}]}{[\text{TO}]}$$

was finally calculated.

GCMS was utilized primarily in the recombination experiments to help identify complex product species.

Hamming & Foster (9) provided a thorough introduction to the subject of mass spectroscopy, while McLafferty (10) concentrated on the interpretation of mass spectra, with emphasis on the identification of unknown compounds. Reference to standard spectra of many common compounds is available in the EPA/NIH Mass Spectra Data Base (11).

3.4.4 Nuclear Magnetic Resonance Spectroscopy (NMR)

Once the molecular weight and the constitutive functional groups of a compound were determined, the distribution of the protons and the carbons in the molecule could help narrow down the possible chemical structures, and in some cases could point to the precise structure for that compound. A Bruker WM500 High Resolution Nuclear Magnetic Resonance Spectrometer was used to obtain both the proton and carbon-13 NMRs of certain fractions of the recombination products. These samples were usually of very low concentration due to the limited capacity of the HPLC injection size, so that high resolution NMR was required. These NMRs were run by the Southern California Regional NMR Facilities on the California Institute of Technology campus. For samples with sufficiently high concentrations, such as authentic samples to which our unknowns were compared, a Varian Model EM390 90 MHz NMR were utilized.

The application of proton and carbon-13 NMRs to identify the chemical structures of recombination products will be discussed in Chapters 5 and 6.

For reference, the text by Emsley, Feeney, and Sutcliffe (12) deals in detail with high resolution NMR spectroscopy, covering background theory, spectra

analysis, and surveying major applications. The book by McFarlane and White (13) is a practical manual on various experimental techniques. For a survey of the application of NMR to aromatic compounds, the book by Memory and Wilson (14) is recommended. Finally, the Aldrich Library of NMR Spectra (15) provides standard NMRs for a large number of compounds.

REFERENCES

- [1] McNair, H. M. and Bonelli, E. J., 'Basic Gas Chromatography,' Varian Instrument Division Offices, Palo Alto, California, 5th Edition, 1969
- [2] Freeman, R. R. (ed.), 'High Resolution Gas Chromatography,' Hewlett-Packard, USA, 1979
- [3] Bone, R. L., 'Kinetics and Mechanisms of the Co-Oxidation of Aldehydes and Model Organic Sulfur Compounds in Studies Related to the Oxo-Desulfurization of Fuel Oil and Coal,' Ph.D. Thesis, Department of Chemical Engineering, California Institute of Technology, Pasadena, California, 1981
- [4] Spectra-Physics, 'Liquid Chromatograph Instruction Manual: Model 3500B,' Spectra-Physics, Santa Clara, California, 1975
- [5] Williams, D. H. and Fleming, I., 'Spectrophotometric Methods in Organic Chemistry,' McGraw-Hill Book Company, London, Great Britain, Second Edition, 1973
- [6] Johnson, E. L. and Stevenson, R., 'Basic Liquid Chromatography,' Varian Associates, Inc., Palo Alto, California, 1978
- [7] Simpson, C. F. (Ed.), 'Practical High Performance Liquid Chromatography,' Heyden, New York, 1976
- [8] Snyder, L. R. and Kirkland, J. J., 'Introduction to Modern Liquid Chromatography,' A Wiley-Interscience Publication, John Wiley & Sons, Inc., New York, 1974
- [9] Hamming, M. C. and Foster, N. G., 'Interpretation of Mass Spectra of Organic Compounds,' Academic Press, Inc., New York, 1972

- [10] McLafferty, F. W., 'Interpretation of Mass Spectra,' W. A. Benjamin, Inc., Advanced Book Program, Reading, Massachusetts, Second Edition, 1973
- [11] Heller, S. R. and Milne, G. W. A., 'EPA/NIH Mass Spectra Data Base,' Volumes I - III, NSRDS-NBS 63, U.S. Government Printing Office, Washington, D.C., 1978
- [12] Emsley, J. W., Feeney, J., and Sutcliffe, L. H., 'High Resolution Nuclear Magnetic Resonance Spectroscopy,' Pergamon Press, 1965
- [13] McFarlane, W. and White, R. F. M., 'Techniques of High Resolution Nuclear Magnetic Resonance Spectroscopy,' Butterworth & Co., Ltd., London, Great Britain, 1972
- [14] Memory, J. D. and Wilson, N. K., 'NMR of Aromatic Compounds,' A Wiley-Interscience Publication, John Wiley & Sons, Inc., New York, 1982
- [15] Pouchert, C. J., 'The Aldrich Library of NMR Spectra,' Volumes I and II, Aldrich Chemical Company, Inc., Milwaukee, Wisconsin, Edition II, 1983

FIGURE 3.1

^1H NMR OF 1-NAPHTHOL-OH vs. 1-NAPHTHOL -OD

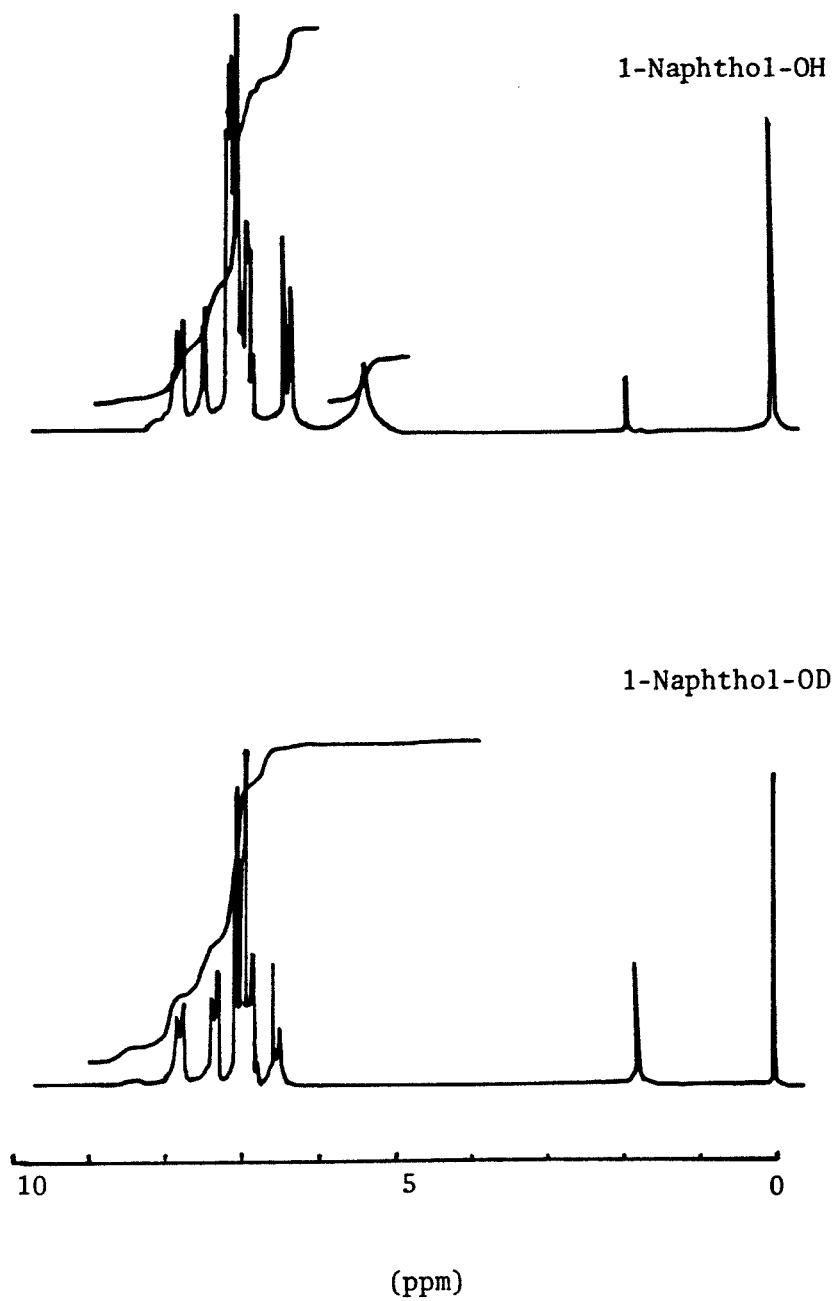


FIGURE 3.2

HPLC OF BPE + TO THERMOLYSIS PRODUCTS

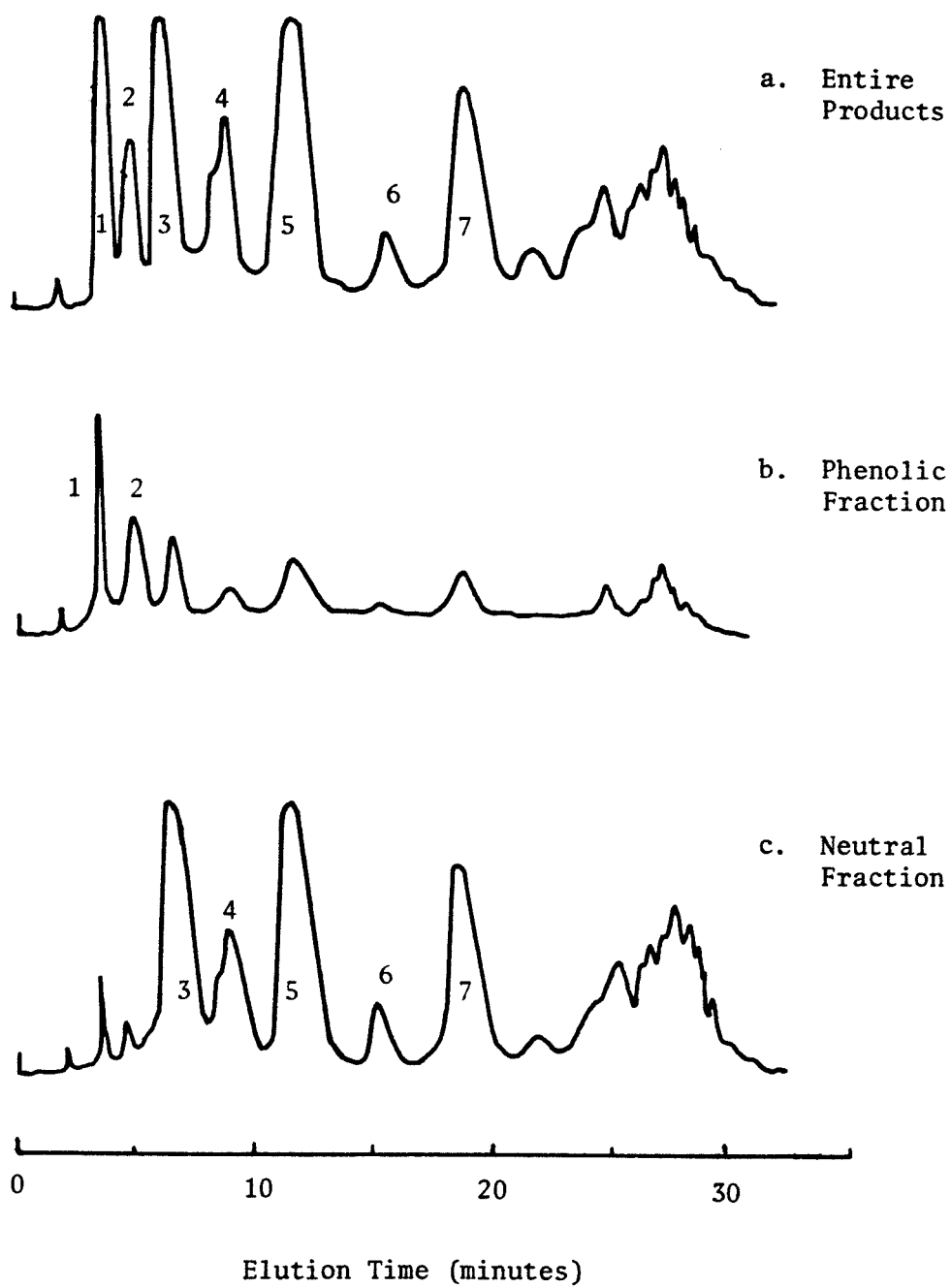


FIGURE 3.3

GC OF BB + PD + MN (+BP) THERMOLYSIS PRODUCTS vs.

GC OF AUTHENTIC MIXTURE OF TO, PD, MN, BP, AND BB

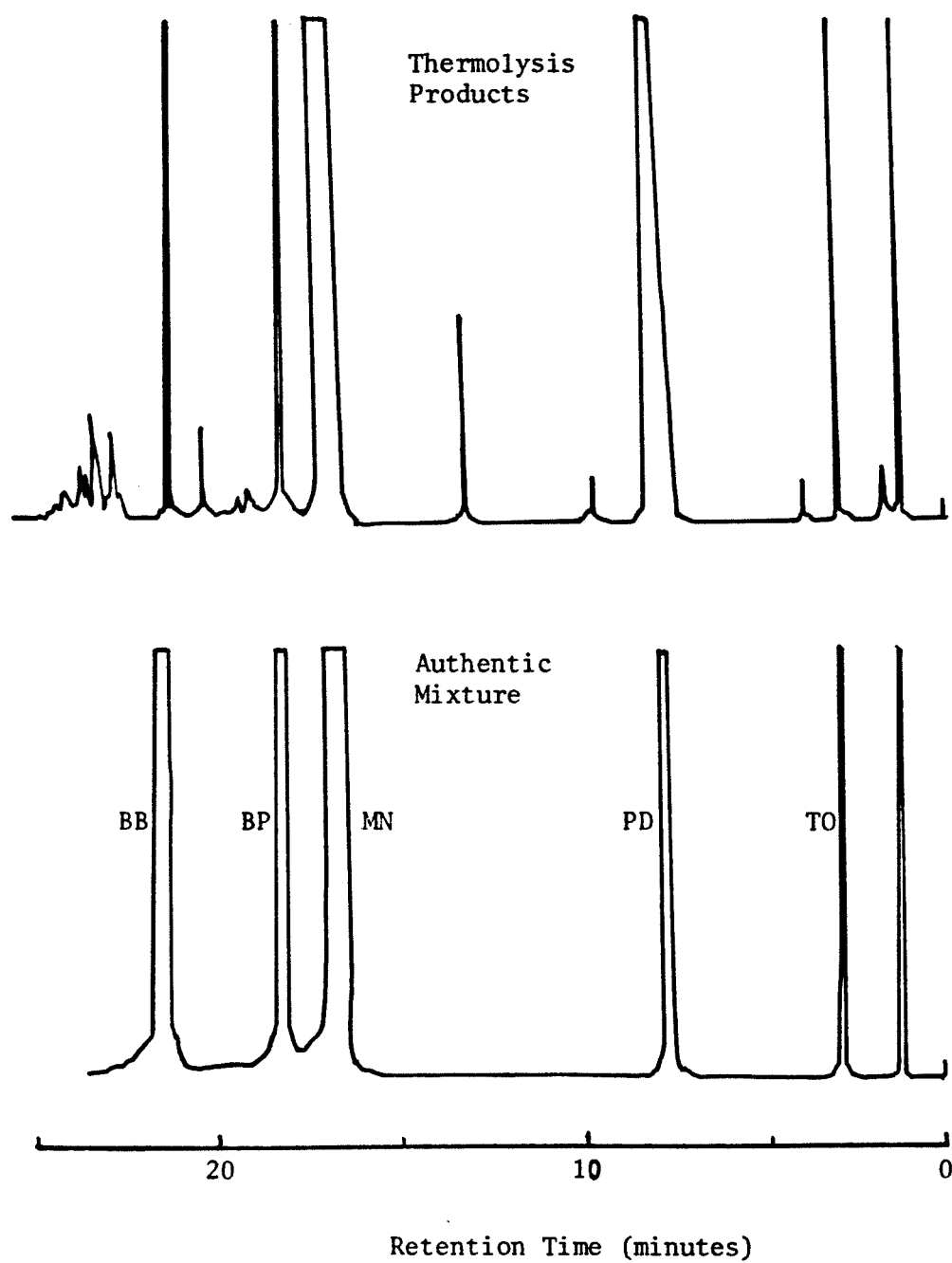


FIGURE 3.4

SCHEMATIC OF LIQUID CHROMATOGRAPHY SYSTEM

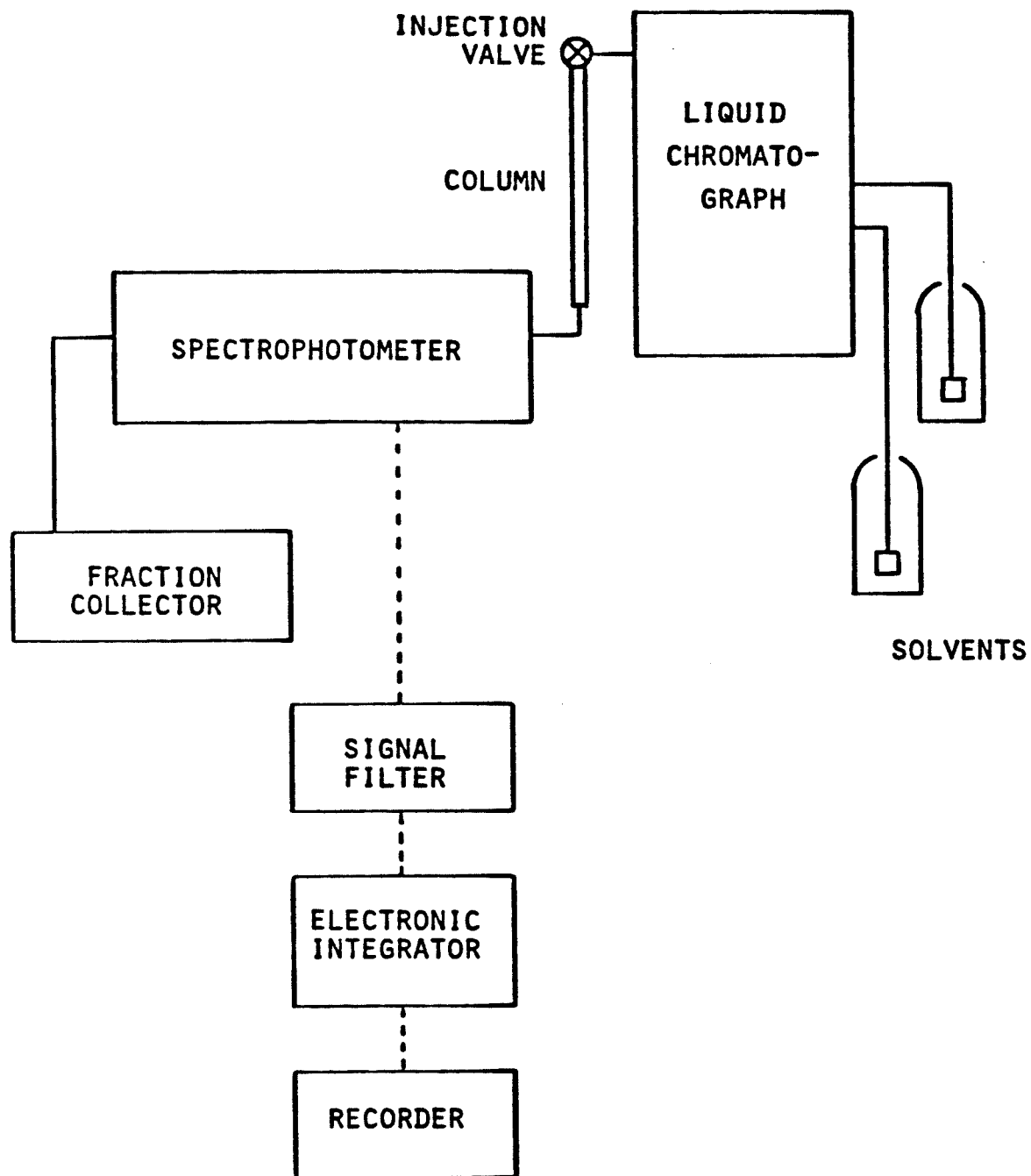
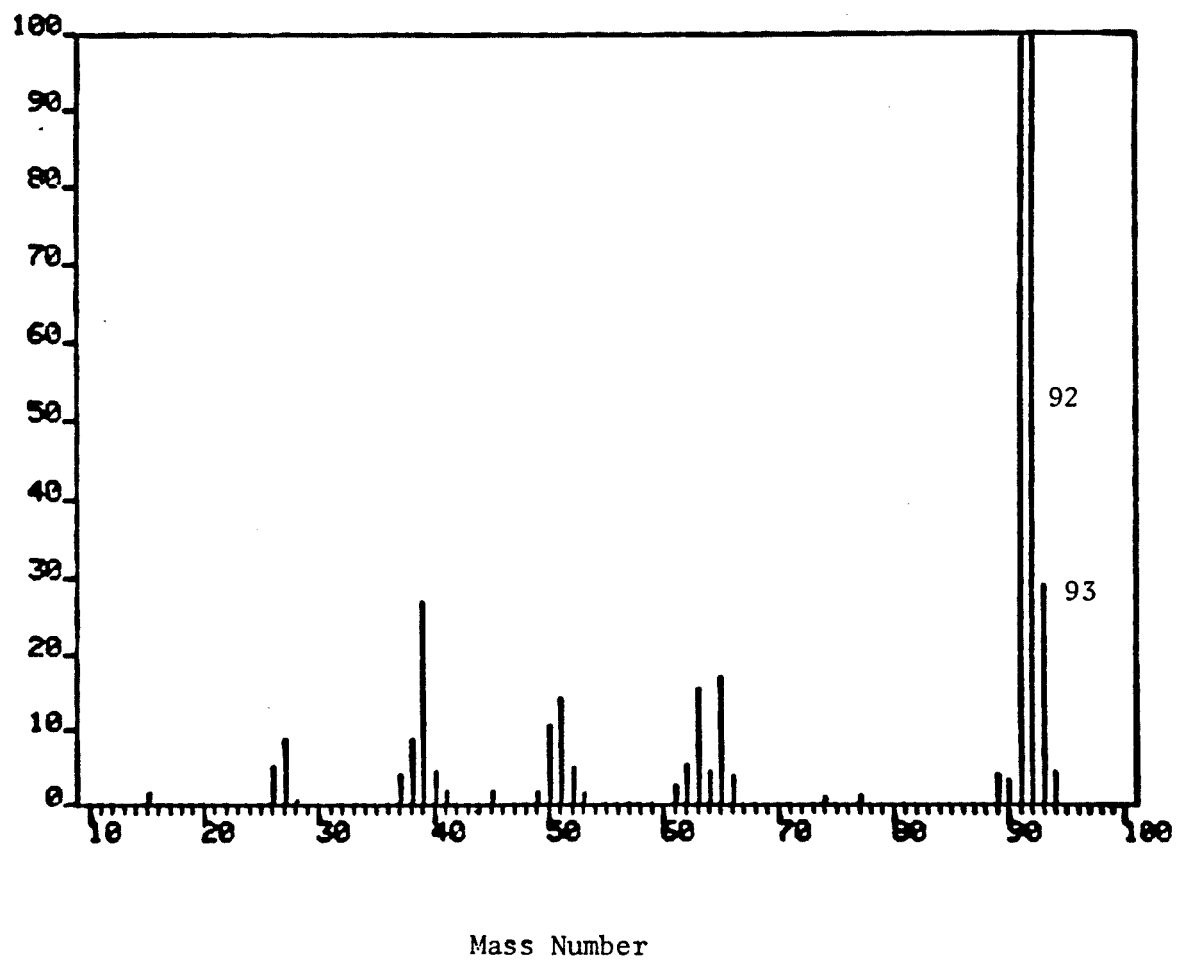


FIGURE 3.5

GCMS INTENSITY SCAN OF BB + PD + MN THERMOLYSIS PRODUCTS
SHOWING THE TOLUENE SIGNALS



CHAPTER 4

HYDROGEN ABSTRACTION EXPERIMENTS

4.1 Introduction

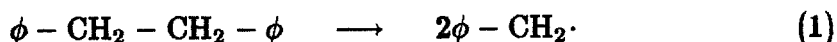
The purpose of this set of experiments was to determine the rate parameters associated with hydrogen abstraction by both a carbon-centered radical, such as the benzyl radical ($\phi - \text{CH}_2\cdot$) and an oxygen-centered radical, such as the phenoxy radical ($\phi - \text{O}\cdot$). The hydrogen atom could come from either a hydrocarbon, such as the methyl hydrogen in methyl naphthalene, or from a phenol, such as the hydroxyl hydrogen in phenol. Table 4.1 shows the two model compound mixtures employed for these experiments. Each mixture was chosen so that the rate of hydrogen abstraction from phenol or naphthol was the only unknown parameter. The other rate parameters were obtained from the literature or from previous experimental results (for example, 1, 2, 3, 4), or were estimated by thermochemical techniques (5). The model compounds were chosen to contain certain representative structures found in coal itself, namely the ethylene and ether bridges and the fused aromatic clusters. The model compounds were also selected in such a manner that minimized the different types of free radicals in the reaction systems. For instance, 1,2-diphenyl ethane (bibenzyl) was employed because it dissociates to produce a single type of radical, the benzyl radical. Finally, the relatively simple structures of these model compounds reduced the number and complexity of undesirable high molecular weight products of recombination. In the following sections, each of the two experimental systems will be discussed with respect to the rate parameters under

consideration and the kinetic analysis through which these rate parameters were derived.

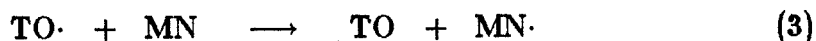
4.2 Thermolysis of Bibenzyl + Phenol OD + 1 Methylnaphthalene

4.2.1 Rate Parameters of Interest

Thermolysis of bibenzyl (BB) has been extensively studied (3, 6, 7). Above 350°C, the ethylene bridge dissociates to produce two benzyl radicals:



The benzyl radical (henceforth represented as $\text{TO}\cdot$) could abstract a hydrogen atom either from 1-phenol-OD (PD) or from 1-methylnaphthalene (MN):



The rate parameters for reaction (3) were obtained by comparison with similar reactions in the literature (1). The rate values for reaction (2) were the only unknowns. The use of deuterated phenol allowed differentiation between the toluene resulting from abstraction from PD and from MN. The initial mole ratio of BB to PD to MN of 1:4:4 provides a large excess of PD and MN for every benzyl radical created to assure that reactions (2) and (3) are indeed the most important abstraction reactions for the benzyl radical. The ratio $[\text{TOD}]/[\text{TO}]$ can be shown to be approximately proportional to the ratio k_2/k_3 (see subsection 4.2.2). Thus, given the experimental values of $[\text{TOD}]/[\text{TO}]$, as determined by GCMS, and given the known value of k_3 , a first estimate of k_2 can be calculated.

The final value of k_2 would be obtained through a least-squares minimization method. The next subsection discusses how computer modeling is used to accomplish this goal.

4.2.2 Kinetic Modeling

Table 4.2 shows the free-radical mechanism employed in modeling this reaction system. There are three groups of reactions. The first is the dissociation reaction, or radical initiation reaction. Reaction (1) is the only initiation reaction in this case. The second group, consisting of reactions (2) through (13), consists of propagation reactions. One radical abstracts hydrogen to form a molecule and generate another radical, keeping the total number of radicals constant. To select these propagation reactions, we look at all the molecules from which a benzyl radical can abstract a hydrogen atom. They are PD, MN, and also BB because BB is not completely dissociated and the resulting $BB\cdot$ radical is quite stable. The subsequent radicals $PH\cdot$, $MN\cdot$, and $BB\cdot$ will next abstract from PD, MN, and BB. They will further abstract from TO, which is a major product from the first series of abstractions. TOD is not included as a hydrogen donor because the abstraction from PD to form TOD is much slower than from MN or BB, and the resulting concentration of TOD is much lower than that of TO. The resulting 12 reactions are called the primary propagation reactions. They involve abstraction from only the major hydrogen donors present in the early phase of thermolysis. For example, abstraction from PH, a secondary product, is not considered because at low conversion of BB the radical activities are not extensive and the majority of phenol is present as PD. Similarly, abstractions from deuterated MN and BB are ignored. For this reason, most experiments

were limited to less than 20 percent conversion of BB to avoid unnecessary complications due to secondary reactions.

The third group consists of recombination, or termination reactions, reactions (14) through (23). In this case two radicals collide with each other to form a stable molecule, resulting in a net loss of two radicals from the system. The recombination reactions are determined by considering all possible permutations between the existing radicals, namely $\text{TO}\cdot$, $\text{PH}\cdot$, $\text{MN}\cdot$, and $\text{BB}\cdot$. Once again, these are the primary recombination reactions, involving only those radicals occurring in the early phase of BB thermolysis. Furthermore, with the exception of BB, all recombination products are assumed to be stable and undergo no further abstraction reactions. These termination reactions indeed provide a radical 'sink' and allow for products of recombination to accumulate as thermolysis progresses.

The omission of secondary propagation and termination reactions would lead to inaccuracy in model results. As will be shown presently, however, even the most abundant of the recombination products are present only in relatively small concentrations. The secondary products would account for an even smaller fraction of the total product mixture. It appears, then, that the error resulting from omission of the secondary reactions is quite small at low conversions.

The assignment of rate values to each of the aforementioned reactions deserves some comment. First, the bond dissociation energy of 65 kcal/mol and the A factor of $10^{15.9}$ for BB were reported by Miller & Stein (3). Other investigators reported slightly different values. For example, Sato (6) gave $E_a = 60.9$ kcal/mol and $A = 10^{14}$. Poutsma (7) gave $E_a = 61.5$ kcal/mol and $A = 2.5 \times 10^{14}$. It turned out that an activation energy of 63 kcal/mol and an A factor of $10^{15.9}$ gave the most satisfactory agreement with our data. Next,

the activation energies for hydrogen abstraction by benzyl radicals were taken to be 9 kcal/mol (1). The activation energy for abstraction by the bibenzyl radical, however, was calculated by group additivity to be 12.5 kcal/mol. The larger activation energy was mainly due to the increased stability of the bibenzyl radical (a secondary radical) in comparison with the benzyl radical (a primary radical). In either case, $A = 10^7$. Finally, all free-radical recombination reactions were assigned an activation energy of zero. These termination reactions were assumed to be diffusion controlled and to have no steric hindrance. Rates of diffusion-limited reactions were estimated from the viscosity of the mixture using the Stokes-Einstein equation (8)

$$k_{\text{diff}} = \frac{8RT}{3 \times 10^3 \eta}$$

where η is the viscosity of the reactant mixture which is liquid at the reaction temperature. For saturated liquids at high temperatures, the corresponding states correlations can be used in conjunction with the acentric factor (9) to yield the equation

$$\eta_L \xi = (\eta_L \xi)^{(0)} + \omega(\eta_L \xi)^{(1)}$$

where

$$\xi = \frac{T_c^{\frac{1}{6}}}{M^{\frac{1}{2}} P_c^{\frac{2}{3}}}$$

where M is the molecular weight and, to a good approximation,

$$(\eta_L \xi)^{(0)} = 0.015174 - 0.02135T_r + 0.0075T_r^2$$

$$(\eta_L \xi)^{(1)} = 0.042552 - 0.07674T_r + 0.0340T_r^2$$

in the range $0.76 \leq T_r \leq 0.98$. The units for η , T , and P are centipoises, degrees Kelvin, and atmospheres, respectively.

The critical constants for the reactant mixture are also calculated by the corresponding states method. For the pseudocritical temperature T_{cm} , a simple mole fraction average method, often called Kay's rule, gives

$$T_{cm} = \sum_j y_j T_{cj}$$

For the pseudocritical pressure, a mole fraction average is not satisfactory when the critical pressures and volumes of all the components are dissimilar. Instead, the modified Prausnitz and Gunn combination (10) is employed to yield the relationship

$$P_{cm} = \frac{R \left(\sum_j y_j Z_{cj} \right) T_{cm}}{\sum_j y_j V_{cj}}$$

The acentric factor is given by the approximation (11)

$$\omega_m = \sum_j y_j \omega_j$$

The critical constants for each of the simple compounds can be found in Reid, *et al.* (12). For larger, more complicated model compounds such as bibenzyl, Lydersen's method (13), which employs structural contributions, is applied. The relations are

$$T_c = T_b \left[0.0567 + \sum \Delta_T + \left(\sum \Delta_T \right)^2 \right]^{-1}$$

$$P_c = M \left(0.34 + \sum \Delta_P \right)^{-2}$$

$$V_c = 40 + \sum \Delta_v$$

where T_b is the boiling point and the unit for V_c is cubic centimeters per gram mole. The Δ quantities are the Lydersen's critical-property increments and are evaluated by summing contributions from various atoms or groups of atoms (13).

Finally, the concentration of each reactant species in the mixture at reaction temperature is estimated from the critical properties using the method of Gunn and Yamada (14):

$$\frac{V}{V_{sc}} = V_r^{(0)}(1 - \omega\Gamma)$$

where

$$V_{sc} = \frac{RT_c}{P_c} (0.2920 - 0.0967\omega)$$

For $0.8 < T_r < 1.0$,

$$V_r^{(0)} = 1.0 + 1.3(1 - T_r)^{\frac{1}{2}} \log(1 - T_r) - 0.50879(1 - T_r) - 0.91534(1 - T_r)^2$$

For $0.2 < T_r < 1.0$,

$$\Gamma = 0.29607 - 0.09045T_r - 0.04842T_r^2$$

Table 4.3 summarizes the diffusion-limited rates of the termination reactions associated with the thermolysis of BB + PD + MN, as well as the concentration of each of the three reactants, at reaction temperatures between 387 and 425°C.

Table 4.4 summarizes the model results as compared with experimental data for the thermolysis of BB + PD + MN. The data are divided into three sections. First, the ratio k_2/k_3 was obtained as follows. Toluene (TO) and deuterated toluene (TOD) were distinguished by the use of GCMS (see Chapter 3), which yielded the relative concentrations of masses 93 (TOD) and 92 (TO). From reactions (2), (3), and (4), the ratio of [TOD] to [TO] can be written as

$$\frac{[TOD]}{[TO]} = \frac{k_2 \int [TO\cdot][PD]dt}{k_3 \int [TO\cdot][MN]dt + k_4 \int [TO\cdot][BB]dt}$$

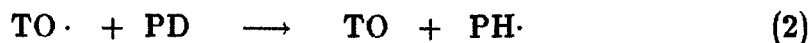
For low conversion of BB, [PD], [MN], and [BB] were approximately constant. Further, $k_3 = k_4$. Thus the equation reduces to

$$\frac{[TOD]}{[TO]} = \frac{k_2}{k_3} \frac{[PD]}{[MN] + [BB]}$$

Given the initial concentrations of PD, MN, and BB, a first approximation of the ratio k_2/k_3 could be calculated. Iteration on the value of k_2/k_3 eventually yielded BB conversion that agreed with experimental data. The product ratio of $[TOD]/[TO]$ also agreed with the experimental value determined by GCMS. The resulting ratio $k_2/k_3 = 0.077$ was then used at various reaction temperatures and residence times. In the second section of Table 4.4, the computer model was employed to simulate thermolysis at temperatures from 387 to 425°C, at a constant residence time of 1 hour. The model results agree well with the experimental data, as shown graphically in Figure 4.1. In the third section of Table 4.4, the conversion of BB was kept under 20 percent at all temperatures by varying the residence time. As explained above, the low conversion of BB would allow omission of secondary reactions in the free-radical mechanism without significant inaccuracy in the model results. The model values from this section were next used to calculate k_2 . In the Arrhenius form, the ratio k_2/k_3 can be written as follows:

$$\frac{k_2}{k_3} = \frac{A_2}{A_3} \exp \left[- \frac{E_{a2} - E_{a3}}{RT} \right]$$

We note that the value $k_2/k_3 = 0.077$ was satisfactory in predicting BB conversion and $[TOD]/[TO]$ over a range of temperatures and residence times. From the above relationship, this must mean that E_{a2} must be close to E_{a3} because a small difference in the two activation energies would result in the exponential term being nonzero and thus temperature dependent. Given $\log_{10} A_3 = 7$, $\log_{10} A_2$ can then be calculated to be 5.9. Thus for the reaction



we estimated $E_{a2} = 9$ kcal/mol, and $\log_{10} A_2 = 5.9$.

It might have appeared more reasonable to iterate for k_2/k_3 at lower conversions of BB, (third group of data in Table 4.4). At high conversions of BB, however, the experimental data were more accurate, giving more accurate results. As it turned out, k_2/k_3 was very insensitive to variations in temperature and reaction time.

The kinetic isotope effect, the change of reaction rate due to deuterium substitution, must now be considered. To a good approximation, all the differences are attributable to the change in mass, which manifests itself primarily in the frequencies of vibrational modes (15). The frequencies (or rather, the wave numbers) in two isotopically substituted molecules will be in the ratio

$$\frac{\tilde{\nu}_1}{\tilde{\nu}_2} = \left(\frac{\mu_2}{\mu_1} \right)^{\frac{1}{2}}$$

where μ is the reduced mass.

Given the stretching wave number of the C-H or O-H bond of 3100 cm^{-1} (5), the wave number of the C-D bond was calculated to be 2275 cm^{-1} .

For a linear activated complex, Johnson and Parr (16) gave the following equation for the kinetic isotope effect:

$$\frac{k_H}{k_D} = \frac{\tilde{\nu}_{iH}}{\tilde{\nu}_{iD}} \left(\frac{\Gamma_H}{\Gamma_D} \right)^* \prod \left(\frac{\Gamma_H}{\Gamma_D} \right)^{\dagger} \prod \left(\frac{\Gamma_D}{\Gamma_H} \right)^r \left(\frac{\sigma_H}{\sigma_D} \right)$$

where

$\tilde{\nu}_i \equiv$ imaginary wave number of the activated complex,

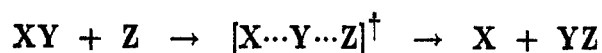
$\Gamma^* \equiv$ tunneling correction factor,

$\Gamma^{\dagger} \equiv$ quantum correction factor for real vibrations of the activated complex,

$\Gamma^r \equiv$ quantum correction factor for real vibrations of the reactants,

$\sigma \equiv$ reaction path degeneracy.

Literature calculations showed that tunneling correction did not significantly improve the accuracy of the rate ratio, and thus the tunneling correction factor was ignored from our calculations. Next, literature showed that a linear, three-atom model was nearly as satisfactory as a very tedious nine-atom model in the case of $\text{CF}_3^\bullet + \text{CD}_3\text{H}$ (17). Thus a three-atom model was employed as an approximation:



For this model, there existed one stretching vibration and two bending vibrations for the activated complex, and one stretching vibration for the reactant. Further, $\frac{\sigma_{\text{H}}}{\sigma_{\text{D}}} = 1$. The equation for the kinetic isotope effect was thus reduced to:

$$\frac{k_{\text{H}}}{k_{\text{D}}} = \frac{\tilde{\nu}_{\text{iH}}}{\tilde{\nu}_{\text{iD}}} \left(\frac{\Gamma_{\text{sH}} \Gamma_{\text{bH}}^2}{\Gamma_{\text{sD}} \Gamma_{\text{bD}}^2} \right)^\ddagger \left(\frac{\Gamma_{\text{sD}}}{\Gamma_{\text{sH}}} \right)^r$$

where $\Gamma = 0.5u/\sinh(0.5u)$, $u = h\tilde{\nu}/kT$,

The subscripts s and b refer to stretching and bending modes, respectively.

From the above calculations, $\tilde{\nu}_{\text{C-H}}$ or $\tilde{\nu}_{\text{O-H}} = 3100 \text{ cm}^{-1}$ and $\tilde{\nu}_{\text{C-D}} = \tilde{\nu}_{\text{O-D}} = 2275 \text{ cm}^{-1}$. No data were available for the remaining wave numbers, and the approximate values for the activated complex $[\text{CH}_3 \cdots \text{H} \cdots \text{H}]$ were obtained from the literature (18). Because the H-H and H-O bonds had somewhat similar spectroscopic data, such as the bond dissociation energy, bond order, and Morse parameter, the above complex was deemed to be a fair approximation of $[\phi\text{CH}_3 \cdots \text{H} \cdots \text{O}\phi]$.

At 400°C , the approximate kinetic isotope effect was determined to be $k_{\text{H}}/k_{\text{D}} \cong 1.95$. According to literature data on similar systems, the theoretical

values could be different from the experimental values by as much as a factor of 10. Experimental data (18, 19) indicated, however, that the ratio k_H/k_D for several hydrogen transfer reactions approached unity as the temperature increased. In this work, therefore, the kinetic isotope effect was ignored because the temperatures were on the order of 400°C. It must be cautioned that a detailed study would be necessary to determine the precise extent of the kinetic isotope effect.

Finally, the effect of deuterium scrambling must be considered. The abstraction of deuterium from PD generated the phenoxy radical ($PH\cdot$), which is extremely reactive. It would immediately abstract either H or D from any available donor. (Thermochemical kinetics shows that the abstraction reaction involving $PH\cdot$ has an enthalpy change of -5.8 kcal/mol, indicating a highly exothermic and thermodynamically favorable reaction.) Thus before long, a concentration of PH will begin to build up. Hydrogen abstraction by $TO\cdot$ from PH yields TO, which can not be differentiated from abstraction from MN. However, if the conversion of BB is kept small, the $TO\cdot$ concentration is also small, and the resulting $PH\cdot$ concentration low. With a large excess of initial concentration of PD, the concentration of PH would quite small by comparison. And the ration $[TOD]/[TO]$ would still closely approximate the preference of $TO\cdot$ for abstraction from PH to MN.

4.3 Thermolysis of Benzyl Phenyl Ether + 1 Naphthol OD + 1,2,3,4 Tetrahydronaphthalene

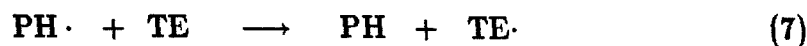
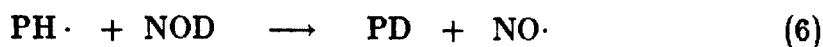
4.3.1 Rate Parameter of Interest

Having estimated the rate of hydrogen abstraction from phenol by a carbon-centered radical, we are now in a position to determine the abstraction rate by an oxygen-centered radical. Benzyl phenyl ether (BPE) was chosen as the initial source of phenoxy radicals because of the readily available value of bond dissociation energy (20, 21). An ether bridge is much weaker than an ethylene bridge, and BPE begins to dissociate above 250°C to produce one benzyl radical and one phenoxy radical:



The abstraction reactions involving $\text{TO}\cdot$ can now be inferred from section 4.2. The reactions of $\text{PH}\cdot$ are of current interest. Abstraction by $\text{PH}\cdot$ from PD would only result in deuterium scrambling. NOD was therefore chosen as the phenolic hydrogen donor. The temperature range selected was low (250 - 350°C) to prevent extensive dissociation of BPE. At such low temperatures, however, MN is not an effective hydrogen donor. Tetralin (TE), a very good hydrogen donor, was thus selected instead of MN for use in this reaction system.

The rate parameters for deuterium abstraction from NOD by $\text{PH}\cdot$ were the only unknowns in this system. The two reactions of consequence are:



By comparing the relative concentrations of PD and PH, the ratio of the rates k_6/k_7 can be estimated. From iteration, the final value of k_6 can be obtained because k_7 is known. The following subsection describes the free-radical model relevant to this reaction system.

4.3.2 Kinetic Modeling

The free-radical mechanism appropriate for this reaction system is shown in Table 4.5. As was the case in the previous system, reaction (1) is the only radical initiation reaction, where the dissociation of the ether bridge yields one benzyl radical and one phenoxy radical. The propagation reactions include reactions (2) through (17). The possible hydrogen (and deuterium) donors are NOD, TE, BPE, and TO. The relevant radicals are $\text{TO}\cdot$, $\text{PH}\cdot$, $\text{NO}\cdot$, $\text{TE}\cdot$, and $\text{BPE}\cdot$. We note that there are two oxygen radicals, the phenoxy and the naphthoxy radicals. In order to distinguish between abstraction by the phenoxy radical from a hydrocarbon and from a phenol, NOD had to be used instead of PD. The use of NOD results in a new radical, the naphthoxy radical, which accounts for four additional propagation reactions. Already we see the importance of limiting the number of radicals to keep the number of elementary reactions to a minimum. Once again, these sixteen reactions are the primary propagation reactions. Abstraction from PH, for example, is neglected on the grounds that its concentration is much lower than that of NOD at low conversions of BPE. Thus the experiments were controlled to achieve no more than 20 percent conversion of BPE so that the omission of secondary reactions would not lead to significant error in the kinetic modeling.

The recombination reactions include reactions (18) through (32). They in-

volve the bimolecular interactions of all radicals with one another. With five major radicals, $\text{TO}\cdot$, $\text{PH}\cdot$, $\text{NO}\cdot$, $\text{TE}\cdot$, and $\text{BPE}\cdot$, their permutations yield 15 reactions. With the exception of BPE, all products of recombination are assumed to be stable. Even BB, the product of benzyl radical recombination, is assumed to undergo no further reaction because of the low reaction temperatures.

It is possible to reduce the number of elementary reactions further without jeopardizing the validity of the model results. Given the small initial concentration of BPE relative to those of NOD and TE, the abstraction reactions from BPE to produce the radical $\text{BPE}\cdot$, and thus the subsequent termination reactions involving $\text{BPE}\cdot$, could be omitted without serious penalty. For a large number of intermediates it is often necessary to reduce the number of reactions with a small sacrifice in accuracy in order to obtain a more manageable system and save computer time. In the present case the reaction system is relatively simple, involving only 32 elementary reactions. The reactions involving BPE and $\text{BPE}\cdot$ will therefore remain in the model for completeness.

The assignment of rate values is discussed next. Kamiya *et al.* (21) gave the value of $E_a \cong 50$ kcal/mol, and Schlosberg *et al.* (4) reported $E_a = 52 \pm 5$ kcal/mol while $\log_{10} A$ was taken to be 16.0 for the dissociation of benzyl phenyl ether. The activation energies for all hydrogen abstraction reactions were taken to be 9 kcal/mol, as in the previous system. Also, for most reactions, $\log_{10} A = 7.0$. For reactions (2), (13), and (16), however, the results of section 4.2.2 can now be used, assuming that the different resonance stabilization energies would not have a significant effect on these rate parameters. Ladacki & Szwarc (22), studying a system of aromatic bromides, concluded that increasing the size of the π -electron system had no appreciable effect on the C-Br bond dissociation energy. By analogy, we assume that the value of the A factor determined for ab-

straction from PD can be used for abstraction from NOD. That is, for reactions (2), (13), and (16), $\log_{10} = 5.9$. The recombination reactions were assumed to be diffusion-limited and their rates were estimated from the mixture's viscosity, as outlined in subsection 4.2.2. The diffusion-controlled rate values for the thermolysis of BPE + NOD + TE, as well as the concentration of each of the reactants, at reaction temperatures between 250 and 350°C, appear in Table 4.6.

Table 4.7 summarizes the model results vs. experimental data for the thermolysis of BPE + NOD + TE. Following the scheme discussed in subsection 4.2.2, a first estimate of k_6/k_7 could be obtained from the experimentally determined ratio of $[PD]/[PH]$. This rate ratio was determined to be 1.65. The experimental conversion of BPE was much larger than predicted by the model, and any amount of adjustment on k_6 would not remedy the disagreement. Instead, adjustment was made on the value of E_{a1} , the activation energy for BPE dissociation. By lowering E_{a1} to 47 kcal/mol, the predicted conversion of BPE became very close to the experimental value, as shown in the first section of Table 4.7. The adjustment of 3 kcal/mol in the activation energy was within reason, and certainly within the margin of ± 5 kcal/mol given by Schlosberg (4). Moreover, the agreement between model results and experimental values were so good that k_6 need not be further adjusted. The value k_6/k_7 was used for the rest of the calculations, with the results appearing in the second section of Table 4.7. The 'low conversion' results are also plotted in Figure 4.2, showing very good agreement between model predictions and experimental data. In contrast to the BB experiments, where the reaction time was at least 15 minutes, the BPE experiments involved reaction time of only 5 minutes, due to the higher reactivity of the ether bridge. Because the reactor heatup time was on the order

of 1 minute, decreasing the reaction time any further would render temperature history imprecise. Low conversions of BPE were thus achieved by lowering the reaction temperature while maintaining the reaction time constant at 5 minutes.

As described previously, the constancy of k_6/k_7 over temperature implies that $E_{a6} = E_{a7}$. Given $\log_{10} A_7 = 7.0$, $\log_{10} a_6$ can be calculated as 7.2. Thus for the reaction



we estimated $E_{a7} = 9 \text{ kcal/mol}$, and $\log_{10} A_7 = 7.2$. This reaction is thus only slightly faster than the abstraction from a hydrocarbon, in contrast to the finding by Mahoney & DaRooge (23), who reported that the abstraction from a phenol was much more rapid than from a hydrocarbon. This difference might be due to the difference in reaction temperatures. Mahoney & DaRooge carried out their reactions at 60°C. The difference between the chemistry of the donor solvents might become less significant at high temperatures, such as in this study.

Finally, the kinetic isotope effect was again ignored due to the high reaction temperatures.

4.4 Summary

Free-radical mechanisms were proposed to explain the thermolysis of model compound mixture containing ethylene and ether bridges. Rate parameters were determined for the abstraction of hydroxyl hydrogen atoms from phenol or naphthol by the benzyl and phenoxy radicals resulting from bridge dissociation. In the first set of experiments, 1,2-diphenyl ethane (BB) dissociated to

yield two benzyl radicals. The benzyl radical either abstracted a hydrogen atom from 1-methylnaphthalene (MN), generating another carbon-centered radical, or it abstracted a deuterium atom from phenol-OD (PD), generating a phenoxy radical. Computer modeling was used to analyze the experimental data and estimate abstraction rate parameters. The results revealed that the benzyl radical preferentially abstracted from MN over PD, the rate of abstraction from MN being roughly 13 times as fast as that from PD. This result is in reasonable accord with the fact that the benzyl radical is more stable than the phenoxy radical.

In the second set of experiments, benzyl phenyl ether (BPE) was employed to generate the benzyl radical and the phenoxy radical. The phenoxy radical then either abstracted hydrogen from 1,2,3,4-tetrahydronaphthalene (TE), generating a carbon-centered radical TE·, or it abstracted deuterium from naphthol-OD (NOD), generating another oxygen-centered radical, namely the naphthoxy radical (NO·). Computer modeling showed that the phenoxy radical preferentially abstracted from NOD over TE. Even though abstraction from NOD yielded NO·, which was more reactive than TE·, this effect was possibly offset by the more favorable hydrogen-bonding interaction between the phenoxy radical with the O-D group in NOD compared with the C-H group in TE (23). In other words, during the hydrogen (or deuterium) transfer process between the two oxygen-centered radicals, a transition-state complex was formed as follows:



The relative stability of this hydrogen-bonded complex resulted in a lower activation energy and thus abstraction from NOD became more competitive with abstraction from TE.

Yet another contradicting effect was the relative tightness of the activated complex in the oxygen-oxygen system vs. the oxygen-carbon system. Mahoney & DaRooge (23) reported that for the hydrogen atom transfer between peroxy radicals, the oxygen moieties were separated by a shorter distance than for the transfer between a peroxy radical and a hydrocarbon. These researchers claimed that the tightness of the oxygen-oxygen complex would result in a lower value of the preexponential factor in the Arrhenius expression compared with those observed in the oxygen-carbon system.

In the present case, the interplay between the relative reactivity of the naphthoxy radical, the stability of the hydrogen-bonded complex, and the tightness of this activated complex all contributed to the effective rate ratio for hydrogen abstraction by the phenoxy radical from NOD vs. TE of 1.65.

Having estimated the rates of hydrogen abstraction involving the phenoxy radicals, we shall next focus our attention on the recombination reactions associated with certain oxygen model compounds. The rate parameters calculated here will be applied to these new reaction systems to validate the free-radical mechanism by comparing with experimental data, and to determine termination rates. More importantly perhaps is the insight obtained from observing the tendency for a phenoxy radical to engage selectively in certain reactions. This insight will prove useful in formulating mechanistic pathways for radical interactions and predicting the subsequent products of recombination, as will be demonstrated in the next two chapters.

REFERENCES

- [1] Gavalas, G. R., 'Coal Pyrolysis,' Coal Science and Technology; 4, Elsevier Scientific Publishing Co., Amsterdam, The Netherlands, 1982
- [2] Allen, D. T. and Gavalas, G. R., *Int. J. Chem. Kinetics*, 1983, 15, 219
- [3] Miller, R. E. and Stein, S. E., *J. Phys. Chem.*, 1981, 85, 580
- [4] Schlosberg, R. H., Davis, Jr., W. H. and Ashe, T. R. *Fuel*, 1981, 60, 201
- [5] Benson, S. W., 'Thermochemical Kinetics: Methods for the Estimation of Thermochemical Data and Rate Parameters,' John Wiley & Sons, Inc., New York, Second Edition, 1976
- [6] Sato, Y., *Fuel*, 1979, 58, 318
- [7] Poutsma, M. L., *Fuel*, 1980, 59, 335
- [8] Ingold, K. U., 'Rate Constants for Free Radical Reactions in Solutions,' Chapter 2, National Research Council of Canada, Ottawa, Canada
- [9] Letsou, A. and Steil, L. I., *A. I. Ch. E. J.*, 1973, 19, 409
- [10] Prausnitz, J. M. and Gunn, R. D., *A. I. Ch. E. J.*, 1958, 4, 430, 494
- [11] Joffe, J., *Ind. Eng. Chem. Fundam.*, 1971, 10, 532
- [12] Reid, R. C., Prausnitz, J. M. and Sherwood, T. K., 'The Properties of Gases and Liquids,' McGraw-Hill Book Company, New York, Third Edition, 1977
- [13] Lydersen, A. L., 'Estimation of Critical Properties of Organic Compounds,' *Univ. Wisconsin Col. Eng. Exp. Stn., Rep. 3*, Madison, Wisconsin, April 1955
- [14] Gunn, R. D. and Yamada, T., *A. I. Ch. E. J.*, 1971, 17, 131
- [15] Lawry, T. H. and Richardson, K. S., 'Mechanism and Theory in Organic Chemistry,' Harper & Row, Publishers, Inc., New York, 1976

- [16] Johnston, H. S. and Parr, C., *J. Am. Chem. Soc.*, 1963, **85**, 2544
- [17] Johnston, H. S., 'Gas Phase Reaction Rate Theory,' The Ronald Press Company, New York, 1966
- [18] Arthur, N. L. and McDonell, J. A., *J. Chem. Phys.*, 1972, **56**(6), 3100
- [19] Schlosberg, R. H., Szajowski, P. F., Dupre, G. D., Danik, J. A., Kurs, A., Ashe, T. R. and Olmstead, W. N., *Fuel*, 1983, **62**, 690
- [20] Kamiya, Y., Yao, T. and Oikawa, S., *Am. Chem. Soc., Div. Fuel Chem. Preprints*, 1979, **24**(2), 116
- [21] Ladacki, M. and Szwarc, M., *J. Chem. Phys.*, 1952, **20**, 1814
- [22] Mahoney, L. R. and DaRooge, M. A., *J. Am. Chem. Soc.*, 1975, **97**, 4722

FIGURE 4.1
 MODEL RESULTS VS. EXPERIMENTAL DATA
 THERMOLYSIS OF BB + PD + MN, 1 HOUR

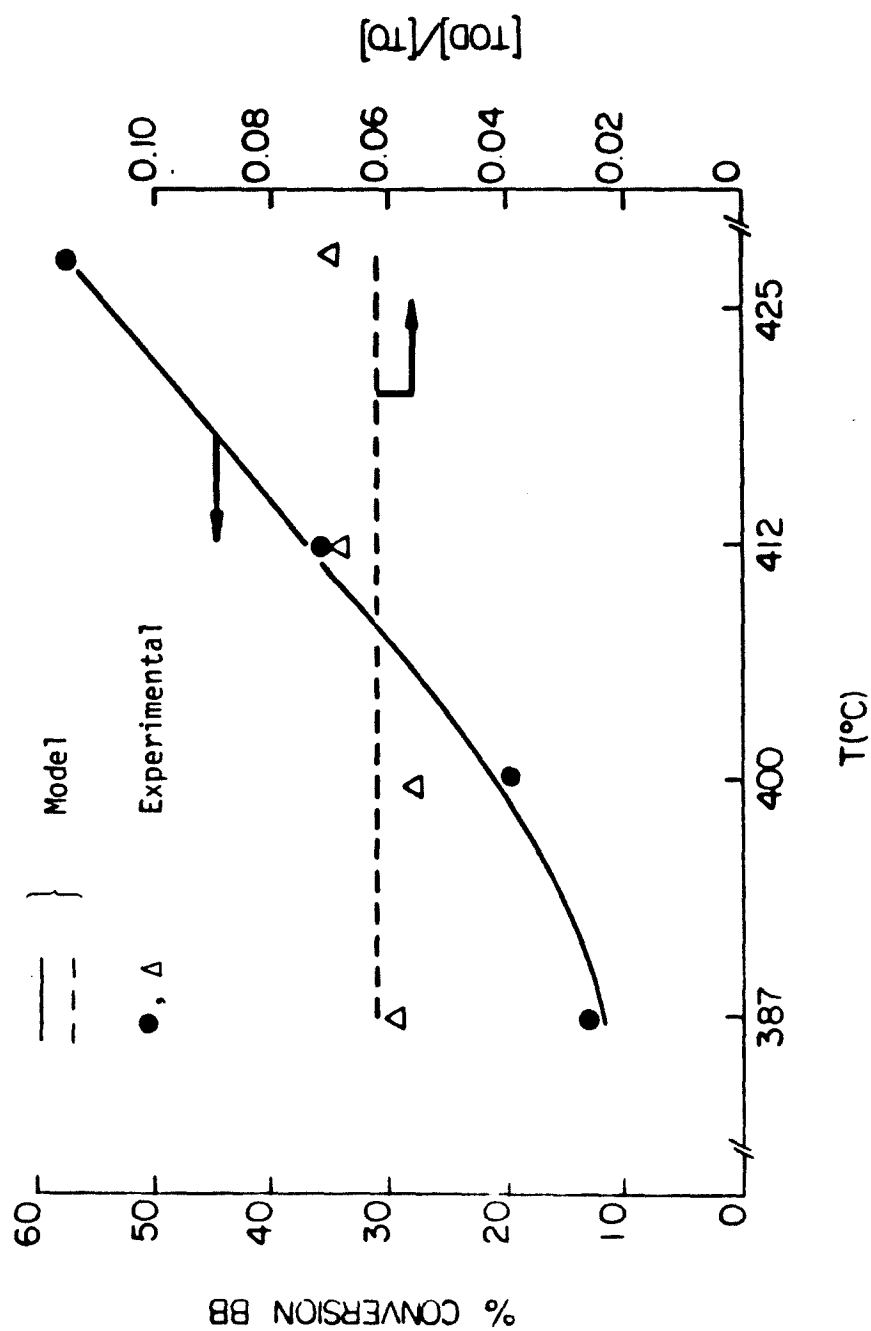


FIGURE 4.2
 MODEL RESULTS VS. EXPERIMENTAL DATA
 THERMOLYSIS OF BPE + NOD + TE, 5 MINUTES

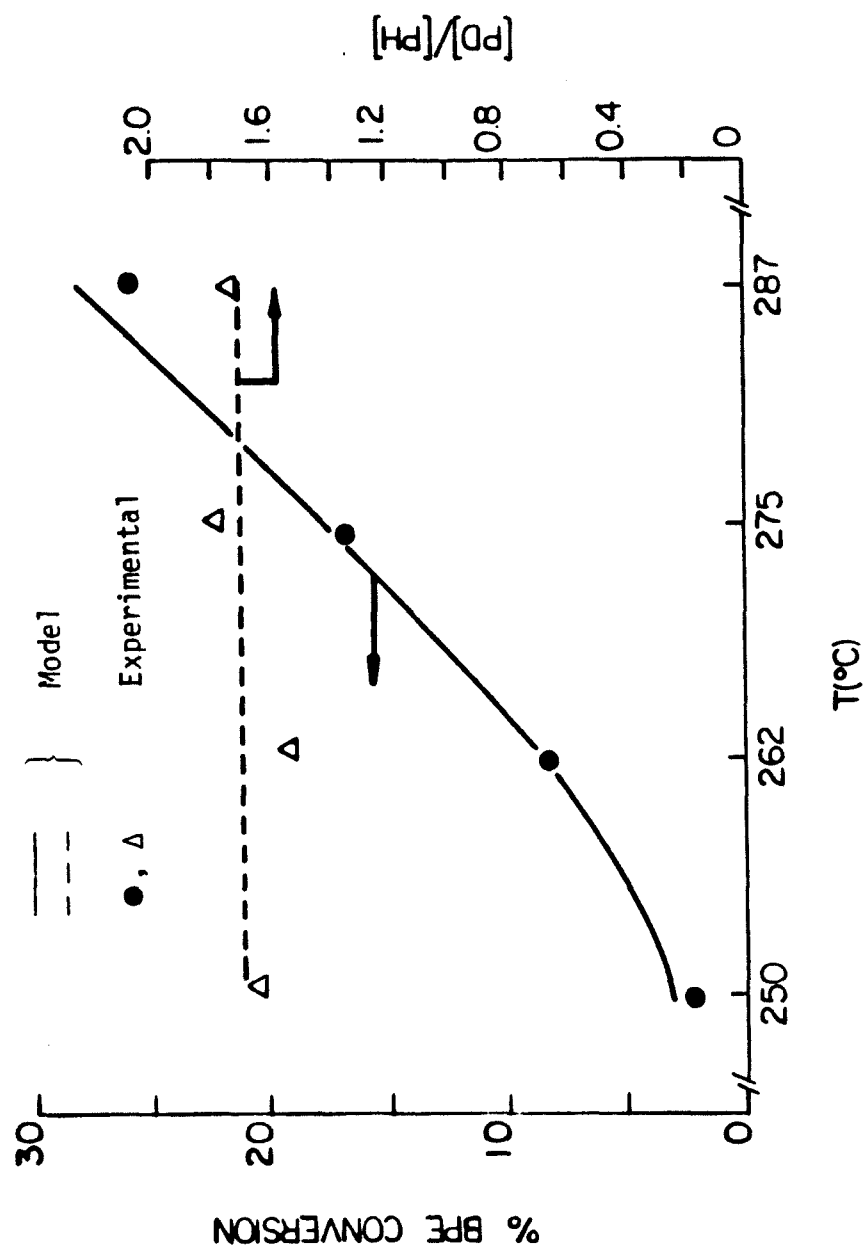
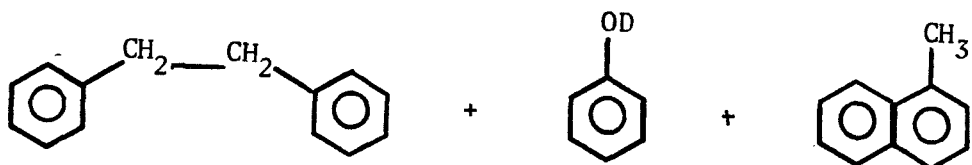


TABLE 4.1

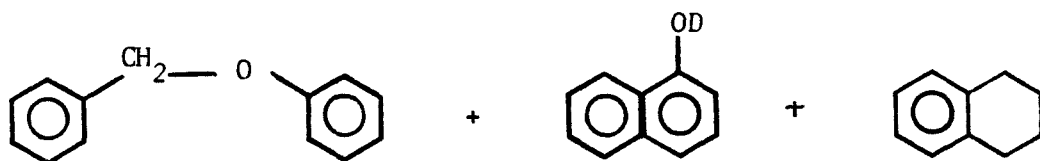
REACTANT MIXTURES FOR THE HYDROGEN ABSTRACTION EXPERIMENTS

1



Mole Ratio: 1:4:4
Temperature: 387-425°C
Reaction Time: 15-60 minutes

2



Mole Ratio: 1:4:4
Temperature: 250-350°C
Reaction Time: 5-10 minutes

TABLE 4.2

THERMOLYSIS MECHANISM FOR BB + PD + MN

NO.	REACTION	$\log_{10} A^a$	E^b
INITIATION			
1	BB \longrightarrow TO \cdot + TO \cdot	15.9	63.0
PROPAGATION			
2	TO \cdot + PD \longrightarrow TOD + PH \cdot	5.89	9.0
3	TO \cdot + MN \longrightarrow TO + MN \cdot	7.0	9.0
4	TO \cdot + BB \longrightarrow TO + BB \cdot	7.0	9.0
5	PH \cdot + TO \longrightarrow PH + TO \cdot	7.0	9.0
6	PH \cdot + MN \longrightarrow PH + MN \cdot	7.0	9.0
7	PH \cdot + BB \longrightarrow PH + BB \cdot	7.0	9.0
8	MN \cdot + TO \longrightarrow MN + TO \cdot	7.0	9.0
9	MN \cdot + PD \longrightarrow MN + PH \cdot	5.89	9.0
10	MN \cdot + BB \longrightarrow MN + BB \cdot	7.0	9.0
11	BB \cdot + TO \longrightarrow BB + TO \cdot	7.0	12.5
12	BB \cdot + PD \longrightarrow BB + PH \cdot	5.89	12.5
13	BB \cdot + MN \longrightarrow BB + MN \cdot	7.0	12.5
TERMINATION			
14	TO \cdot + TO \cdot \longrightarrow BB		0
15	TO \cdot + PH \cdot \longrightarrow P2		0
16	TO \cdot + MN \cdot \longrightarrow P3		0
17	TO \cdot + BB \cdot \longrightarrow P4		0
18	PH \cdot + PH \cdot \longrightarrow P5		0
19	PH \cdot + MN \cdot \longrightarrow P6		0
20	PH \cdot + BB \cdot \longrightarrow P7		0
21	MN \cdot + MN \cdot \longrightarrow P8		0
22	MN \cdot + BB \cdot \longrightarrow P9		0
23	BB \cdot + BB \cdot \longrightarrow P10		0

TABLE 4.2 (cont'd)

DEFINITION OF SYMBOLS

BB	=	bibenzyl	BB.	=	bibenzyl radical
PD	=	phenol-OD	PH.	=	phenoxy radical
PH	=	phenol-OH			
MN	=	1-methylnaphthalene	MN.	=	methylnaphthalene radical
TO	=	toluene	TO.	=	benzyl radical
TOD	=	deuterated toluene			
P2 - P10	=	recombination products			

^a Units of sec^{-1} for reaction 1
 $\text{mol}^{-1}\text{sec}^{-1}$ for all other reactions

^b Activation energy in kcal/mol

TABLE 4.3

THERMOLYSIS OF BB + PD + MN

 k_{diff} and Reactant Concentrations as a Function of Temperature

Temperature (°C)	$k_{\text{diff}} \times 10^{-8}$ ($\text{M}^{-1} \text{sec}^{-1}$)	Concentration (moles L^{-1})	
		BB	PD = MN
375	1.187	0.619	2.476
387	1.321	0.604	2.414
400	1.495	0.581	2.323
412	1.678	0.561	2.242
425	1.917	0.534	2.136
437	2.173	0.506	2.023
450	2.508	0.463	1.853

TABLE 4.4

MODEL RESULTS VS. EXPERIMENTAL DATA
THERMOLYSIS OF BB + PD + MN

$\frac{k_2}{k_3}$	Temp. (°C)	Time (min)	% BB Conversion Model	% BB Conversion Exptl	(TOD)/(TO) Model	(TOD)/(TO) Exptl	Comment
0.068 (1st approx.) 0.073 0.075 0.077	425	60	52.6	57.2	0.054	0.061	Iteration on k_2
			55.4		0.059		
			56.6		0.060		
			57.4		0.061		
0.077	425 412 400 387	60	57.4	57.2	0.061	0.061	Fixed Residence Time (Fig. 4.1)
			35.3	33.7	0.061	0.065	
			20.8	19.3	0.061	0.056	
			11.2	12.7	0.060	0.059	
0.077	425 412 400 387	10 15 60 60	19.1	17.9	0.061	0.060	Low BB Conversion
			12.8	10.4	0.061	0.063	
			20.8	19.3	0.061	0.056	
			11.2	12.7	0.060	0.059	

TABLE 4.5

THERMOLYSIS MECHANISM FOR BPE + NOD + TE

NO.	REACTION	$\log_{10} A$	E
INITIATION			
1	BPE \longrightarrow TO• + PH•	16.0	47.0
PROPAGATION			
2	TO• + NOD \longrightarrow TOD + NO•	5.89	9.0
3	TO• + TE \longrightarrow TO + TE•	7.0	9.0
4	TO• + BPE \longrightarrow TO + BPE•	7.0	9.0
5	PH• + TO \longrightarrow PH + TO•	7.0	9.0
6	PH• + NOD \longrightarrow PH + NO•	7.22	9.0
7	PH• + TE \longrightarrow PH + TE•	7.0	9.0
8	PH• + BPE \longrightarrow PH + BPE•	7.0	9.0
9	NO• + TO \longrightarrow NOH + TO•	7.0	9.0
10	NO• + TE \longrightarrow NOH + TE•	7.0	9.0
11	NO• + BPE \longrightarrow NOH + BPE•	7.0	9.0
12	TE• + TO \longrightarrow TE + TO•	7.0	9.0
13	TE• + NOD \longrightarrow TED + NO•	5.89	9.0
14	TE• + BPE \longrightarrow TE + BPE•	7.0	9.0
15	BPE• + TO \longrightarrow BPE + TO•	7.0	9.0
16	BPE• + NOD \longrightarrow BPED + NO•	5.89	9.0
17	BPE• + TE \longrightarrow BPE + TE•	7.0	9.0

TABLE 4.5 (cont.)

NO.	REACTION	$\log_{10} A$	E
RECOMBINATION			
18	TO• + TO• \longrightarrow BB		0
19	TO• + PH• \longrightarrow BPE		0
20	TO• + NO• \longrightarrow P1		0
21	TO• + TE• \longrightarrow P2		0
22	TO• + BPE• \longrightarrow P3		0
23	PH• + PH• \longrightarrow P4		0
24	PH• + NO• \longrightarrow P5		0
25	PH• + TE• \longrightarrow P6		0
26	PH• + BPE• \longrightarrow P7		0
27	NO• + NO• \longrightarrow P8		0
28	NO• + TE• \longrightarrow P9		0
29	NO• + BPE• \longrightarrow P10		0
30	TE• + TE• \longrightarrow P11		0
31	TE• + BPE• \longrightarrow P12		0
32	BPE• + BPE• \longrightarrow P13		0

TABLE 4.5 (cont'd)

DEFINITION OF SYMBOLS

BPE = benzyl phenyl ether

NOD = naphthol-OD

NO \cdot = naphthoxy radical

NOH = naphthol-OH

TE = tetralin

P1 - p13 = recombination products

TABLE 4.6

THERMOLYSIS OF BPE + NOD + TE

 k_{diff} and Reactant Concentrations as a Function of Temperature

Temperature (°C)	$k_{\text{diff}} \times 10^{-7}$ ($\text{M}^{-1} \text{sec}^{-1}$)	Concentration (moles L^{-1})	
		BPE	NOD + TE
250	4.353	0.739	2.955
262	4.735	0.719	2.875
275	5.195	0.700	2.798
287	5.669	0.682	2.730
300	6.243	0.664	2.657
312	6.838	0.649	2.595
325	7.565	0.632	2.528
337	8.324	0.617	2.470
350	9.259	0.602	2.408

TABLE 4.7

MODEL RESULTS VS. EXPERIMENTAL DATA
THERMOLYSIS OF BPE + NOD + TE

E_{a1} (kcal/mol)	$\frac{k_6}{k_7}$	Temp. (°C)	Time (min)	% BPE Conversion		(PD/PH)		Comment
				Model	Exptl	Model	Exptl	
50 49 48 47	1.65	350	10	49.8 64.7 76.3 88.5	87.2			Iteration on E_{a1}
47	1.65	325 300	5	57.4 36.1	56.0 33.5			
47	1.65	287 275 262 250	5	27.9 17.5 7.6 2.9	26.1 17.0 7.5 2.4	1.72 1.69 1.67 1.67	1.71 1.78 1.53 1.62	

} Low
BPE
Conversion
(Fig. 4.2)

CHAPTER 5

RECOMBINATION EXPERIMENTS

PART I. REACTIONS OF BENZYL PHENYL ETHER

5.1 Introduction

The object of the recombination experiments was to identify the structures of the major products of recombination involving the phenoxy free radicals. Mechanistic pathways were then proposed to account for formation of these products. The proposed mechanisms were next incorporated into a computer model to determine free radical activities. Finally, the model predictions of product concentrations were compared with the experimental data to check the validity of the kinetic mechanisms. This chapter examines the recombination reactions of the phenoxy radical ($\phi - O\cdot$), which was generated from thermal dissociation of benzyl phenyl ether (BPE). Table 5.1 shows the two model-compound mixtures employed for this purpose. The first set of experiments utilized mixtures of BPE and toluene to study the recombination reactions involving the phenoxy radical and the benzyl radical ($\phi - CH_2\cdot$). In the second set of experiments, where BPE and phenol were the reactants, the emphasis was on the interactions of the phenoxy radicals with one another. The recombination rates were once again assumed to be diffusion-limited. The hydrogen-abstraction reactions involving the phenoxy radical have already been studied in Chapter 4. The previously determined rate parameters were now used in the proposed mechanisms. As in Chapter 4, the model compounds were chosen to minimize the

the number of free radicals. The model compounds chosen were also the simplest structures that contained all the essential features under study, in order to reduce the complexity of the subsequent recombination products.

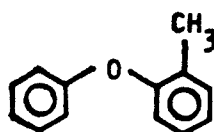
It is essential to emphasize the importance of the ability to 'extrapolate' in model compound studies. For example, the rate parameters for the BPE + 1-naphthol-OD + tetralin system, determined in Chapter 4, can be applied to different reaction mixtures, namely the BPE + toluene and BPE + phenol systems in this chapter. It will next be shown that, as the results of the BPE + toluene mixture are informative for the BPE + phenol system, so will the overall results of the BPE system be useful for the naphthol system, which will be discussed in Chapter 6. The ability to predict the results of one reaction system from another, simpler system will eventually provide the ultimate link between the model compound system and the actual coal-related materials.

5.2 Thermolysis of Benzyl Phenyl Ether + Toluene

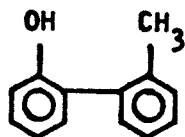
The major radicals in this experimental system were the benzyl radical ($\text{TO}\cdot$) and the phenoxy radical ($\text{PH}\cdot$). Therefore, there existed three possibilities for their recombinations: $\text{TO}\cdot + \text{TO}\cdot$, $\text{PH}\cdot + \text{PH}\cdot$, and $\text{TO}\cdot + \text{PH}\cdot$. In the first instance, several studies (1, 2, 3, 4) have shown that the most predominant product of recombination of two benzyl radicals was bibenzyl (BB). Moreover, it was the $\text{PH}\cdot$ radical, not the $\text{TO}\cdot$ radical, that was of immediate interest. Thus bibenzyl was assumed to be the only product of $\text{TO}\cdot + \text{PH}\cdot$ radical recombination in the modeling section. In the second instance, it turned out that the concentration of the $\text{PH}\cdot$ radical at any given time was very small. The

probability of two $\text{PH}\cdot$ radicals colliding was negligible, as evidenced by the fact that no products of appreciable quantity consisted of two phenoxy groups (as shown by GCMS). Phenol was the major phenolic product. Due to the extreme reactivity of the phenoxy radical, it rapidly abstracted a hydrogen atom from any available source to form phenol. In fact, the absence of $\text{PH}\cdot + \text{PH}\cdot$ products prompted the study of the $\text{BPE} + \text{phenol}$ system, which will be the subject of the following section, section 5.3.

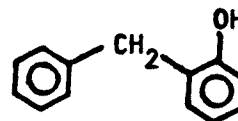
The third instance, where $\text{TO}\cdot$ and $\text{PH}\cdot$ collided to form a product, was therefore of immediate interest. The three possible structures of the resulting product were:



(I)



(II)



(III)

Section 5.2.1 will describe how one of these structures was determined to be the actual product of $\text{TO}\cdot + \text{PH}\cdot$ recombination.

Another major product of recombination resulted from the collision of the radicals $\text{TO}\cdot$ and $\text{BB}\cdot$. The abundance of $\text{BB}\cdot$ was a direct result of the abundance of the $\text{TO}\cdot$ radicals. The predominant product of $\text{TO}\cdot + \text{TO}\cdot$ recombination was bibenzyl, which subsequently acted as a very good hydrogen donor because the resulting $\text{BB}\cdot$ radical was relatively more stable than $\text{TO}\cdot$, and certainly much more stable than $\text{PH}\cdot$. Again, section 5.2.1 will describe the analytical procedures utilized to identify the actual structure of the $\text{TO}\cdot + \text{BB}\cdot$ recombination products.

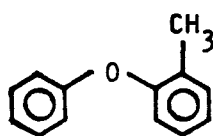
5.2.1 Product Identification

Figure 5.1 illustrates an HPLC chromatogram of the entire products of the thermolysis of a 1:4 molar mixture of BPE + toluene at 325°C, 10 minutes. The major peaks have been labeled 1 through 7, in order of elution time. The small clumps of peaks that eluted much later represent the high-molecular-weight products. These compounds were probably secondary recombination products, that is, compounds resulting from further, extensive reactions of the initial products of recombination. In any case, the total concentration of these products was roughly 10 to 15 percent of total product. From Figure 5.1, there were at least ten such compounds, so that each compound was present in a very small quantity and will be ignored in this study. Focus shall be on the first set of products, or the 'primary' recombination products.

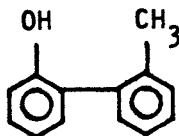
The identities of the two reactants and the most abundant known products were revealed by 'spiking' with authentic samples, as described in Chapter 3. By this method, peaks 1, 3, 4, and 5 were shown to correspond to phenol, toluene, BPE, and bibenzyl, respectively. The entire products were next subjected to chemical separation (Chapter 3). Figure 5.2 compares chromatograms of the phenolic and the neutral fractions to that of the entire products. Besides fraction 1, which was phenol, the only other major phenolic fraction is peak number 2. The rest of the major peaks evidently corresponded to neutral compounds. The three unknown products, corresponding to peaks 2, 6, and 7, were each collected using the liquid chromatograph in the preparative mode (Chapter 3). Each fraction was submitted for GCMS and NMR analysis.

Let us first look at Fraction 2. GCMS of this phenolic fraction indicated a mass of 184 for the parent ion (Figure 5.3). This mass agreed with a product of

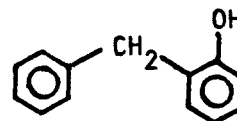
TO· + PH· recombination. Of course, one product was the formation of BPE in a reverse of the dissociation reaction. Fraction 2, however, must correspond to some other product because its elution time was different from that of BPE. The three potential chemical structures of this compound are again shown below:



(i)

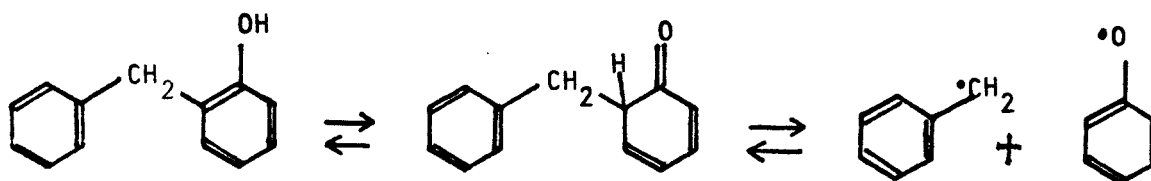


(ii)



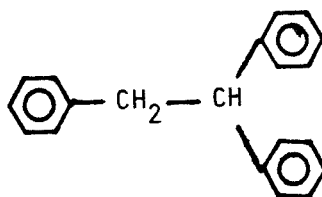
(iii)

Structure (i) was immediately ruled out because it was not phenolic. Proton NMR (Figure 5.4) yielded two singlets, one at 3.9 ppm and one at 5.2 ppm, with integration ratio of roughly 2:1. The singlet at 5.2 ppm corresponded to the hydroxyl proton and the one at 3.9 ppm represented the aliphatic protons. This signal was shifted due to the proximity to a benzene ring. The magnitude of the shift would suggest two benzene rings neighboring these aliphatic protons, thus favoring structure (iii) over structure (ii). A very useful piece of information was the experimental observation that the concentration of fraction 2 decreased as temperature increased, as shown in Figure 5.9 (this figure will be described in more detail presently). Structure (ii) would be stable at the relatively low temperatures studied, the phenyl-phenyl bond dissociation energy being on the order of 90 kcal/mol (5). At first glance, structure (iii) would also appear to be stable, the theoretical bond dissociation energy for the methylene bridge being 86 kcal/mol (5). A closer look, however, revealed that structure (iii) was susceptible to a keto-enol tautomerization, as schematically illustrated below:

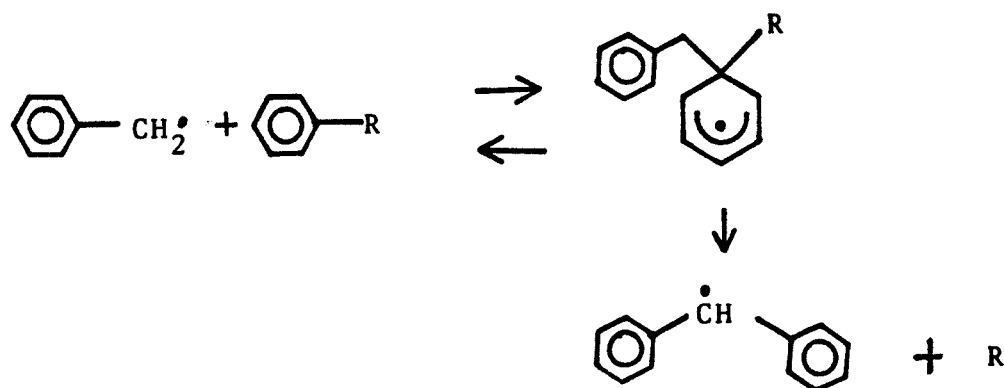


The isomerization reduced the effective bond dissociation energy to about 45 kcal/mol, as experimentally observed by McMillen *et al.* (5). Moreover, only the ortho and para isomers would undergo this type of tautomerization. With all the supporting evidence, it was concluded therefore that fraction 2 was either o-benzyl phenol or p-benzyl phenol (BPH). Structure (iii) represents the ortho isomer.

Fraction 6 was determined by GCMS to have a mass of 258 (Figure 5.5). Proton NMR indicated a singlet at 3.4 ppm and a doublet at 4.3 ppm, with integration ratio of roughly 2:1 (Figure 5.6). The following structure is proposed:



The two groups of aliphatic protons would be shifted and split in agreement with the NMR results. The formation of this molecule was somewhat more complicated. Schlosberg (1) proposed the homolytic aromatic substitution reaction that resulted in formation of the biphenyl methyl radical:

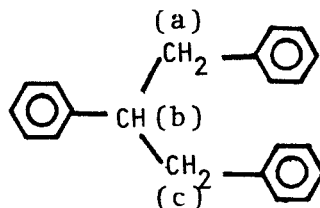


In our case, $\text{R} \equiv \text{CH}_3 - \text{CH}_2 - \phi$ and $\phi\text{-R} \equiv$ bibenzyl. The biphenyl methyl radical could then recombine with the benzyl radical to form structure F6. With the molecular structure in accord with analytical data and with all pathways of formation accounted for, peak 6 was thus assigned the structure F6, or 1,1,2-triphenyl ethane (TPE).

Of course, in addition to recombining to form structure F6, the biphenyl methyl radical could also abstract hydrogen to form biphenyl methane ($\phi\text{-CH}_2\text{-}\phi$). This product was actually found in the chromatogram (as identified by its mass through GCMS). In the HPLC chromatogram of the reaction products (Figure 5.1), it occurred just on the left shoulder of the BPE peak (peak 4). As Figure 5.1 shows, biphenyl methane, and thus TPE, were present only in small amounts. Determination of their concentrations via integration data was therefore inaccurate. This coupled with the fact that TPE was a secondary product containing no phenoxy group, which was our prime interest, justified omission of TPE from our mechanistic model. The omission of TPE eliminated at least two free radicals from the mechanism, significantly reduced the number of elementary reactions and simplified the kinetic model.

Finally, fraction 7 was found to have a mass of 272 (Figure 5.7). The proton

NMR shows two similar multiplets centered at about 2.9 ppm, and one multiplet at 3.2 ppm. The integration ratio of the three multiplets was about 2:2:1 (Figure 5.8). The following molecular structure was proposed:



The protons (a) and (b) are similar, but not identical, so that both are split differently and both shift differently, due to the proximity to the benzene rings. The proton (c) is split by both (a) and (b), and is also shifted by the benzene ring. Thus structure F7 is consistent with both the GCMS and NMR results. Fraction F7 would be easily formed from collision between the $\text{BB}\cdot$ radical and the $\text{TO}\cdot$ radical. The larger concentration of this fraction evidently follows from the abundance of both $\text{BB}\cdot$ and $\text{TO}\cdot$. Consequently, it was concluded that peak 7 in the chromatogram of the products of the reaction $\text{BPE} + \text{TO}$ corresponded to structure F7, or 1,2,3-triphenyl propane (TPP).

In summary, peaks 1, 6, and 7 in Figure 5.1 have been identified as benzyl phenol (BPH), 1,1,2-triphenyl ethane (TPE), and 1,2,3-triphenyl propane (TPP). Another secondary product, biphenyl methane, was also detected. TPE and biphenyl methane, however, were present in very small concentrations that did not warrant their inclusion in the kinetic model. It was considered sufficient to have identified TPE and BP as minor products of $\text{BPE} + \text{toluene}$ thermolysis. The validity of the free-radical model will be satisfactorily demonstrated by its ability to match the concentrations of bibenzyl, BPH, and TPP with

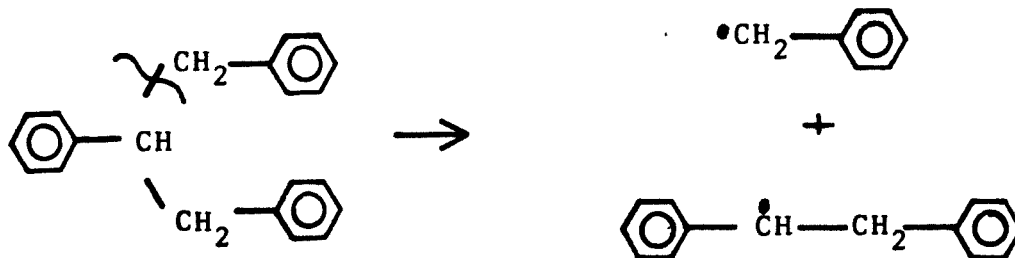
experimental data. This will be the topic of the next section.

5.2.2 Kinetic Modeling

The mechanism illustrated in Table 5.2 was employed in modeling the BPE + toluene system. There are four initiation reactions: the dissociation of the ether bridge in BPE, the dissociation of the methylene bridge in BPH, and the dissociations of the ethylene bridges in bibenzyl and TPP. Even though BPH, bibenzyl, and TPP were secondary recombination products, the incorporation of their dissociation reactions into the overall mechanistic model is necessary due to the low activation energies of the dissociation reactions. The propagation reactions include the abstraction by the $\text{TO}\cdot$, $\text{PH}\cdot$, $\text{BPE}\cdot$, and $\text{BB}\cdot$ radicals from toluene, phenol, BPE, and bibenzyl. The recombination reactions consist of the bimolecular collisions between the radicals $\text{TO}\cdot$, $\text{PH}\cdot$, $\text{BPE}\cdot$, and $\text{BB}\cdot$. As mentioned above, collision between two benzyl radicals was assumed to produce only bibenzyl, as represented by reaction (15) (see Table 5.2). Reaction (16) illustrates the formation of BPH by recombination of $\text{TO}\cdot$ and $\text{PH}\cdot$. The formation of TPP from collision of $\text{TO}\cdot$ and $\text{BB}\cdot$ is represented by reaction (18). The remainder of the products of recombination are simply labeled P1 through P7. Note that, as discussed in section 5.2.1, reactions leading to the formation of biphenyl and 1,1,2-triphenyl ethane (TPE) have been omitted from this mechanism. This resulted in considerable reduction in the total number of elementary reactions while little accuracy in model results was sacrificed.

Except for BPH and TPP dissociation, most of the initiation and propagation reactions in this mechanism have already been previously encountered. For these reactions, the appropriate rate parameters have simply been taken

directly from Chapter 4. In the dissociation of the methylene bridge in BPH, the effective bond dissociation energy was taken to be 45 kcal/mol, as reported by McMillen (5). In the case of TPP, the dissociation was assumed to yield the benzyl radical and the bibenzyl radical, as represented schematically below:



Thermochemical methods (6) showed that the activation energy for this cleavage was roughly 3 kcal/mol lower than that for the ethylene bridge dissociation in bibenzyl. This result made intuitive sense because the bibenzyl (secondary) radical should be more stable than the benzyl (primary) radical. By analogy (7, 8, 9), then, the rate parameters for the dissociation of TPP was taken to be $E_a = 60$ kcal/mol and $\log_{10} A = 15.9$. The diffusion-controlled rates of recombination were estimated from the viscosity of the mixture using the Stokes-Einstein equation, as described by Ingold (10). The concentrations of BPE and toluene at various reaction temperatures were calculated from the critical properties of the mixture using the method of Gunn & Yamada (11). Both sets of calculations were outlined in section 4.2.2. The necessary physical constants appear in Reid *et al.* (12).

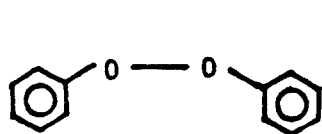
The model successfully predicted the conversions of BPE and toluene over the temperature range 300 - 375°C, as shown in Table 5.3. The good agreement between model results and experimental data on the yields of BPH, bibenzyl, and TPP is illustrated in Figure 5.9. The steady decrease in BPH concentra-

tion with increasing temperature was correctly predicted by the model because the effective bond dissociation energy for the methylene bridge cleavage of 45 kcal/mol, rather than the theoretical value of 86 kcal/mol, was incorporated into the mechanism. The concentrations of bibenzyl and TPP first increased with temperature, then gradually decreased as the temperature exceeded 350°C. This decline was attributed to further dissociation of bibenzyl and TPP. Reactions (3) and (4) (see Table 5.2) accounted for their dissociation, and allowed the model to produce parallel results with experimental values (Figure 5.9). The radicals generated from breakup of bibenzyl and TPP underwent still further recombination reactions, eventually forming larger and more complex molecules at long reaction times. In fact, the concentrations of products heavier than TPP increased steadily with temperature. These products were equivalent to the undesirable tar residues in coal liquefaction. Their structures and mechanistic pathways of formation, however, lie outside the scope of this work.

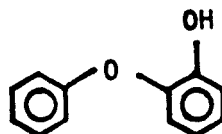
In summary, the thermolysis of BPE + toluene were carried out at 300 - 375°C for 15 minutes and the products were identified to be phenol, benzyl phenol, bibenzyl, TPP, and smaller amounts of biphenyl and TPE. Compounds larger than TPP accounted for about 10 - 15 percent of the total products. They were, however, not considered in this work. A computer model, incorporating the dissociation rates for benzyl phenol, bibenzyl, and TPP, correctly predicted the experimental results on the conversions of BPE and toluene and the yields of BPH, bibenzyl, and TPP, as illustrated graphically in Figure 5.9.

5.3 Thermolysis of Benzyl Phenyl Ether + Phenol

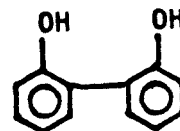
In the previous section, the recombination products derived from two benzyl radicals or from a benzyl and a phenoxy radical. The transient concentration of the phenoxy radical was too small to permit collision of two such radicals with one another. To investigate the recombination reactions among phenoxy radicals, phenol was utilized instead of toluene as a reactant, so that hydrogen abstraction from phenol would yield $\text{PH}\cdot$, increasing the concentration of this radical. The product of recombination had one of the following structures:



(i)



(ii)



(iii)

which will be identified presently.

Since dissociation of BPE gave the benzyl radical as well as the phenoxy radical, products containing the benzyl group were also present in this system, such as benzyl phenol and bibenzyl. Secondary products resulting from the $\text{BB}\cdot$ radical, however, would exist in small amounts due to the low concentration of bibenzyl. Therefore, 1,2,3-triphenyl propane (TPP), and certainly 1,1,2-triphenyl ethane (TPE), two secondary products identified in the previous system, would not be major products of this reaction. This presents no problem in any case, because these products did not contain the phenoxy radical, and thus would not be pertinent to this study. Note that in order to boost the phenoxy radical concentration, a reactant mixture have been selected in which

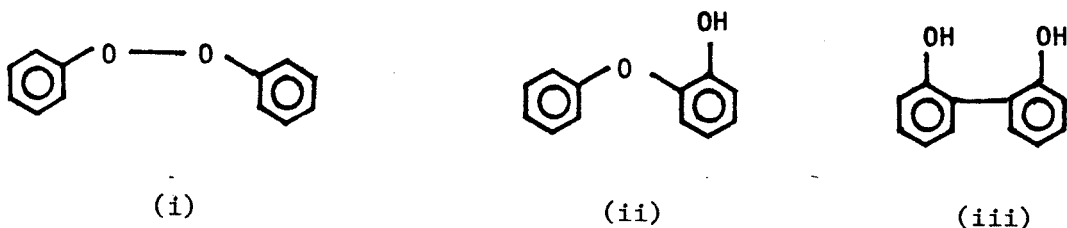
there are no good hydrogen donors. The result was larger concentrations of free-radicals that could not easily abstract hydrogen and eventually recombine to form heavy, undesirable products. Attention will only be focussed on the few primary products that will reveal the behavior of the phenoxy radical.

5.3.1 Product Identification

Figure 5.10 shows an HPLC chromatogram of the entire products of thermolysis of a 1:2 molar mixture of BPE + phenol. The major peaks were labeled 1 through 6, in order of elution time. Note that this chromatogram was run at a lower flow rate and lower initial ratio of acetonitrile to water than in the case of the BPE + toluene system. The early peaks were therefore separated farther apart from one another than those in Figure 5.1. In this manner, attention could be paid to the phenolic compounds, which eluted early in the chromatogram. A large fraction of the product mixture, up to 30 percent, contained compounds of higher molecular weights than bibenzyl, but they were also outside the scope of this study.

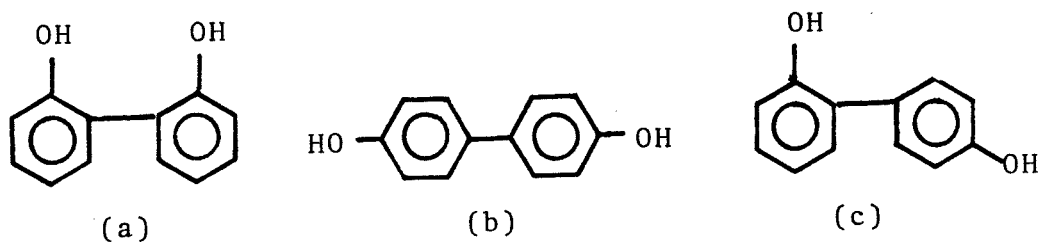
By 'spiking' the product mixture with authentic samples, peaks 2, 4, 5, and 6 were identified as phenol, toluene, BPE, and bibenzyl, respectively. Chemical separation (see Figure 5.10 a, b, c) indicated that peaks 1, 2, and 3 were phenolic, while the rest of the compounds of interest were neutral. The unknown products corresponding to peaks 1 and 3 were fractionated by the liquid chromatograph. Each fraction was purified and then subjected to GCMS and NMR analysis.

GCMS of fraction 1 revealed a mass of 186 for the parent ion (Figure 5.11), suggesting a product of $\text{PH}\cdot + \text{PH}\cdot$ recombination. The possible chemical structures of this compounds are:



The oxygen-oxygen bridge is known to be extremely weak. Under the reaction conditions studied, this bond would break as soon as it was formed. Structure (i) was thus eliminated from consideration. The proton NMR of fraction 1 (Figure 5.12) indicated that the integration ratio of aromatic protons to hydroxyl protons was roughly 4:1. This evidence pointed to structure (iii) as the appropriate molecular structure. Structure (iii), or biphenol, was also a more logical choice than structure (ii) on the grounds that this compound eluted very early in the HPLC, indicating very strong polarity (13).

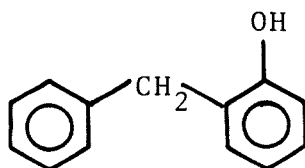
The configuration of biphenol was further identified by the use of Carbon-13 NMR. Figure 5.13 illustrates that there are six different types of carbon atoms in this molecule. Consider the following possibilities:



Configuration (a) is the only one with six different types of carbons. In structure (b), due to the extreme symmetry, only four different signals should have been observed. On the contrary, a nonsymmetric molecule such as (c)

would result in 12 signals because all carbons are different. Thus Fraction 1 was clearly 1,1-biphenol, or structure (a).

Fraction 3 was determined by GCMS to have a mass of 184. Proton NMR yielded a singlet that was shifted to 3.9 ppm, indicating two neighboring benzene rings. The concentration of fraction 3 decreased with rising temperature, as shown in Figure 5.14. This information was identical to that described in section 3.2, and the corresponding molecule would be benzyl phenol:



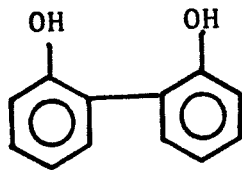
In fact, the process of identification proceeded much faster in this instance. Given the existence of both $\text{TO}\cdot$ and $\text{PH}\cdot$, previous experience already suggested that benzyl phenol would be one of the recombination products. Experience also dictated the particular range of mass numbers in the GCMS to investigate. Finally, temperature dependence among the reaction products was quickly detected. Insight from one model compound system was demonstrated here again to help simplify work in a different mixture of compounds.

Now that peak 1 has been identified as biphenol and peak 3 as benzyl phenol, the next step is to model this reaction system. The validity of the proposed free-radical mechanism will be based upon the success of the model in matching the concentrations of biphenol and benzylphenol with experimental results. Even though heavier products accounted for as much as 30 percent of the total reaction products due to the absence of a good hydrogen donor in the

reactant mixture, they will be ignored in modeling so that attention can be paid to the products of recombination of the phenoxy radicals, which is the heart of this particular reaction system.

5.3.2 Kinetic Modeling

Table 5.4 shows the free-radical mechanism designed to account for thermolysis of BPE + phenol. This mechanism is virtually identical to the one for the BPE + toluene system (Table 5.2), with the exception that the dissociation reaction of TPP has been omitted due to its low concentration. Thus there are three initiation reactions, those of BPE, BPH, and bibenzyl. The propagation reactions include the abstraction by the $\text{TO}\cdot$, $\text{PH}\cdot$, $\text{BPE}\cdot$, and $\text{BB}\cdot$ radicals from toluene, phenol, BPE, and bibenzyl. The recombination reactions consist of the interactions between the above four radicals. Reaction (16) represents the formation of bibenzyl from two benzyl radicals, while reaction (17) accounts for the formation of BPH from $\text{TO}\cdot$ and $\text{PH}\cdot$ recombination. Collision between $\text{TO}\cdot$ and $\text{BB}\cdot$ is represented in reaction (19) as simply producing a product p2, as opposed to TPP because TPP is not of interest in this section. Reaction (20), on the other hand, represents the recombination of two phenoxy radicals to form the product of current interest, biphenol (BIP), whose molecular structure is shown below:



The rest of the products were unimportant to this study, and were marked p1 through p7. The rate parameters were virtually identical to those in the BPE + toluene system, and the discussion concerning the various rate values appears in section 5.2.2.

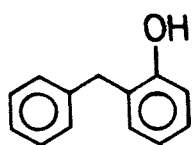
The model is first shown by Table 5.5 to be in good agreement with experiments with respect to the conversions of BPE and phenol. Next, Figure 5.14 demonstrates graphically that the model simulated the empirical yields of BPH and BIP reasonably well over the range of temperatures under study. Again, BPH steadily decreased with increasing temperature. BIP, on the contrary, rose monotonically with temperature. The theoretical dissociation energy of the phenyl-phenyl bond was about 90 kcal/mol (5). The model consequently left out the dissociation reaction of BIP, and correctly paralleled experimental results.

In short, the thermolyses of BPE + phenol were done at 325, 375, and 400°C, with the reaction time of 10 minutes. The recombination products of interest were biphenol (BIP) and benzyl phenol (BPH). A larger portion of the product – up to 30 percent – consisted of compounds heavier than bibenzyl, but these compounds were irrelevant as far as primary recombination reactions of the phenoxy radical were concerned. The mechanistic model incorporated the dissociation rates for BIP and BPH and satisfactorily predicted the conversions of BPE and phenol, as well as the yields of BPH and BIP.

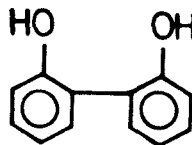
5.4 Summary

In the experiments involving benzyl phenyl ether, the phenoxy radical was generated from the dissociation of the ether bridge. This radical then combined

with either the benzyl radical or with another phenoxy radical. The resulting products of recombination were of primary interest. Through analytical means, the two predominant products were determined to be benzyl phenol and biphenol:



Benzylphenol



Biphenol

Certain other hydrocarbon products that did not contain the phenoxy group were also detected and identified. Most rate parameters were taken directly from the hydrogen-abstraction experiments (Chapter 4). The remaining rate values were obtained from analogy with similar reactions. The diffusion-limited rate of recombination for each reaction system was calculated from the mixture's viscosity at reaction conditions. The proposed kinetic mechanisms utilizing these rate parameters (Tables 5.2 and 5.4) yielded results in good agreement with empirical data (Figures 5.9 and 5.14).

One important conclusion from the aforementioned results is that the rate parameters from the above kinetic mechanisms were taken from the hydrogen abstraction experiments using different reactant mixtures at different reaction conditions. Yet the model successfully predicted the experimental results of the above systems, namely the recombination experiments involving benzyl phenyl ether. Another noteworthy point is that the existence of benzyl phenol in the

BPE + toluene system prompted speculation of its existence in the BPE + phenol system. As a result of the experience from the former system, one unknown compound in the latter system was quickly identified. The ability to extend information from one set of model compounds to explain the behavior of another compound mixture will continue to be emphasized. It is in this manner that the more complex sets of reactions in this work will be modeled and mechanistic pathways determined.

REFERENCES

- [1] Schlosberg, R. H., Davis, Jr., W. H., and Ashe, T. R. *Fuel*, 1981, **60**(3), 201
- [2] Schlosberg, R. H., Ashe, T. R., Pancirov, R. J., and Donaldson, M., *Fuel*, 1981, **60**(2), 155
- [3] Poutsma, M. L., *Fuel*, 1980, **59**, 335
- [4] Miller, R. E. and Stein, S. E., *J. Phys. Chem.*, 1981, **85**, 580
- [5] McMillen, D. F., Ogier, W. C., and Ross, D. S., *Am. Chem. Soc. Preprints*, 1981, **26**(2), 181
- [6] Benson, S. W., 'Thermochemical Kinetics: Methods for the Estimation of Thermochemical Data and Rate Parameters,' John Wiley & Sons, Inc., New York, Second Edition, 1976
- [7] Gavalas, G. R., 'Coal Pyrolysis,' Coal Science and Technology; **4**, Elsevier Scientific Publishing Company, Amsterdam, The Netherlands, 1982
- [8] Allen, D. T., 'Modeling the Reactions of Coal Liquids,' Ph.D. Thesis, Department of Chemical Engineering, California Institute of Technology, Pasadena, California, 1983
- [9] Allen, D. T. and Gavalas, G. R., *Int. J. Chem. Kinetics*, 1983, **15**, 219
- [10] Ingold, K. U., 'Rate Constants for Free Radical Reactions in Solutions,' Chapter 2, National Research Council of Canada, Ottawa, Canada, 1981
- [11] Gunn, R. D. and Yamada, T., *Am. Inst. Chem. Eng. J.*, 1971, **17**, 131
- [12] Reid, R. C., Prausnitz, J. M., and Sherwood, T. K., 'The Properties of Gases and Liquids,' McGraw-Hill Book Company, New York, Third Edition, 1977

- [13] William, D. H. and Fleming, I., 'Spectroscopic Methods in Organic Chemistry,' McGraw-Hill Book Company (UK), London, Great Britain, Second Edition, 1973

FIGURE 5.1

HPLC OF BPE + TO THERMOLYSIS PRODUCTS

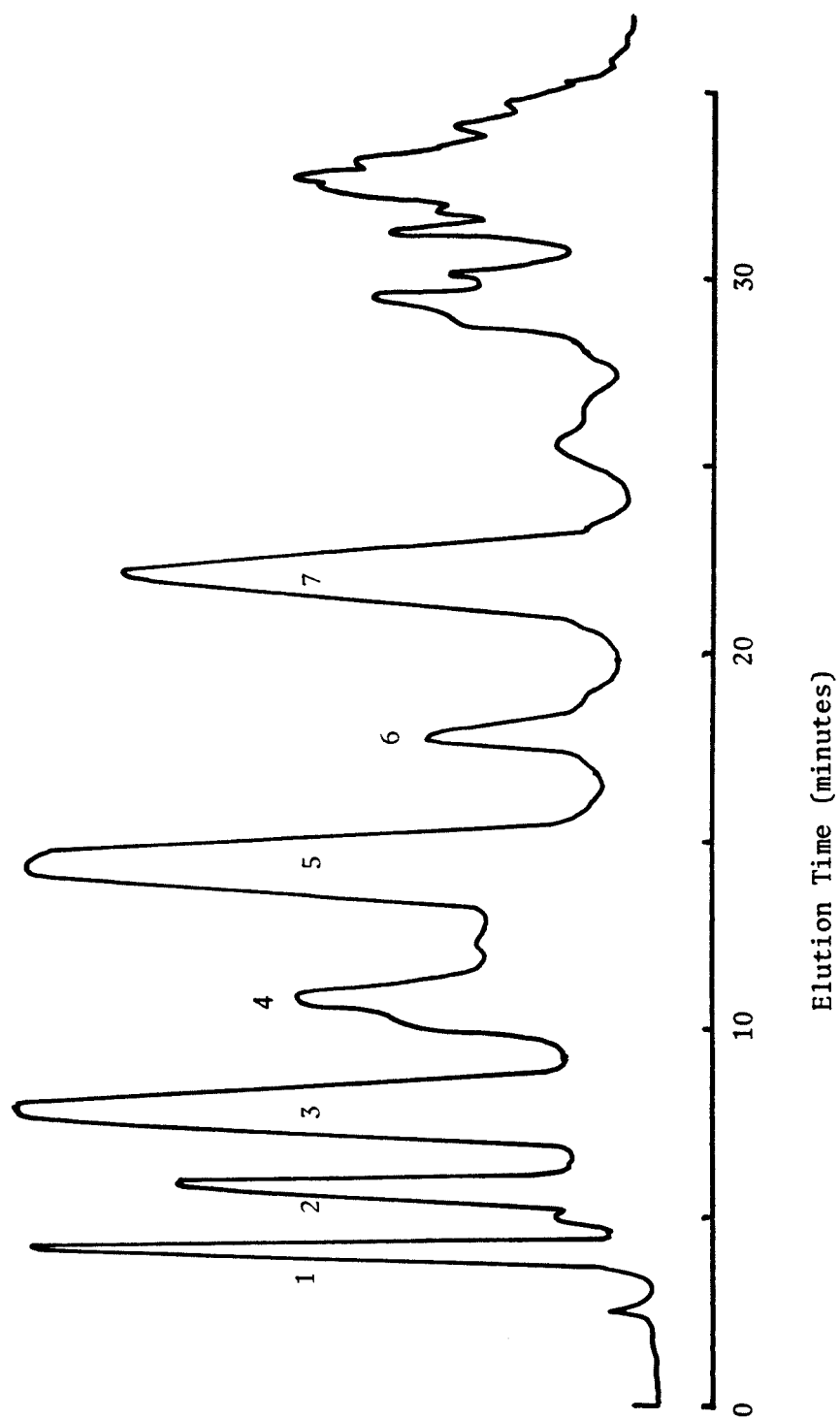


FIGURE 5.2

HPLC OF BPE + TO THERMOLYSIS PRODUCTS

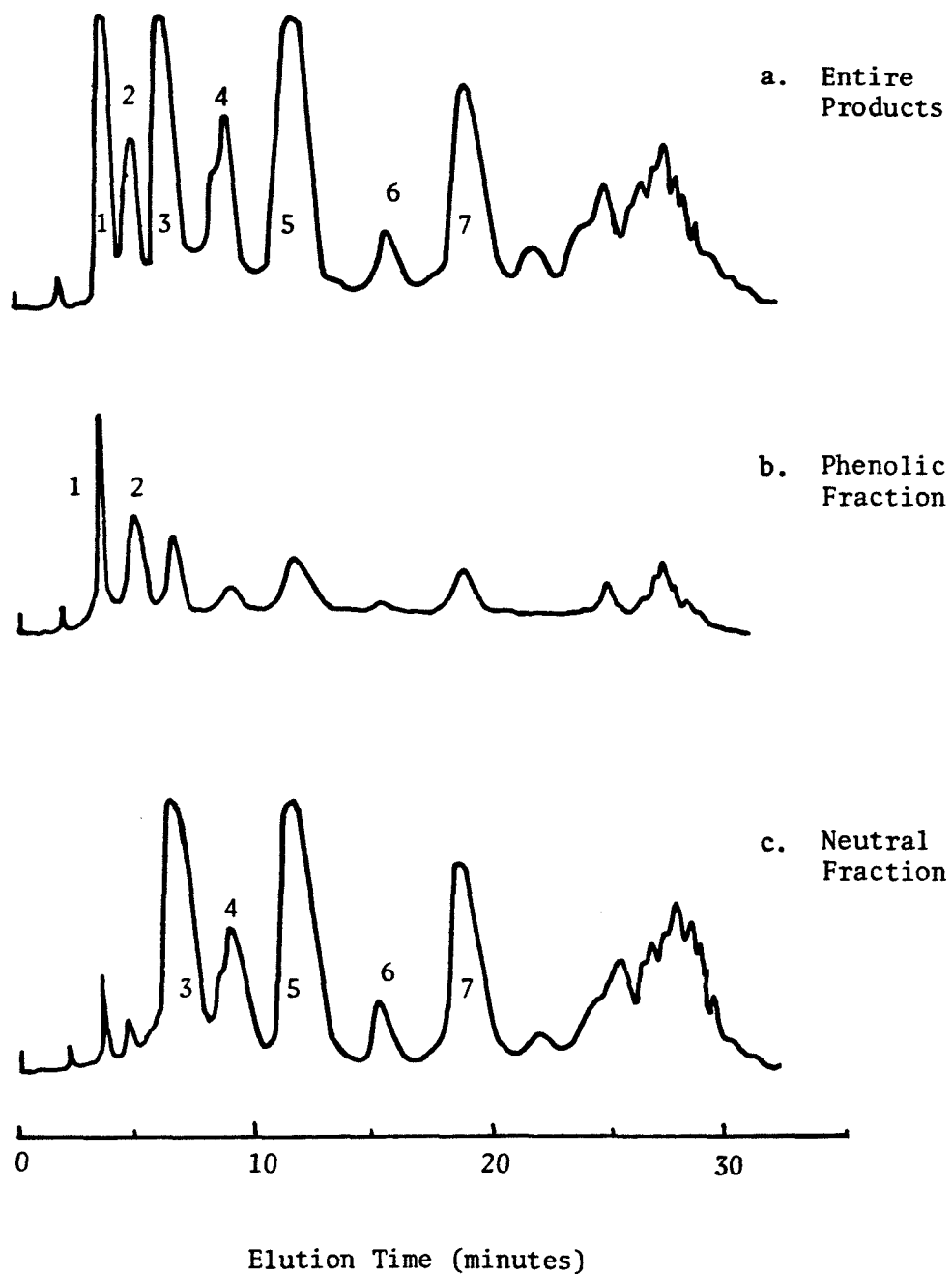


FIGURE 5.3

GCMS OF BPE + TO THERMOLYSIS PRODUCTS: FRACTION F2

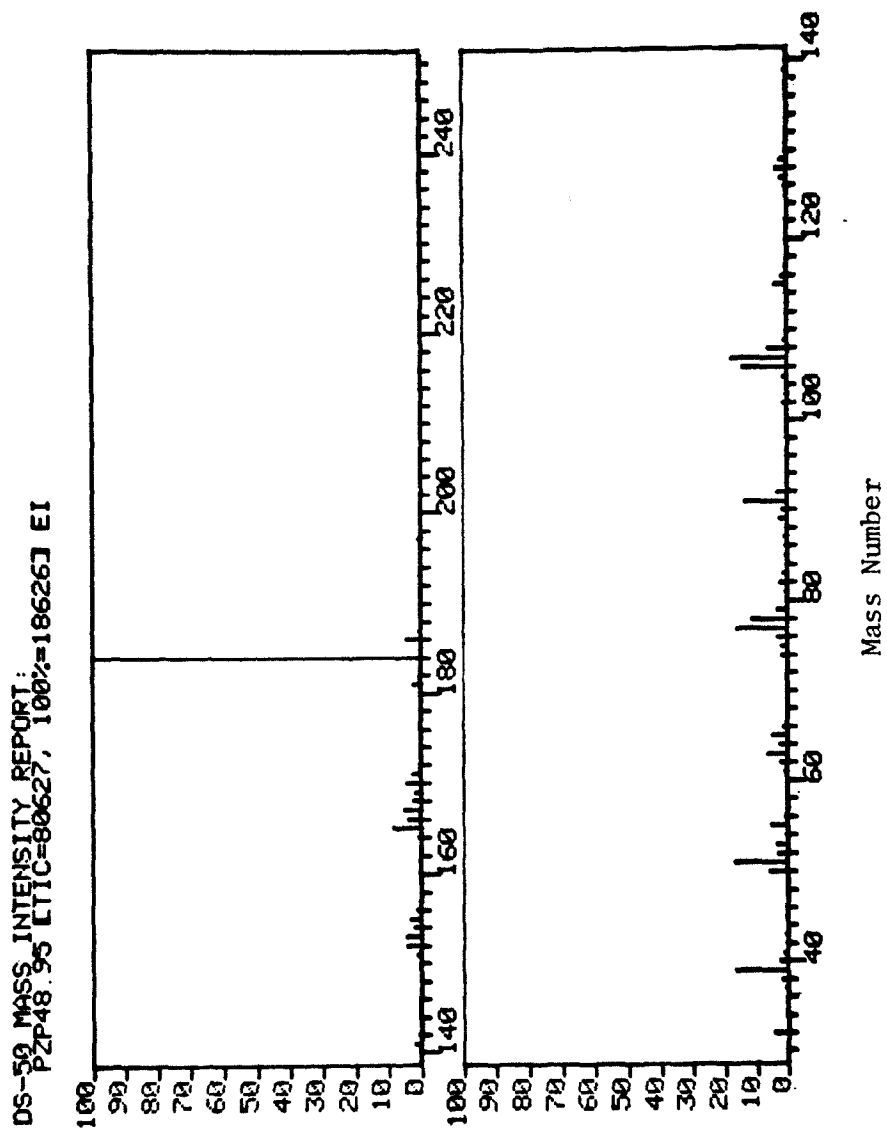


FIGURE 5.4

^1H NMR OF BPE + TO THERMOLYSIS PRODUCTS: FRACTION F2

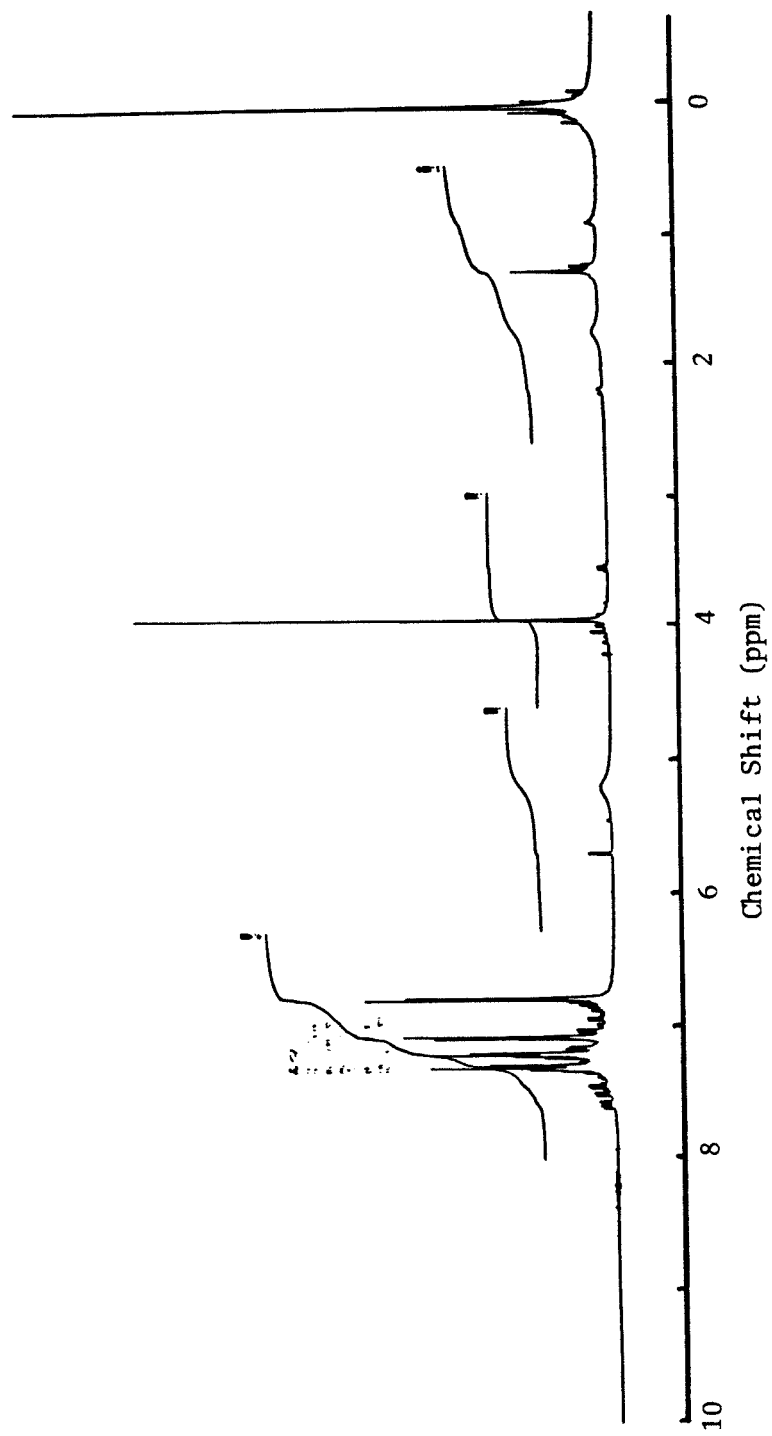


FIGURE 5.5

GCMS OF BPE + TO THERMOLYSIS PRODUCTS: FRACTION F6

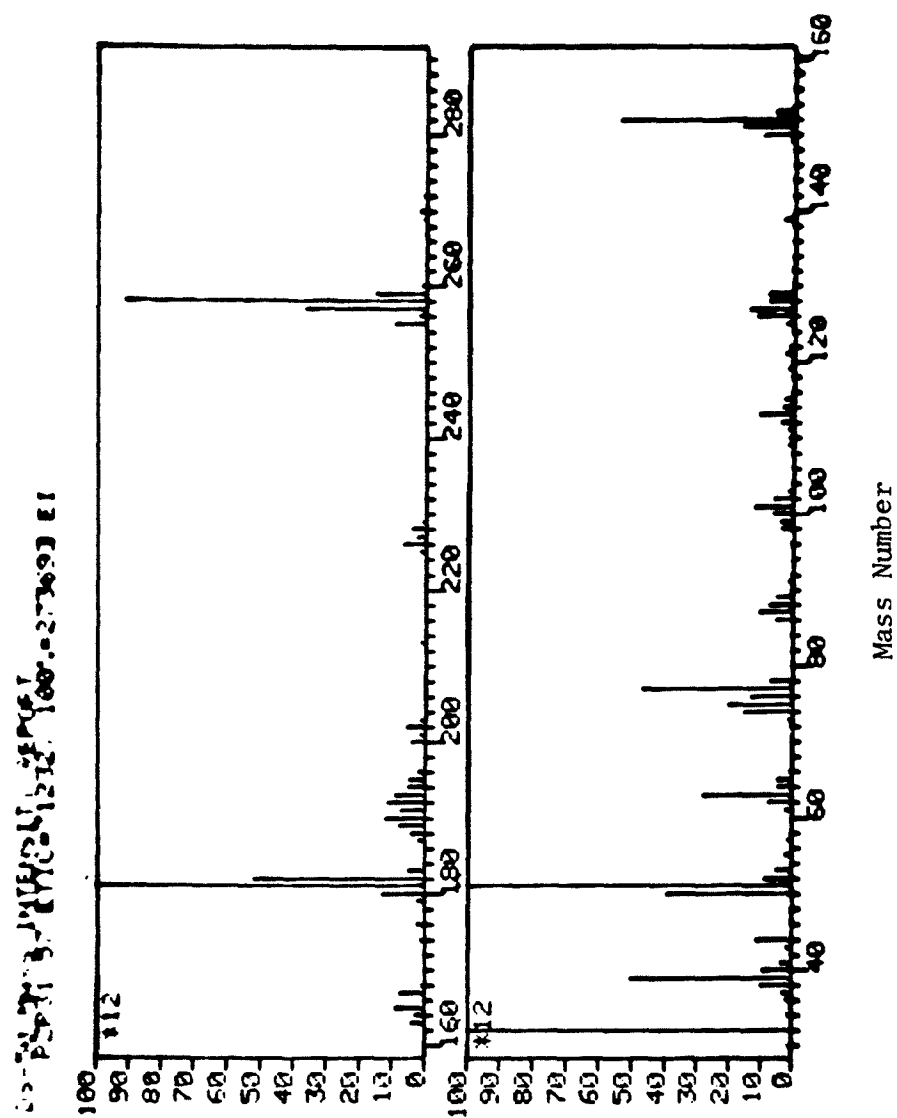


FIGURE 5.6

^1H NMR OF BPE + TO THERMOLYSIS PRODUCTS: FRACTION F6

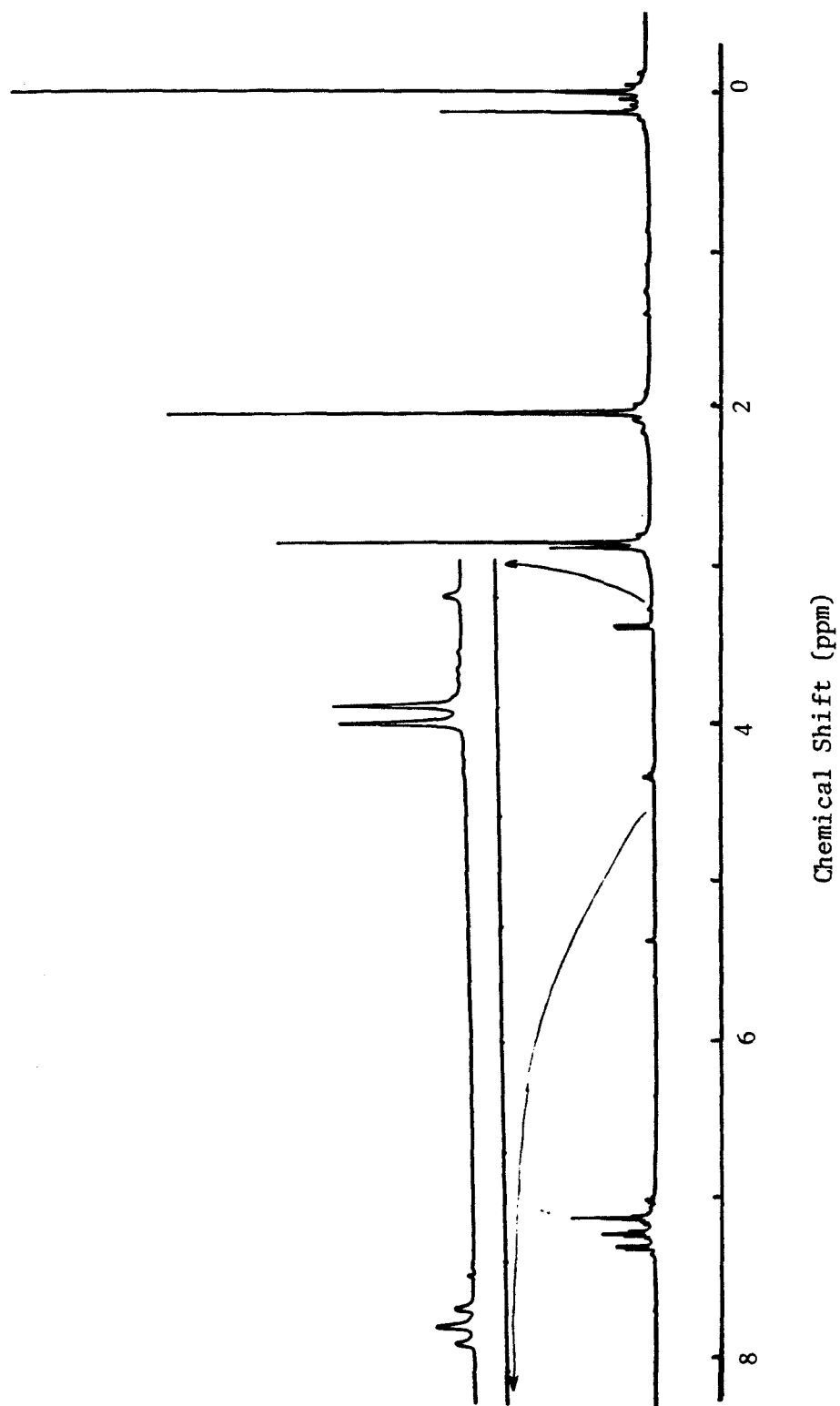


FIGURE 5.7

GCMS OF BPE + TO THERMOLYSIS PRODUCTS: FRACTION F7

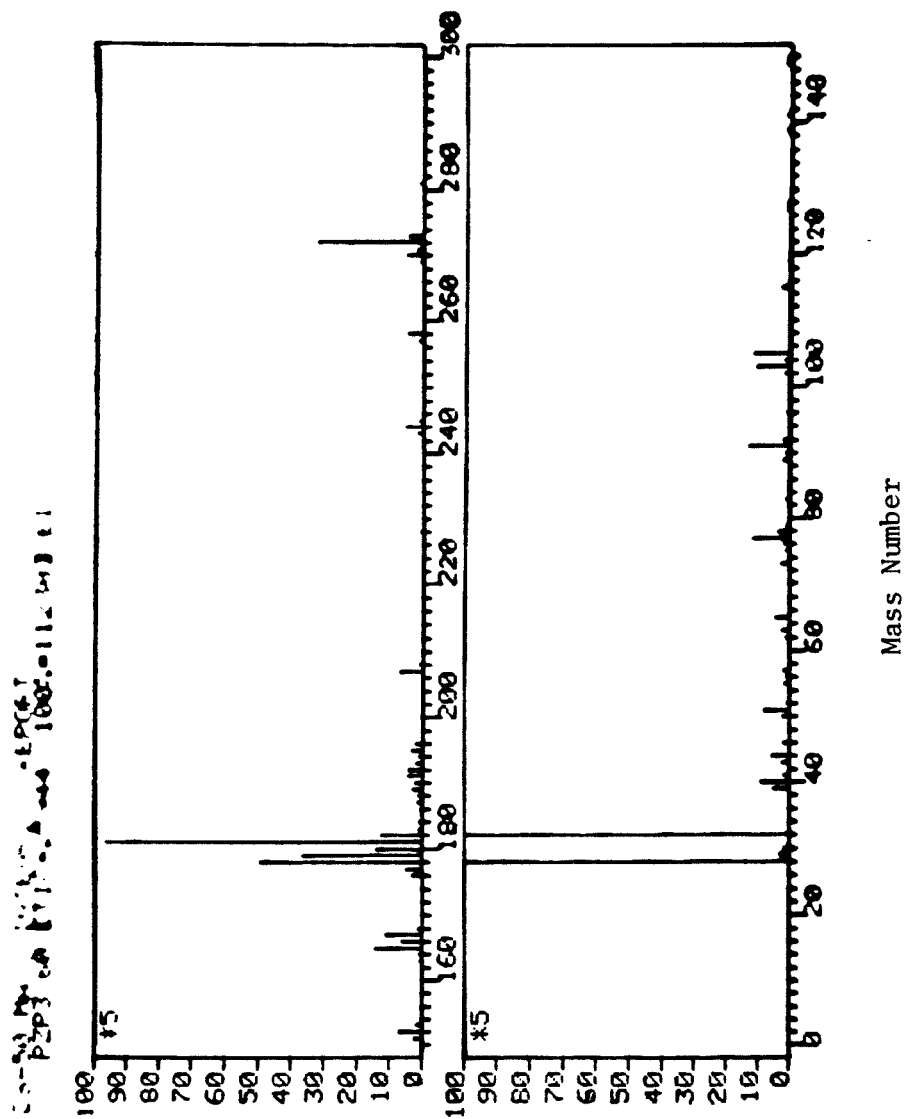


FIGURE 5.8

^1H NMR OF BPE + TO THERMOLYSIS PRODUCTS: FRACTION F7

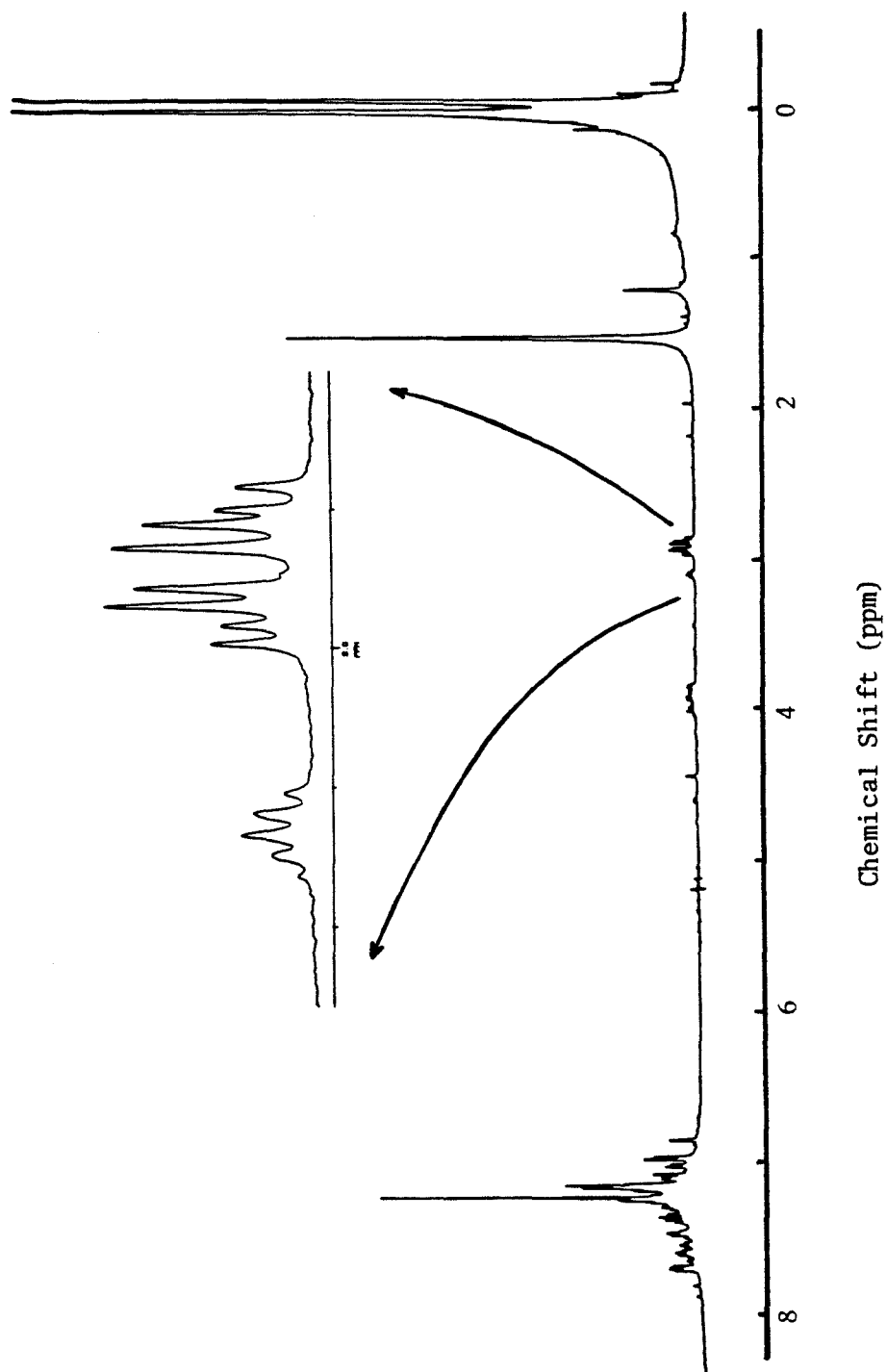


FIGURE 5.9

MODEL RESULTS VS. EXPERIMENTAL DATA
THERMOLYSIS OF BPE + TO, 15 MINUTES

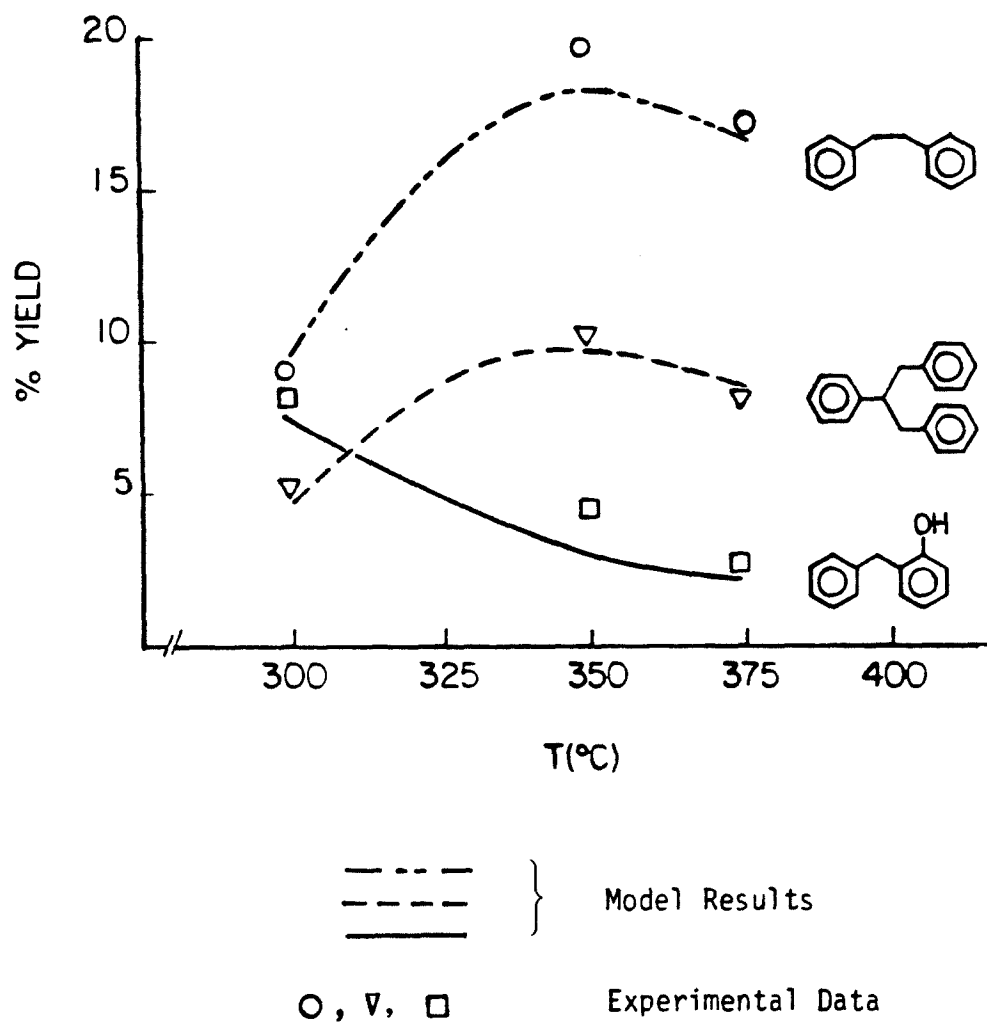


FIGURE 5.10

HPLC OF BPE + PH THERMOLYSIS PRODUCTS

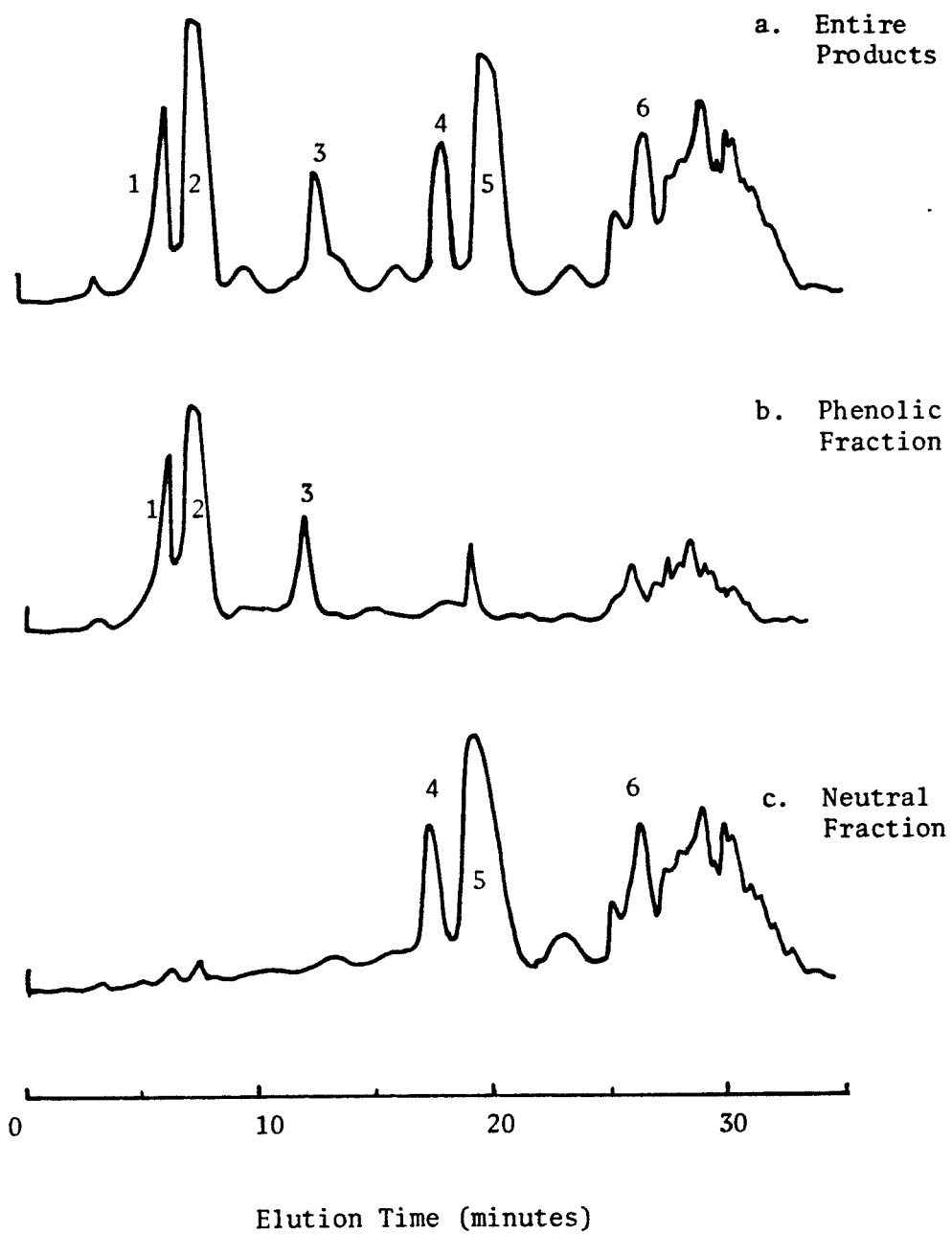


FIGURE 5.11

GCMS OF BPE + PH THERMOLYSIS PRODUCTS: FRACTION F1

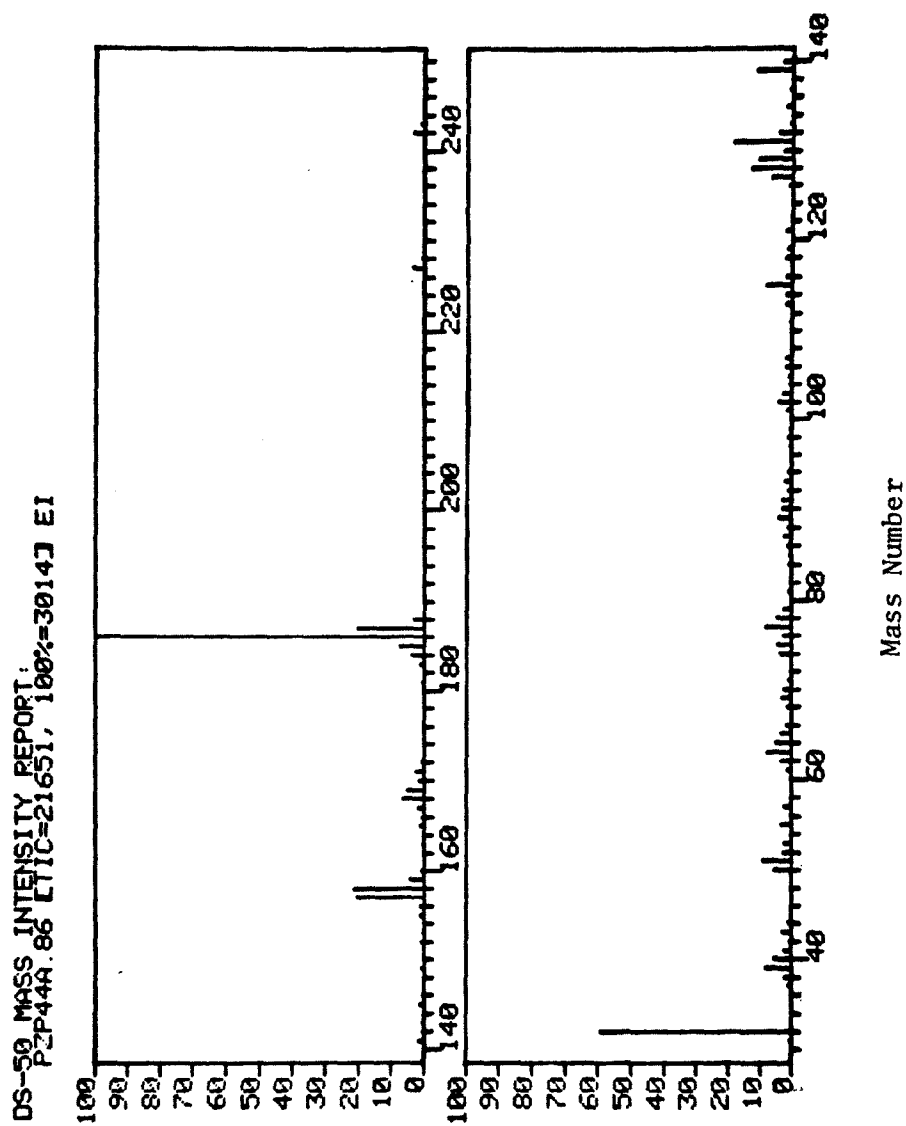


FIGURE 5.12
 ^1H NMR OF BPE + PH THERMOLYSIS PRODUCTS: FRACTION F1

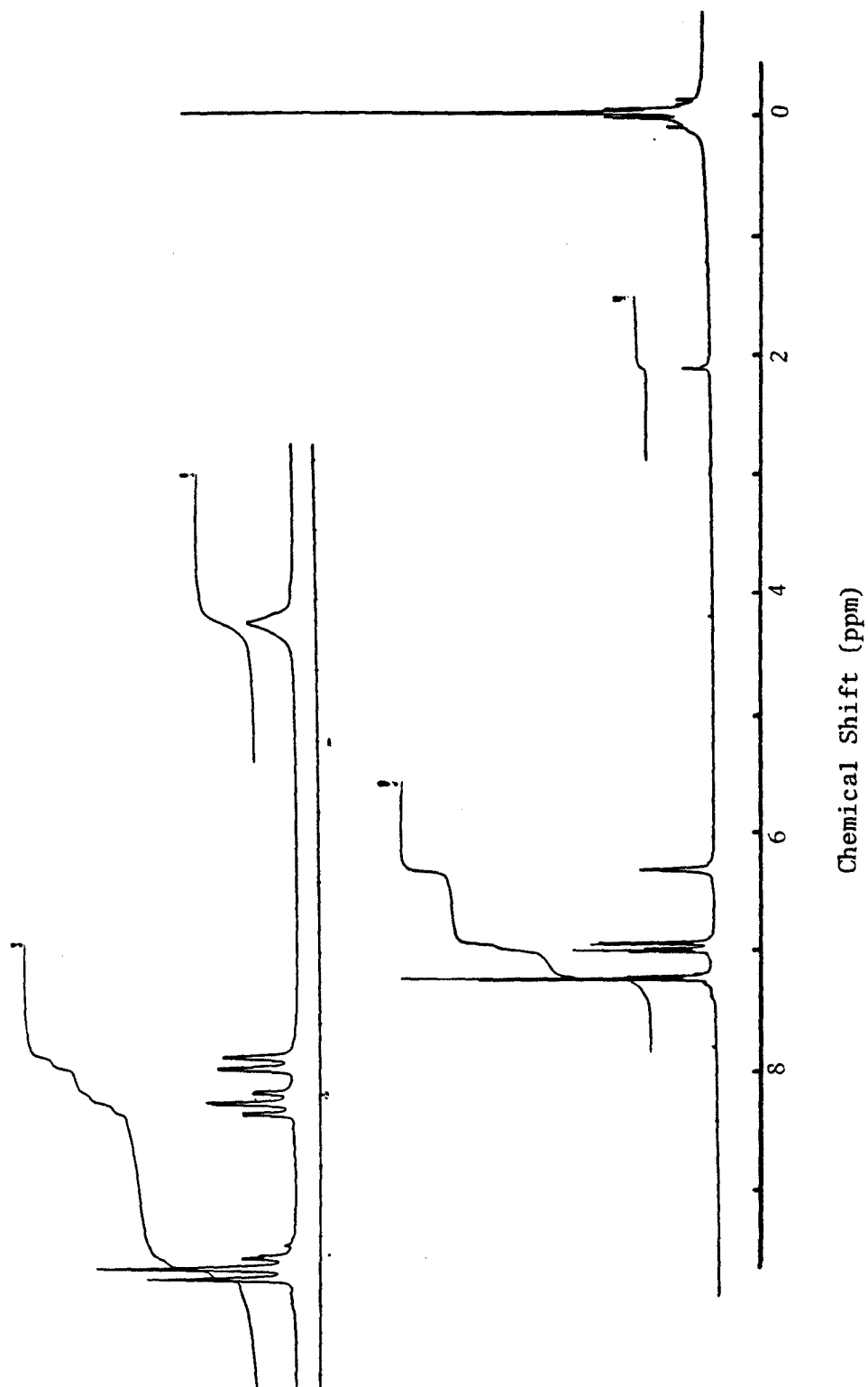


FIGURE 5.13

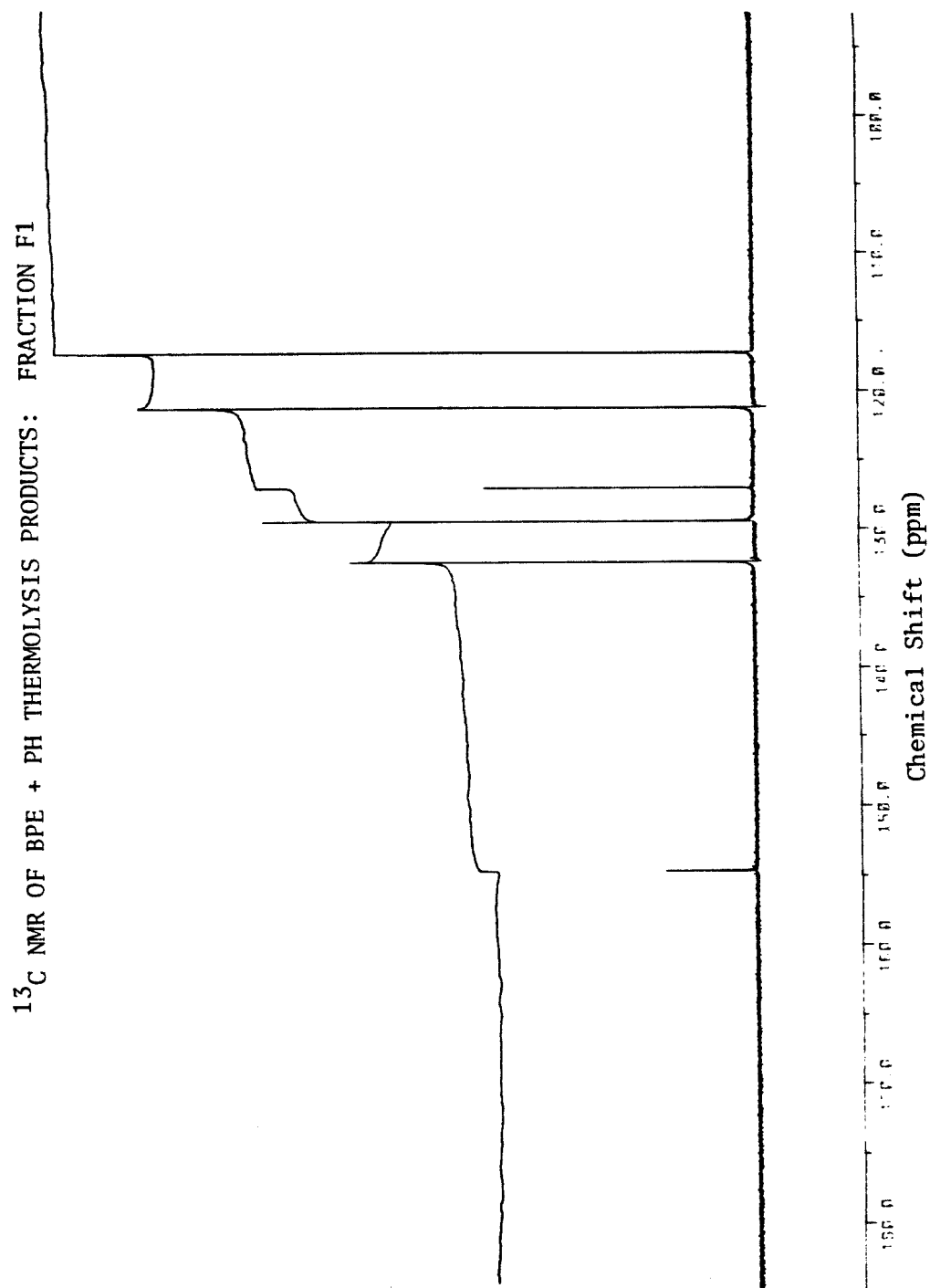


FIGURE 5.14

MODEL RESULTS VS. EXPERIMENTAL DATA
THERMOLYSIS OF BPE + PH, 15 MINUTES

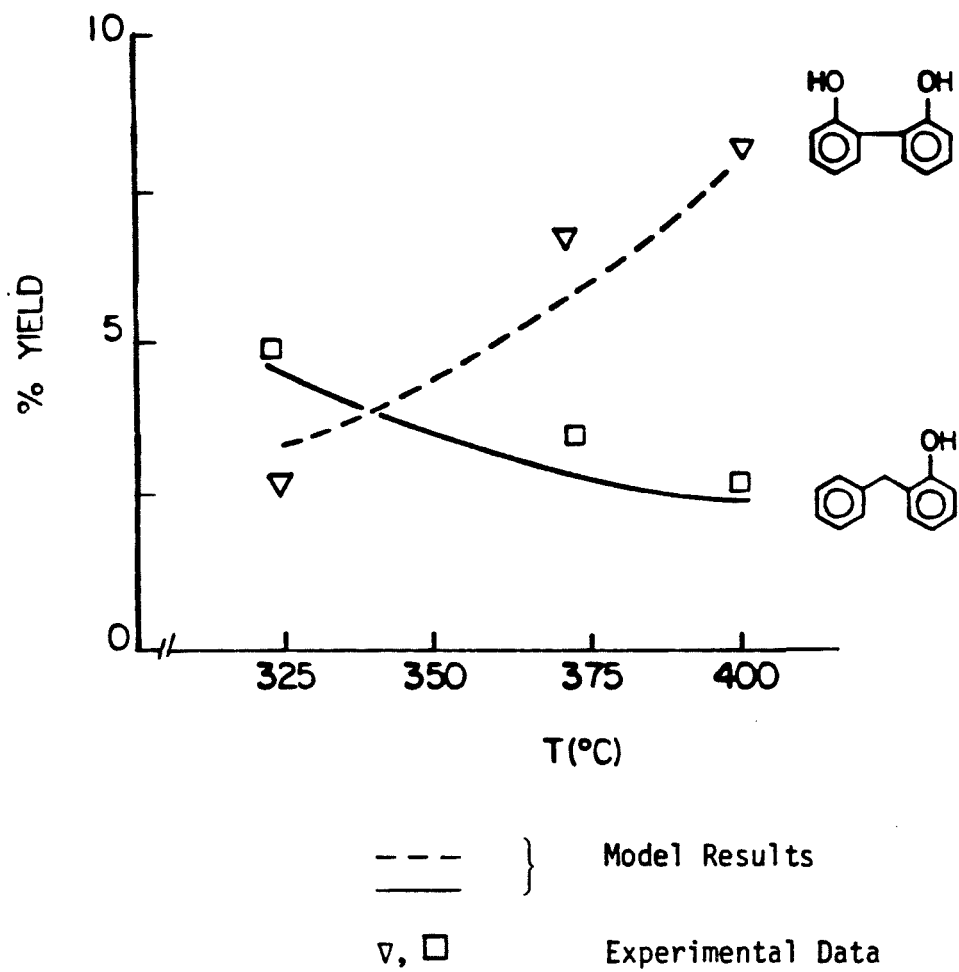
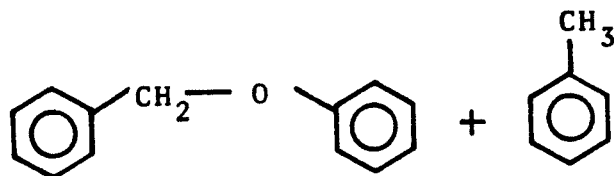


TABLE 5.1

REACTANT MIXTURES FOR THE RECOMBINATION EXPERIMENTS

PART I BENZYL PHENYL ETHER

1

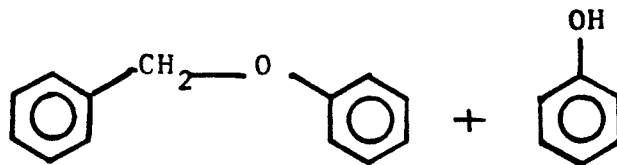


Mole Ratio: 1:4

Temperature: 300-375°C

Reaction Time: 10-15 minutes

2



Mole Ratio: 1:2

Temperature: 325-400°C

Reaction Time: 10 minutes

TABLE 5.2

THERMOLYSIS MECHANISM FOR BPE + TO

NO.	REACTION	$\log_{10} A$	E_a
INITIATION			
1	BPE \longrightarrow TO \cdot + PH \cdot	16.0	47
2	BPH \longrightarrow TO \cdot + PH \cdot	12.0	45
3	BB \longrightarrow TO \cdot + TO \cdot	15.9	63
4	TPP \longrightarrow TO \cdot + BB \cdot	15.9	60
PROPAGATION			
5	TO \cdot + BPE \longrightarrow BPE \cdot + TO	7.0	9.0
6	TO \cdot + PH \longrightarrow PH \cdot + TO	5.9	9.0
7	TO \cdot + BB \longrightarrow BB \cdot + TO	7.0	9.0
8	PH \cdot + BPE \longrightarrow BPE \cdot + PH	7.0	9.0
9	PH \cdot + TO \longrightarrow TO \cdot + PH	7.0	9.0
10	PH \cdot + BB \longrightarrow BB \cdot + PH	7.0	9.0
11	BPE \cdot + TO \longrightarrow TO \cdot + BPE	7.0	9.0
12	BPE \cdot + PH \longrightarrow PH \cdot + BPE	5.9	9.0
13	BPE \cdot + BB \longrightarrow BB \cdot + BPH	7.0	9.0
14	BB \cdot + TO \longrightarrow TO \cdot + BB	7.0	12.5
15	BB \cdot + PH \longrightarrow PH \cdot + BB	5.9	12.5
16	BB \cdot + BPE \longrightarrow BPE \cdot + BB	7.0	12.5
RECOMBINATION			
17	TO \cdot + TO \cdot \longrightarrow BB		0
18	TO \cdot + PH \cdot \longrightarrow BPH		0
19	TO \cdot + BPE \cdot \longrightarrow P1		0
20	TO \cdot + BB \cdot \longrightarrow TPP		0
21	PH \cdot + PH \cdot \longrightarrow P2		0
22	PH \cdot + BPE \cdot \longrightarrow P3		0
23	PH \cdot + BB \cdot \longrightarrow P4		0
24	BPE \cdot + BPE \cdot \longrightarrow P5		0
25	BPE \cdot + BB \cdot \longrightarrow P6		0
26	BB \cdot + BB \cdot \longrightarrow P7		0

TABLE 5.2 (cont'd)

DEFINITION OF SYMBOLS

BPE = benzyl phenyl ether

PH = phenol

TO = toluene

BPH = benzyl phenol

BB = bibenzyl

TPP = triphenyl propane

P1 - p7 = recombination products

TABLE 5.3

MODEL RESULTS VS. EXPERIMENTAL DATA
THERMOLYSIS OF BPE + TO

Temp (°C)	Time (min)	% BPE Conversion		% to Conversion	
		Model	Exptl	Model	Exptl
300	15	27.3	39.1	9.1	10.2
350	10	73.5	71.2	14.2	15.7
350	15	89.9	85.1	16.1	17.2
375	15	100	100	14.7	18.1

TABLE 5.4

THERMOLYSIS MECHANISM FOR BPE + PH

NO.	REACTION	$\log_{10} A$	E_a
INITIATION			
1	$BPE \longrightarrow TO\cdot + PH\cdot$	16.0	47
2	$BPH \longrightarrow TO\cdot + PH\cdot$	12.0	45
3	$BB \longrightarrow TO\cdot + TO\cdot$	15.9	63
PROPAGATION			
4	$TO\cdot + BPE \longrightarrow BPE\cdot + TO$	7.0	9.0
5	$TO\cdot + PH \longrightarrow PH\cdot + TO$	5.9	9.0
6	$TO\cdot + BB \longrightarrow BB\cdot + TO$	7.0	9.0
7	$PH\cdot + BPE \longrightarrow BPE\cdot + PH$	7.0	9.0
8	$PH\cdot + TO \longrightarrow TO\cdot + PH$	7.0	9.0
9	$PH\cdot + BB \longrightarrow BB\cdot + PH$	7.0	9.0
10	$BPE\cdot + TO \longrightarrow TO\cdot + BPE$	7.0	9.0
11	$BPE\cdot + PH \longrightarrow PH\cdot + BPE$	5.9	9.0
12	$BPE\cdot + BB \longrightarrow BB\cdot + BPH$	7.0	9.0
13	$BB\cdot + TO \longrightarrow TO\cdot + BB$	7.0	12.5
14	$BB\cdot + PH \longrightarrow PH\cdot + BB$	5.9	12.5
15	$BB\cdot + BPE \longrightarrow BPE\cdot + BB$	7.0	12.5
RECOMBINATION			
16	$TO\cdot + TO\cdot \longrightarrow BB$		0
17	$TO\cdot + PH\cdot \longrightarrow BPH$		0
18	$TO\cdot + BPE\cdot \longrightarrow P1$		0
19	$TO\cdot + BB\cdot \longrightarrow P2$		0
20	$PH\cdot + PH\cdot \longrightarrow BIP$		0
21	$PH\cdot + BPE\cdot \longrightarrow P3$		0
22	$PH\cdot + BB\cdot \longrightarrow P4$		0
23	$BPE + BPE\cdot \longrightarrow P5$		0
24	$BPE + BB\cdot \longrightarrow P6$		0
25	$BB + BB\cdot \longrightarrow P7$		0

TABLE 5.4 (cont'd)

DEFINITION OF SYMBOLS

BPE = benzyl phenyl ether

PH = phenol

TO = toluene

BB = bibenzyl

BPH = benzyl phenol

BIP = biphenol

P1 - p7 = recombination products

TABLE 5.5

MODEL RESULTS VS. EXPERIMENTAL DATA

THERMOLYSIS OF BPE + PH

Temp (°C)	Time (min)	% BPE Conversion		% PH Conversion	
		Model	Exptl	Model	Exptl
325	10	37	39	5.1	6.0
375	10	87	91	11.9	13.2
400	10	100	100	12.7	14.0

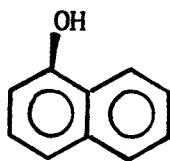
CHAPTER 6

RECOMBINATION EXPERIMENTS

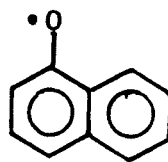
PART II. REACTIONS OF 1-NAPHTHOL

6.1 Introduction

Organic matter in coal consists of fused aromatic clusters, each of which typically contains two to three condensed rings (1, 2). This thesis thus far has only dealt with benzene rings, as were the cases with bibenzyl and benzyl phenyl ether. In order to study the effects of condensed aromatic nuclei on the phenoxy radical, 1-naphthol was selected as a source of the naphthoxy radical:



Naphthol



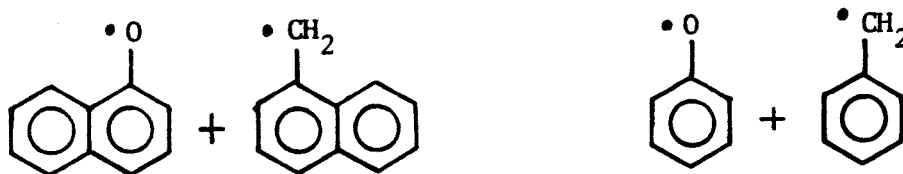
Naphthoxy radical

Table 6.1 illustrates the three model compound systems and the reaction conditions chosen for this purpose. The first set of experiments was designed to investigate the thermolysis of blank 1-naphthol. As opposed to phenol, which is quite stable at liquefaction temperatures, 1-naphthol has been found to undergo considerable thermolysis even in the absence of any other reactants (3, 4). Already, the resonance stabilizing effect of the fused ring structure has manifested itself in this simplest case. The objectives of these experiments were therefore to explain the mechanistic pathways for the thermal dissociation of 1-naphthol,

and to determine the associated rate parameters.

The second set of experiments utilized mixtures of 1-naphthol and bibenzyl to study the recombination reactions involving the naphthoxy radical and the benzyl radical ($\phi - \text{CH}_2\cdot$). The rate parameters for the hydrogen-abstraction reactions involving the naphthoxy radical have already been determined in Chapter 4 and were now used in the proposed mechanisms. The recombination rates were again assumed to be diffusion-controlled.

In the third set of experiments, a 1:2 molar mixture of 1-naphthol + 1-methylnaphthalene was employed to investigate the recombination pathways of the naphthoxy and the methyl naphthalene radicals. The objective here was to examine a condensed-ring analog of the phenoxy-benzyl radical recombination discussed in Chapter 5

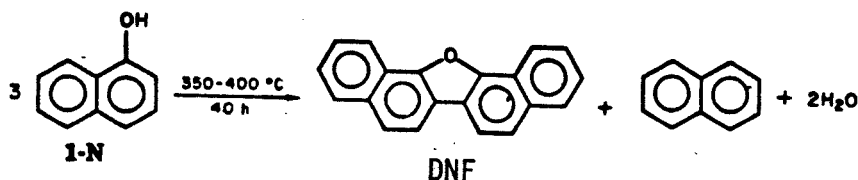


It will be demonstrated that certain aspects of the kinetic behavior of the naphthoxy radical can be speculated from the knowledge of the reactions of the phenoxy radical.

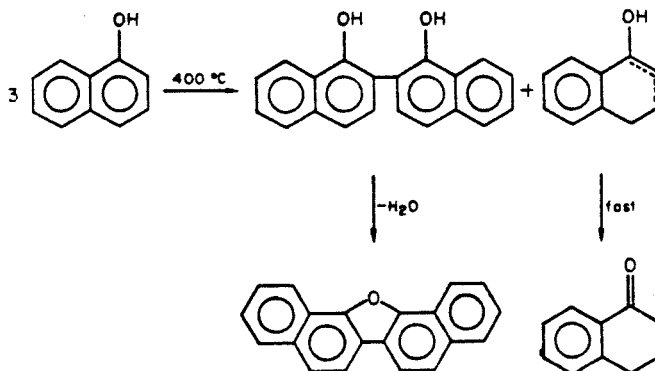
6.2 Thermolysis of 1 Naphthol

As mentioned in Chapter 1, a limited number of studies have focussed on 1-naphthol thermolysis (3 - 6). Dinaphthofuran was invariably the predominant final product, while binaphthol, tetralone, naphthalene, water, and a host of

final product, while binaphthol, tetralone, naphthalene, water, and a host of other products were reported in smaller concentrations. Merz and Weith (3) assigned a partial stoichiometry to the reaction:



Hall (4) proposed that ether formation preceded the furan formation. Poutsma (5) suggested the following reaction scheme to account for the major products:



He determined a global rate for ring coupling and hydrogen transfer reaction to be proportional to the concentration of naphthol raised to the power of roughly 2.5. He also provided quantitative accounts of product formation. To supplement the above information, this section attempts to explain the *elementary* reactions that describe the dissociation of 1-naphthol, and to suggest the mechanistic pathways for radical recombination. The aforementioned studies provided useful guidelines as to the identities of the thermolysis products. The molecular structures of these products are useful in that they reflect the kinetic behavior

of the parent naphthoxy radical, particularly in comparison with the phenoxy radical.

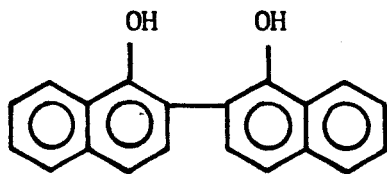
Another objective of the 1-naphthol thermolysis study was to estimate the rate parameters associated with the elementary reactions at liquefaction temperatures. A final goal, of course, was to put together a kinetic mechanism consisting of these elementary reactions and the estimated rate parameters. The mechanism was then validated by its ability to simulate empirical results, from our own experiments and also from the literature.

6.2.1 Product Identification

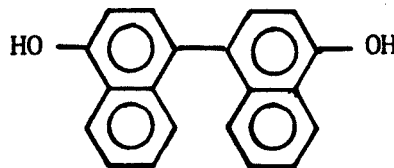
An HPLC chromatogram of the thermolysis products of 1-naphthol at 425°C for 15 minutes is illustrated in Figure 6.1. The peaks of significance have been labeled 1 through 5, in order of elution time. Note that although no good hydrogen donors were present in the reactant mixture, the chromatogram of the products appears quite clean. Other than the labeled compounds, the remaining peaks accounted for less than 10 percent of total products. Obviously, mechanistic pathways existed for thermodynamically favorable dissociation of 1-naphthol and recombination of the subsequent free radicals.

'Spiking' with authentic samples revealed that peaks 1, 3, and 5 were 1-naphthol, naphthalene, and dinaphthofuran, respectively. Peak 2 was found to have the same elution time as binaphthol and tetralone, both of which eluted within 15 seconds of each other. This peak was fractionated and mass identification by GCMS confirmed that binaphthol and tetralone were the two products contained in peak 2. Further, the only possible structure of binaphthol was 2,2'-binaphthalene-1,1'-diol because this is the only configuration that can condense

to form dinaphthofuran. For example, the configuration of 1,1'-binaphthalene-4,4'-diol would not permit furan formation from loss of a H_2O molecule.



2,2'-binaphthalene-1,1'-diol

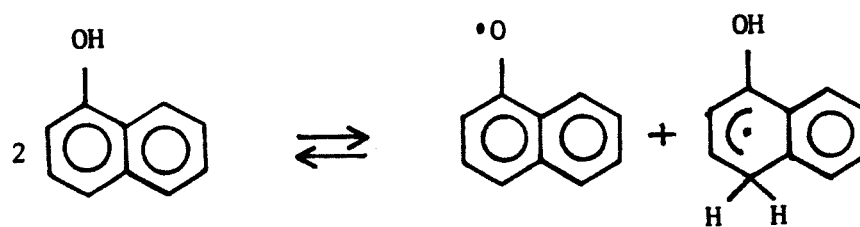


1,1'-binaphthalene-4,4'-diol

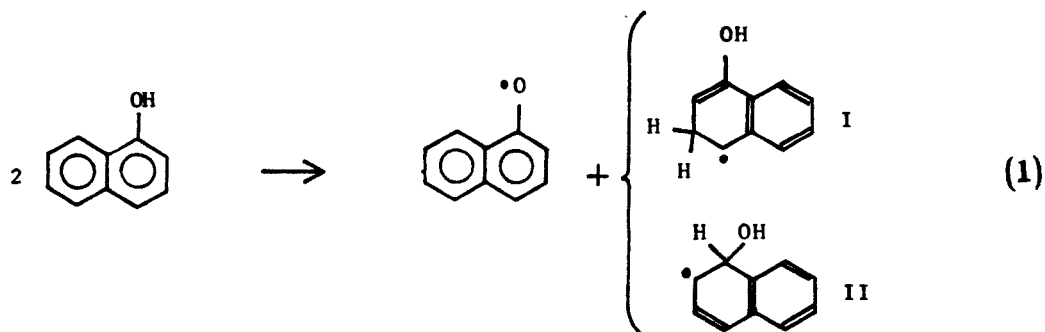
Peak 4 was unidentifiable due to its small concentration. The integration data showed that peak 4 represented a concentration smaller than peak 3, or naphthalene. Yet naphthalene was a minor product of 1-naphthol thermolysis, accounting for less than 3 percent of the total amount of naphthol consumed. It was thus assumed that omission of the compound corresponding to peak 4 from the model would not seriously affect kinetic analysis. The presence of binaphthol, tetralone, dinaphthofuran as major products, and naphthalene as a minor product of 1-naphthol thermolysis agreed with Poutsma's experimental results (4). In the next section, a mechanistic scheme will be advanced to explain the formation of these thermolysis products.

6.2.2 Kinetic Modeling

Poutsma (4) suggested the following bimolecular hydrogen transfer reaction to account for naphthol dissociation:



He estimated the activation energy of this step to be about 50 kcal/mol. Comparison with similar hydrogen transfer reactions (7, 8, 9) yielded an approximate value for the A factor of $10^{10} - 10^{11}$. In this section, the following reverse disproportionation reaction is proposed:



This reaction varies slightly from Poutsma's reaction, the difference being the more explicit structures of the radical $\text{C}_{10}\text{H}_9\text{O}\cdot$. Allen (11), in his study of dihydronaphthalene thermolysis, demonstrated that reverse disproportionation was the dominant step for radical initiation:

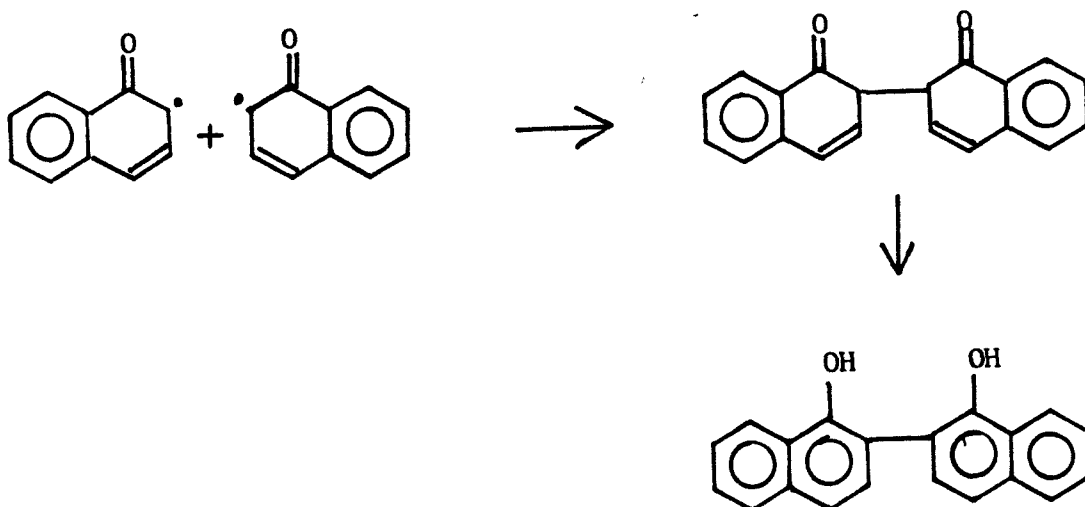


The existence of this reaction would tend to reinforce the proposed reaction (1). Further evidence in support of the reverse disproportionation reaction, as well

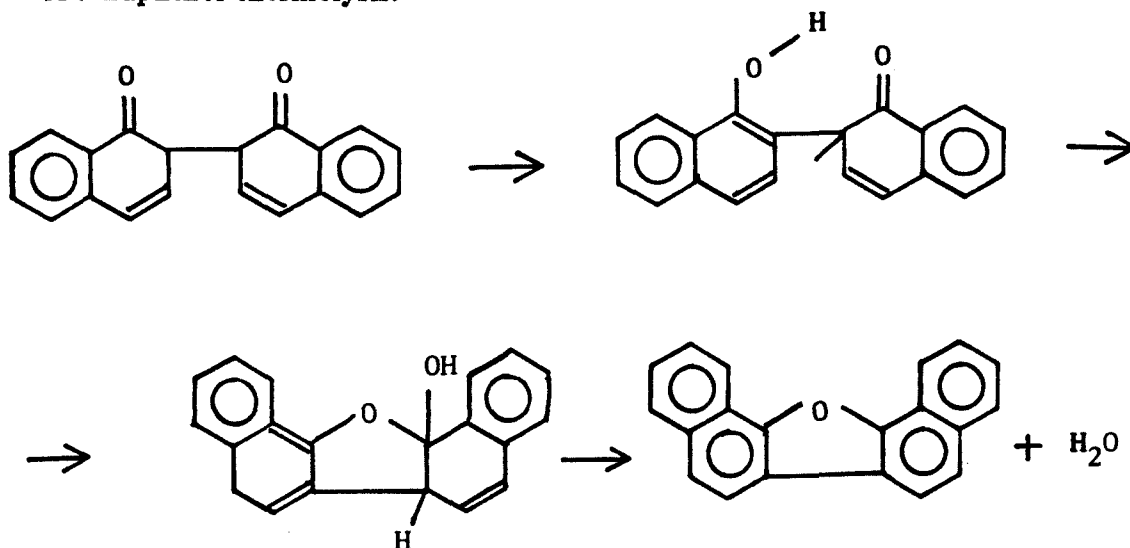
as mechanistic pathways for formation of the major thermolysis products from radicals I and II, will now be presented.

6.2.2.1 Binaphthol and Dinaphthofuran Formation

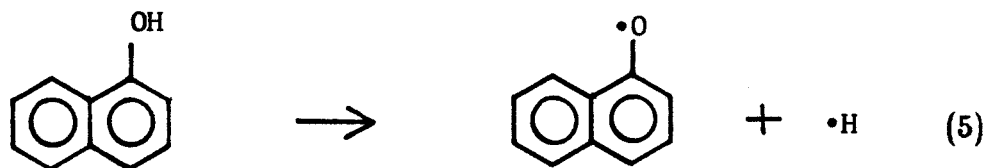
Binaphthol was generally believed to result from recombination of two naphthoxy radicals (4). The mechanistic pathways are outlined below:



where the last step is the rapid keto-enol tautomerization. The above scheme also leads to formation of dinaphthofuran (DNF), which is the dominant product of 1-naphthol thermolysis:



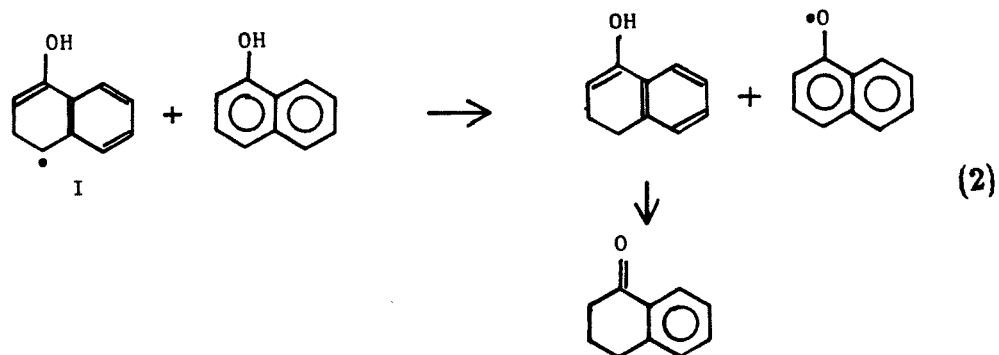
The reaction



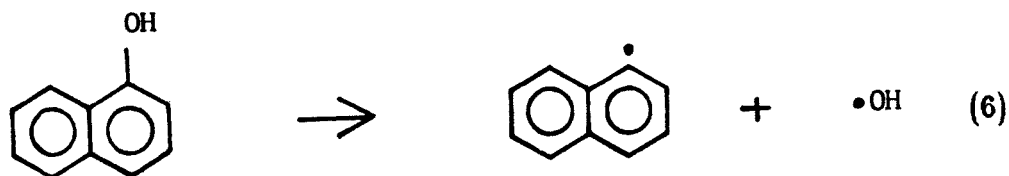
has an activation energy of about 83 kcal/mol (10). Clearly this reaction would not be responsible for generation of the naphthoxy radical at liquefaction temperature. With an activation energy of about 50 kcal/mol, reverse disproportionation (reaction (1)) provided a satisfactory alternative to reaction (5) with respect to naphthoxy generation, and eventual binaphthol and DNF formation.

6.2.2.2 Tetralone and Naphthalene Formation

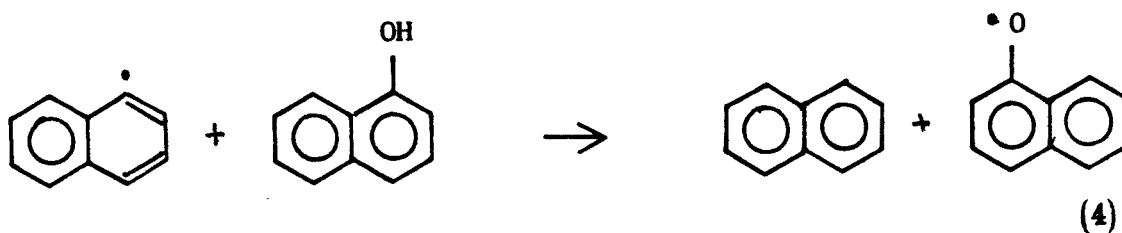
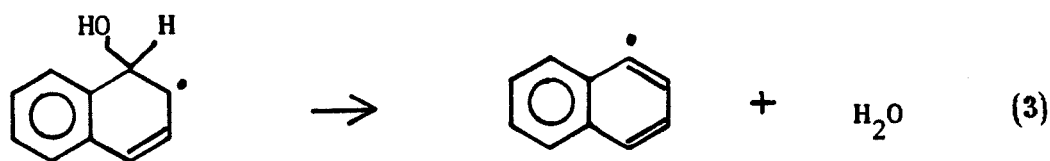
Radical I in reaction (1) can account for tetralone formation via the following mechanism:



Naphthalene was observed in small concentrations as one of the products of 1-naphthol thermolysis. The reaction

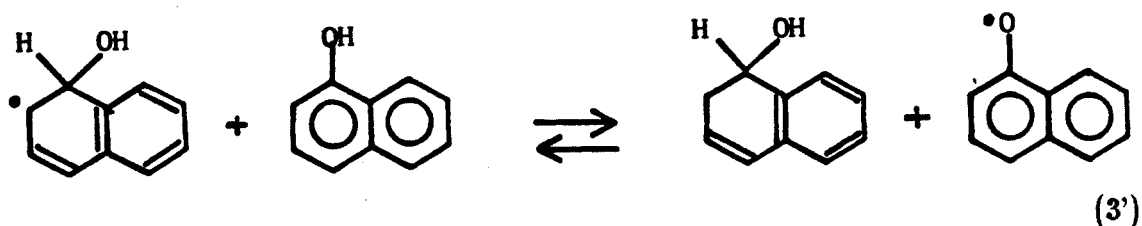


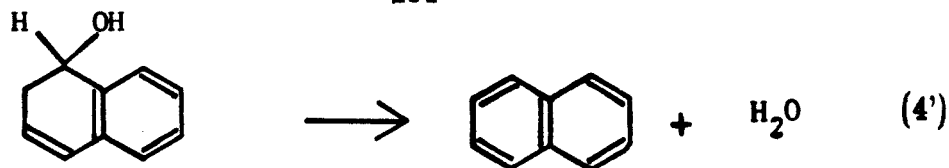
is, however, even less likely than reaction (5), for its activation energy is greater than 100 kcal/mol (12, 13). Poutsma hypothesized that tetralone was a better hydrogen acceptor than naphthol and could undergo hydrogenation, followed by hydration and dehydration to form naphthalene. The following mechanistic scheme appears to be more straightforward:



The high activation energy of reaction (3), due to the extremely unstable naphthyl radical, would explain the small yield of naphthalene, as observed experimentally.

A possible alternative scheme is shown below:



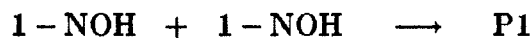


Insufficient information prohibited determination of the 'correct' mechanism. The actual pathway could involve a concerted reaction, for example, rather than a free radical reaction. This work sought to present possible pathways for product formation. For the purpose of modeling 1-naphthol thermolysis, reactions (3) and (4) were selected. Their inclusion in the model, however, does not imply their superiority over reactions (3') and (4').

Note that both reactions (2) and (3) & (4) generate a naphthoxy radical, consistent with the experimental observation that binaphthol, and subsequently DNF, were the dominant thermolysis products.

6.2.2.3 Kinetic Experiments

Kinetic experiments have been conducted using mixtures of 1-naphthol and biphenyl (a diluent) at various dilution ratios. If reaction (1) was to be the rate limiting step, the formation of each product would have to be dependent on the square of the initial concentration of 1-naphthol:



so that

$$\frac{d[\text{P1}]}{dt} = k[1\text{-NOH}]^2$$

where 1-NOH represents 1-naphthol and P1 is a thermolysis product. If the conversion of 1-naphthol was kept sufficiently small, the value $[1\text{-NOH}]$ could be

taken as constant, $[1 - \text{NOH}]_0$, so that

$$[\text{P1}]_f - [\text{P1}]_i = k[1 - \text{NOH}]_0^2 \Delta t$$

where $[\text{P1}]_f$ and $[\text{P1}]_i$ are the final and initial concentration of P1, respectively.

With $[\text{P1}]_i$ being zero and Δt constant, we obtain

$$[\text{P1}] = K[1 - \text{NOH}]_0^2$$

Figure 6.2 illustrates the plot of concentrations of naphthalene, binaphthol, and DNF, as a function of initial naphthol dilution. Naphthalene and DNF exhibit quadratic dependence on $[1 - \text{NOH}]_0$. Although binaphthol appears to show a linear dependence, this result could be due to the fact that binaphthol is the intermediate product, ultimately yielding DNF upon dehydration. Nevertheless, the second order dependence on $[1 - \text{NOH}]_0$ exhibited by naphthalene and DNF offered further support of the proposed bimolecular disproportionation reaction (1).

In summary, the mechanistic scheme diagrammed in Figure 6.3 has been advanced to explain the dissociation of 1-naphthol. Note that this mechanism does not create a hydrogen atom (as reaction (5) would). The hydrogen atom would have abstracted another hydrogen atom very rapidly to form a hydrogen molecule. Thus this mechanism further agreed with Poutsma's observation that no hydrogen gas was detected (4).

Table 6.2 shows the entire mechanism for thermolysis of 1-naphthol, incorporating reactions (1) through (4) to account for naphthol dissociation, as well as formation of tetralone and naphthalene. Here, radicals I and II were both labeled $\text{NOH}\cdot$ for convenience. The recombination of two naphthoxy radicals

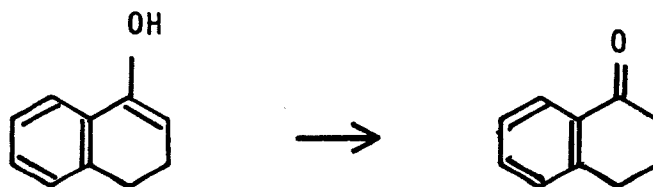
(reaction (5) in Table 6.2) was assumed to yield only binaphthol, while the collision of the naphthoxy radical and radical I or II (reaction (7) in Table 6.2) gave back two molecules of naphthol in a reverse of reaction (1). Binaphthol was further dehydrated to give dinaphthofuran, as represented by reaction (6) in Table 6.2. The remainder of the termination reactions were inconsequential, and their products were simply labeled P1 through P7.

The activation energy for reaction (3) was estimated by thermochemical methods to be 18.1 kcal/mol (see Chapter 2). The value of 10^{14} for the corresponding A factor was obtained by analogy with similar reactions (12). Reactions (2) and (4) had been encountered in the hydrogen-abstraction experiments (Chapter 4) and the rate parameters were taken directly from that chapter.

The recombination reactions were assumed to be diffusion-limited, as before. It turned out, through iteration, that the activation energy for reaction (1) had to be lowered to 48.5 kcal/mol to correctly parallel experimental results. The variation of 1.5 kcal/mol from Poutsma's reported value was indeed very reasonable, especially considering that Poutsma's value was estimated by a series of assumptions.

Table 6.3 illustrates the ability of the proposed mechanistic scheme to model Poutsma's experimental data on 1-naphthol conversion at 400°C over the reaction times of 5 to 75 minutes. Note that the model remains valid even for high conversions of 1-naphthol (≥ 50 percent), indicating that the exclusion of secondary and tertiary elementary reactions resulted in no significant loss of accuracy. Figure 6.4 compares model results with Poutsma's data on the relative yields of the major thermolysis products. The agreement was very good in the cases of naphthalene, binaphthol, and DNF yields. The model result on tetralone concentration was slightly larger than Poutsma's data at reaction times

over 15 minutes. This was attributed to the fact that the model considered the following conversion very rapid



The model did not provide for alternative paths such as hydrogenation reactions that would saturate the ring and yield, for example,



These two compounds were reported in small concentrations by Poutsma. Their formation pathways, however, would involve a series of secondary and tertiary elementary reactions that were not essential to the understanding of the dissociation of 1-naphthol and subsequent interactions of the naphthoxy radical. These reactions were thus omitted from the model to simplify the mechanistic scheme and to focus on the important issues.

In both cases, the slight decline of tetralone with time coincided with the increase in naphthalene. Poutsma theorized that tetralone underwent dehydration and dehydrogenation to form naphthalene. Alternatively, the proposed mechanism for 1-naphthol dissociation, illustrated in Figure 6.3, explained this inverse relationship by the interconversion between radicals I and II. Reaction (4), converting radical II to tetralone, is thermodynamically more favorable than reaction (2), converting radical I to naphthalene. Therefore, the decrease in te-

tralone would result in more radical I available to produce more naphthalene.

In short, the dissociation mechanism advanced for 1-naphthol thermolysis successfully accounted for experimental yields of major products, and explained the behavior of these products with reaction time.

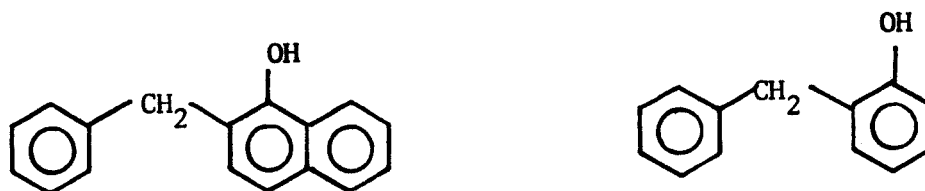
6.3 Thermolysis of 1 Naphthol + Bibenzyl

In Chapter 5, the reaction of benzyl phenyl ether and toluene produced benzyl phenol, a recombination product of the benzyl and phenoxy radicals. In comparison, the model compound mixture 1-naphthol and bibenzyl was designed to study the recombination of the benzyl and naphthoxy radicals. It will become apparent that knowledge of the structure of $\phi - \text{CH}_2\cdot + \phi - \text{O}\cdot$ recombination product provided insight into determining the structure of $\phi - \text{CH}_2\cdot + \text{N} - \text{O}\cdot$ product, where $\text{N} - \text{O}\cdot$ is the naphthoxy radical.

6.3.1 Product Identification

Figure 6.5 shows an HPLC chromatogram of the thermolysis products of the mixture 1-naphthol + bibenzyl at 425°C for 15 minutes. The major peaks have been labelled 1 through 6 in order of elution time. Note that this chromatogram is very similar to the one for 1-naphthol thermolysis (Figure 6.1). In fact, most of the major products could be tentatively identified just by comparing the two chromatograms. It turned out, using the same analytical procedures as described in section 6.2.1, that peaks 1, 3, 4, 6, and 7 corresponded to 1-naphthol, toluene, naphthalene, bibenzyl, and dinaphthofuran, while peak 2 contained both binaphthol and tetralone. Peak 5 was isolated (actually peaks 5

and 6 were isolated in the same fraction due to the similar elution times), and identified by GCMS to have a mass of 234. This mass corresponded to a product of $\phi\text{CH}_2\cdot + \text{NO}\cdot$ recombination. This compound was found to be phenolic, and to maintain a very low concentration as the temperature increased from 425 to 450°C. This behavior was attributed to the dissociation of this compound via keto-enol tautomerization, which became more favorable with rising temperature. Based on the result of $\phi\text{CH}_2\cdot + \phi\text{O}\cdot$ recombination, it was concluded that peak 5 corresponded to benzyl naphthol. The structure of this compound was analogous to benzyl phenol



Knowledge of the structure of benzyl phenol prompted chemical separation to check for the phenolic character of fraction 5. The temperature dependence was also suspected. Only these two tests were performed to successfully identify the structure of this compound. The insight from benzyl phenyl ether + toluene thermolysis reduced the amount of guesswork involved in determining the chemical configuration of the $\phi\text{CH}_2\cdot + \text{NO}\cdot$ recombination product.

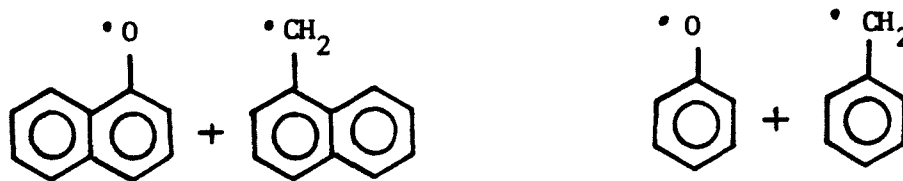
6.3.2 Kinetic Modeling

To check its validity, the dissociation mechanism for 1-naphthol, developed in section 6.2.2, was applied to model the 1-naphthol + bibenzyl thermolysis. Table 6.4 shows the entire kinetic mechanism, incorporating the naphthol dissociation scheme. The rate parameters associated with naphthol were as they appeared in section 6.2.2, and the rate parameters associated with bibenzyl were taken from Chapter 4. Table 6.5 illustrates that the model gives reasonably good agreement with experimental data with respect to the conversion of 1-naphthol and bibenzyl, and the yields of binaphthol and dinaphthofuran. The concentrations of tetralone were somewhat higher than the experimental values, for the reason stated in section 6.2.2. The model concentrations of naphthalene and benzyl naphthol were somewhat lower than the experimental data. This discrepancy was attributed to the inaccuracy of the HPLC integration data. Concentration determination became very prone to error as product concentration was less than 5 percent. The empirical data were obtained for a reaction time of 30 minutes at the expense of total dissociation of benzyl naphthol because the concentrations of the other species were more accurately determined. Their agreement with model results therefore provided a stronger support for the validity of the proposed mechanistic scheme.

6.4 Thermolysis of 1 Naphthol + 1 Methylnaphthalene

As a condensed-ring analogue of $\phi\text{O}\cdot + \text{CH}_2\cdot$ radical recombination discussed in Chapter 5, the 1-naphthol + 1-methylnaphthalene mixture was designed to permit the study of naphthoxy ($\text{NO}\cdot$) - methylnaphthalene ($\text{NCH}_2\cdot$)

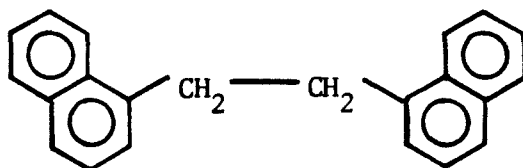
radical recombination



Again, the insight obtained from the single-ring system will prove to be useful in examining the condensed-ring system.

6.4.1 Product Identification

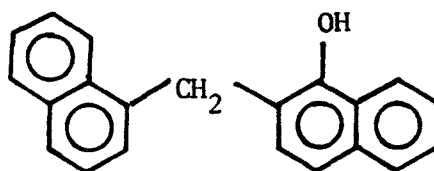
An HPLC chromatogram of the thermolysis products of the model compound system 1-naphthol + 1-methylnaphthalene at 425°C, 15 minutes, appears in Figure 6.5. By comparing elution times with those of authentic compounds and by mass analysis by GCMS, peaks 1, 3, 4, and 7 were identified as 1-naphthol, naphthalene, 1-methylnaphthalene, and dinaphthofuran, respectively. Peak 2 again consisted of both binaphthol and tetralone. Peak 6 was determined to have a mass of 282, corresponding to a product of recombination of two $\text{NCH}_2\cdot$ radicals. From experience with benzyl radical recombination, this peak most likely corresponded to 1,2-binaphthyl ethane.



The abundance of this compound reflected the stability of the methylnaphthalene radical, $\text{MN}\cdot$. The radical did not immediately abstract a hydrogen

atom to form 1-methylnaphthalene, but remained radical long enough to recombine with another MN \cdot radical.

Peak 5 (actually peaks 5 and 6 together) was isolated from the rest of the product mixture by HPLC. The fraction was determined by GCMS to contain a compound of mass 284, corresponding to a product of recombination of NO \cdot + NCH $_2\cdot$. Based on the result of the previous section and of Chapter 5, chemical separation was performed and the result showed that fraction 5 was phenolic. Next, no appreciable growth of this compound with increasing temperature was detected, suggesting again a keto-enol tautomerization that resulted in the lower effective bond dissociation energy of the methylene bridge. This fraction was thus concluded to be 2-naphthoxy, 1-naphthyl methane



As before, experience from the study of simpler model compound system helped to minimize the steps involved in identifying the chemical structure of this recombination product.

6.4.2 Kinetic Modeling

The dissociation scheme for 1-naphthol was again employed in modeling the thermolysis of 1-naphthol + 1-methylnaphthalene. The entire kinetic mechanism for this model compound system appears in Table 6.6. The rate parameters associated with naphthol were as they appeared in section 6.2.2, and the pertinent rate values for 1-methylnaphthalene were taken from Chapter 4. The activa-

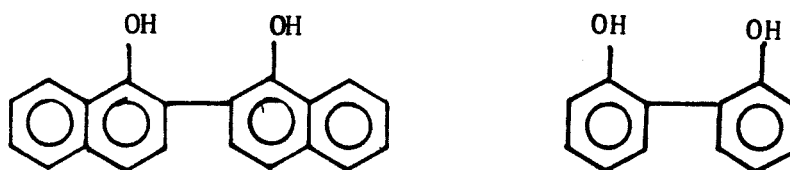
tion energy for ethylene bridge dissociation in dinaphthylethane was reduced to 60 kcal/mol to account for the added stability afforded by the double-ring free radicals (15). Likewise, the effective activation energy for methylene bridge dissociation in naphthoxy naphthyl methane was reduced to 42 kcal/mol. Table 6.7 shows that model results are in reasonable accord with the experimental data at 425° and 450° C, 15 minutes on conversions of 1-naphthol and 1-methylnaphthalene, as well as on yield of dinaphthofuran. The yield of tetralone was again higher than experimentally observed, due to the omission of further reactions of tetralone, as discussed in section 6.2.2. And the yields of naphthalene, binaphthol, and naphthoxy naphthyl methane were smaller than the experimental values due to the low concentrations of these products and the subsequent inaccuracy in integration data. Even though the reaction time was only half that of 1-naphthol + bibenzyl thermolysis, the relative concentration of naphthoxy naphthyl methane was lower than that of benzyl naphthol at 450°C. As discussed above, the more extensive dissociation of naphthoxy naphthyl methane was attributed to the extra stability of both of the resulting free radicals as imparted by the condensed rings. In other words, the effective bond dissociation energy for the methylene bridge was lower when fused aromatic rings were concerned.

6.5 Summary

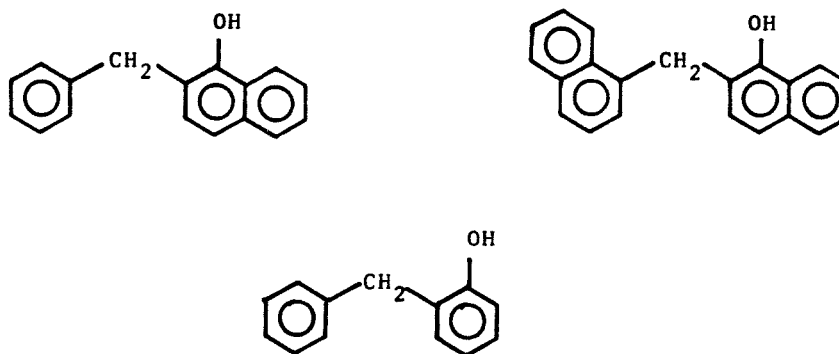
Thermolysis of the three model compound mixtures discussed in this chapter revealed certain differences and similarities between single-ring and double-ring aromatic compounds. The major difference appeared in the noticeable

extent of thermolysis of 1-naphthol, as compared with phenol, which was relatively stable at liquefaction temperatures. A mechanistic scheme was advanced to account for the dissociation of 1-naphthol. The validity of this kinetic mechanism was supported by its success in modeling the other two model compound systems in this chapter, namely, 1-naphthol + bibenzyl and 1-naphthol + 1-methylnaphthalene.

The single-ring and double-ring aromatics investigated in this thesis exhibited similar patterns with respect to product recombination pathways. With reference to the benzyl phenyl ether + phenol mixture studied in Chapter 5, the structure of the product of $\text{NO}\cdot + \text{NO}\cdot$ recombination, namely binaphthol, was analogous to that of $\phi\text{O}\cdot + \phi\text{O}\cdot$ recombination, namely biphenol:



With reference to the benzyl phenyl ether + toluene mixture, the products of $\text{NO}\cdot + \phi\text{CH}_2\cdot$ and $\text{NO}\cdot + \text{MN}\cdot$ recombinations were also analogous to the product of $\phi\text{O}\cdot + \phi\text{CH}_2\cdot$ recombination:



The small concentrations of these products relative to the concentrations of

binaphthol and biphenol were not necessarily due to the tendency of a phenoxy radical to recombine with another phenoxy radical. Rather, as the reaction temperature increased, the carbon-oxygen radical recombination products appeared to undergo substantial dissociation via keto-enol tautomerization. The extra stability of $\text{NO}\cdot$ due to the condensed ring structure resulted in a lower effective activation energy for methylene bridge cleavage in naphthoxy naphthyl methane in comparison to benzyl phenol, accounting for the smaller concentration of the former product relative to the latter. This stability on the other hand was responsible for a large transient concentration of $\text{NO}\cdot$. Thus binaphthol, and subsequently dinaphthofuran, were the predominant products of naphthol thermolysis.

In conclusion, when both carbon and oxygen free radicals were present, the products of oxygen-oxygen and carbon-carbon radical recombination predominated. The lesser amounts of carbon-oxygen recombination products were attributed to the dissociation of the methylene bridges in these products through keto-enol tautomerization. The product of double-ring radical recombination exhibited chemical structures that corresponded to the structures of single-ring radical recombination products. Emphasis was once again placed upon the ability to extrapolate results from a simpler model compound system to predict the behavior of a more complex mixture of model compounds.

REFERENCES

- [1] Dreyden, I. G. G., 'Chemistry of Coal Utilization,' Suppl. Vol., (Ed. H. H. Lowry), John Wiley & Sons, Inc., New York, 1963, Chapters 1 & 6
- [2] Gavalas, G. R. and Oka, M., *Fuel*, 1978, **57**, 285
- [3] Merz V. and Weith, W., *Ber. Dtsch. Chem. Ges.*, 1881, **14**, 187
- [4] Hall, C. C., *Fuel*, 1933, **12**, 419
- [5] Poutsma, M. L. and Dyer, C. W., *J. Org. Chem.*, 1982, **47**(18), 3367
- [6] Raaen, V. F. and Roark, W. H., *Fuel*, 1978, **57**, 650
- [7] Benson, S. W., *Int. J. Chem. Kinetics*, 1980, **12**, 755
- [8] Ayranci, G. and Back, M. H., *Int. J. Chem. Kinetics*, 1981, **13**, 897
- [9] Delliste, D., Richard, C., and Martin, R., *J. Chim. Phys. Phys-Chim. Biol.*, 1981, **78**, 655
- [10] Musso, H., in 'Oxidative Coupling of Phenols,' Taylor, W. I. and Battersby, A. R., Eds., Marcel Dekker, New York, 1967, Chapter 1
- [11] Allen, D. T. and Gavalas, G. R., *Int. J. Chem. Kinetics*, 1983, **15**, 219
- [12] Szwarc, M. and Williams, D., *J. Chem. Phys.*, 1952, **20**(7), 1171
- [13] Ladacki, M. and Szwarc, M., *J. Chem. Phys.*, 1952, **20**(11), 1814
- [14] Benson, S. W., 'Thermochemical Kinetics: Methods for the Estimation of Thermochemical Data and Rate Parameters,' John Wiley & Sons, Inc., New York, Second Edition, 1976
- [15] Gavalas, G. R., 'Coal Pyrolysis,' Coal Science and Technology; **4**, Elsevier Scientific Publishing Company, Amsterdam, The Netherlands, 1982

FIGURE 6.1

HPLC OF 1-NOH THERMOLYSIS PRODUCTS: 425°C, 15 MINUTES

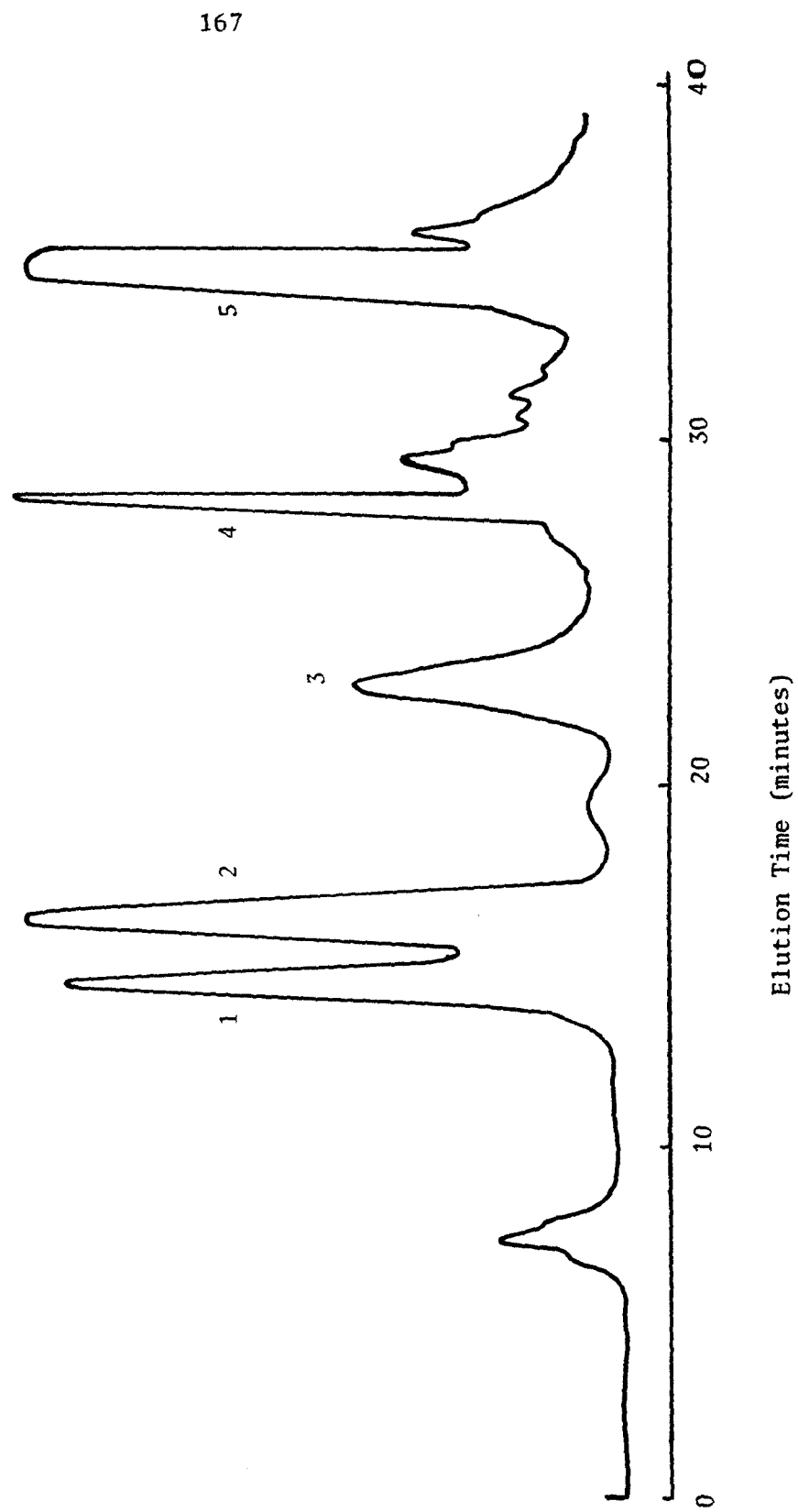


FIGURE 6.2

PRODUCT CONCENTRATION AS A FUNCTION OF NAPHTHOL DILUTION

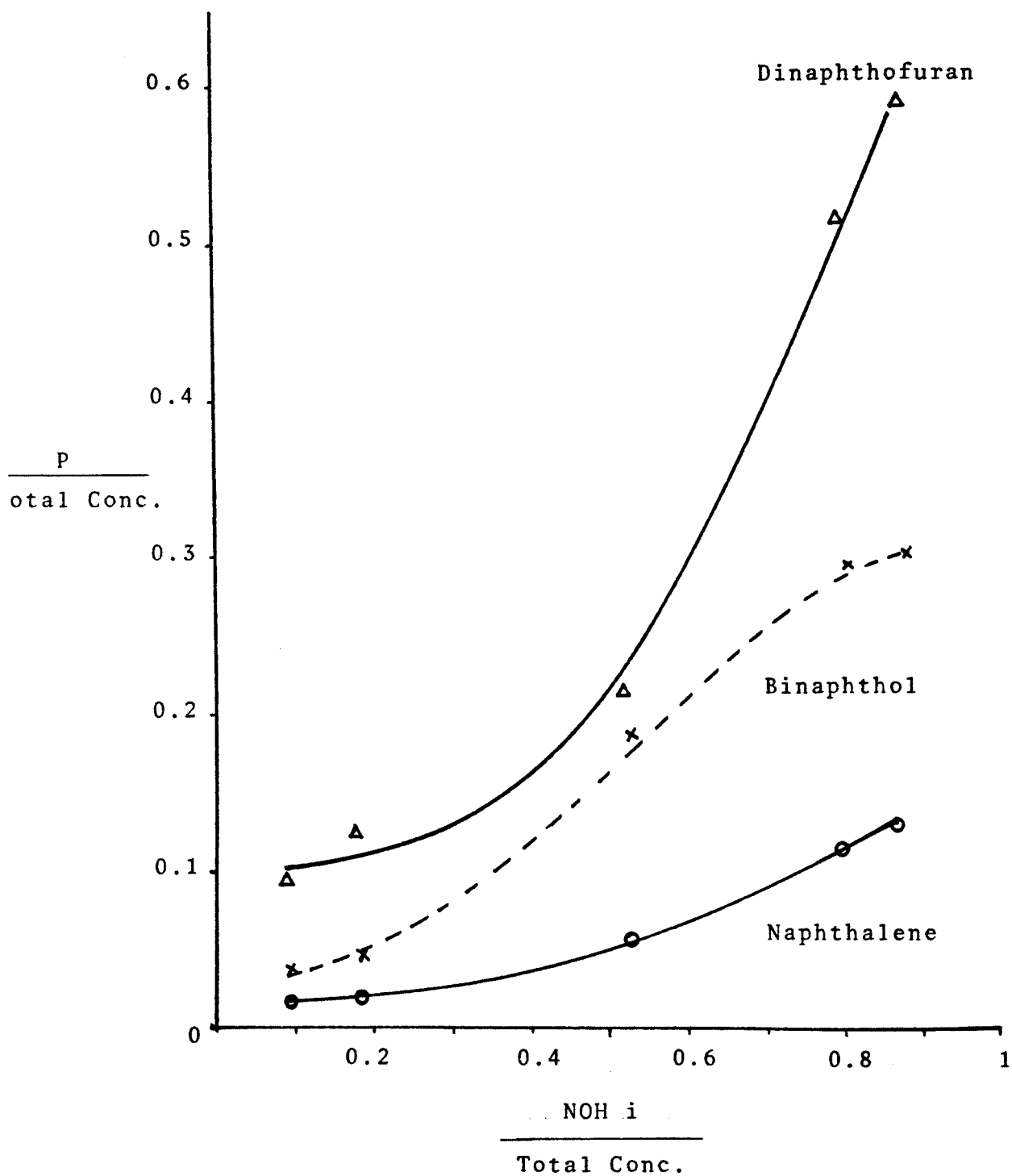


FIGURE 6.3

MECHANISTIC SCHEME FOR 1-NAPHTHOL DISSOCIATION

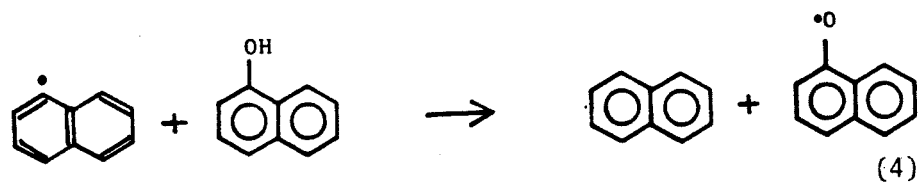
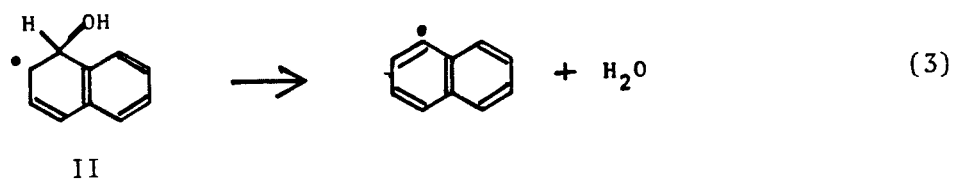
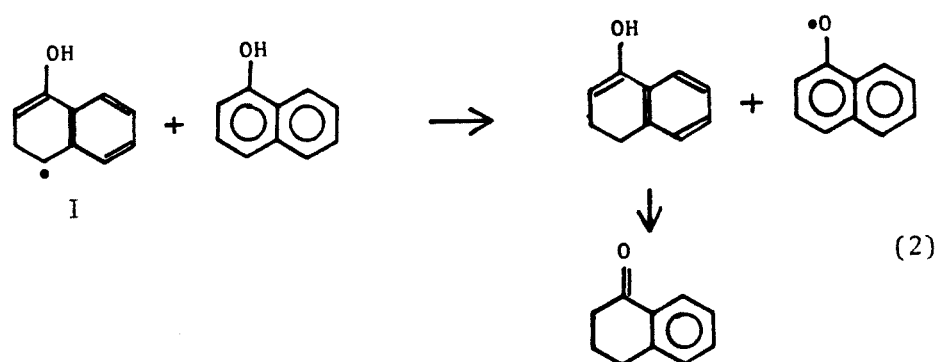
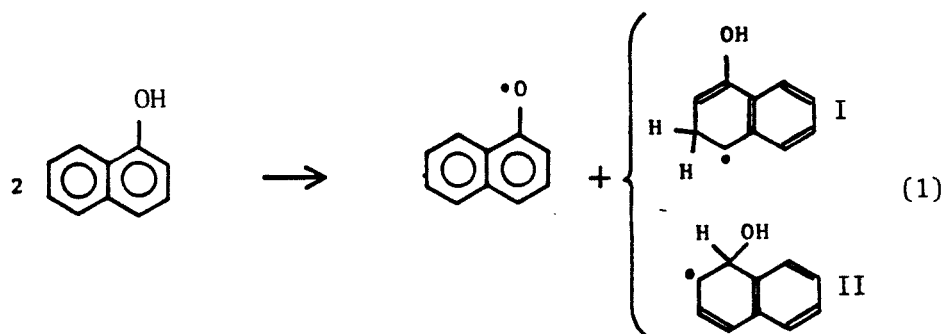


FIGURE 6.4
 MODEL RESULTS (LINES) vs. POUTSMA'S EXPERIMENTAL DATA (POINTS)
 THERMOLYSIS OF 1-NAPHTHOL, 400°C

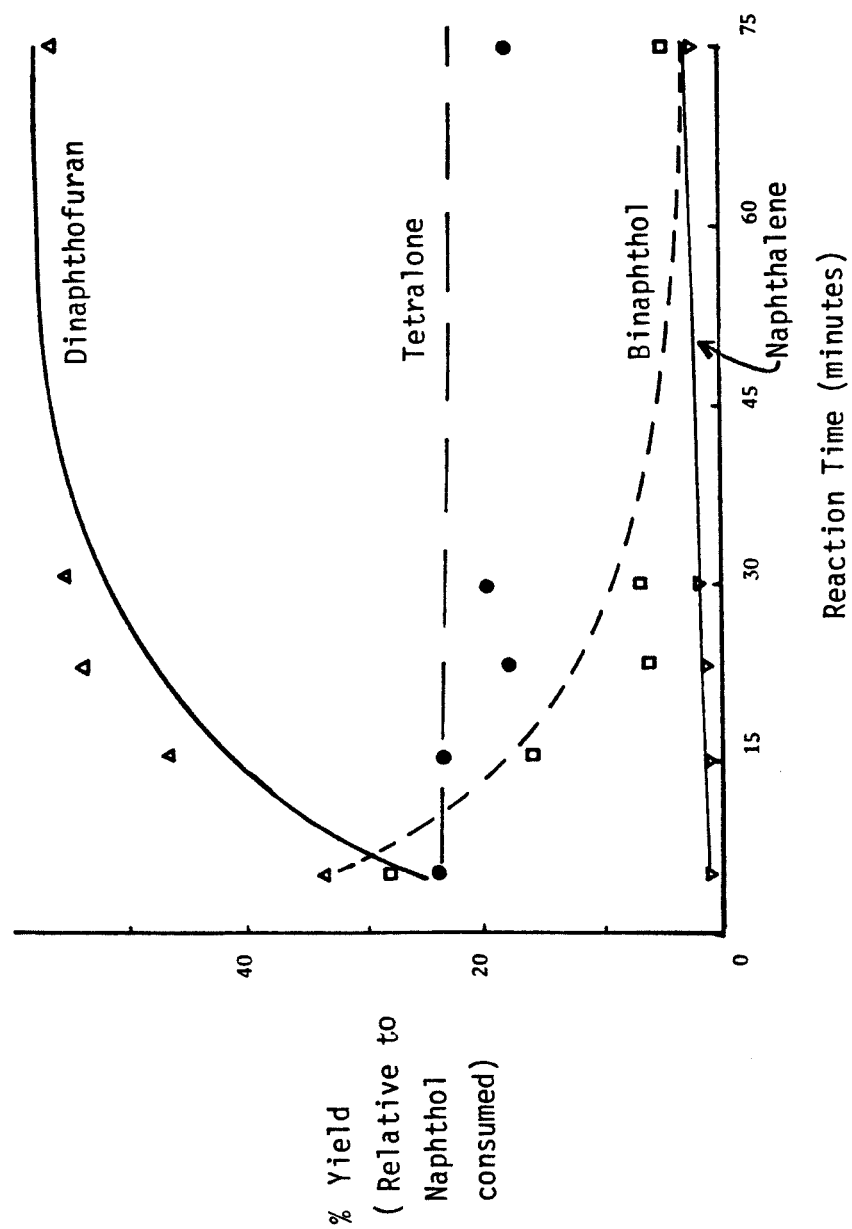


FIGURE 6.5
HPLC OF 1-NOH + BB THERMOLYSIS PRODUCTS
425°C, 15 MINUTES

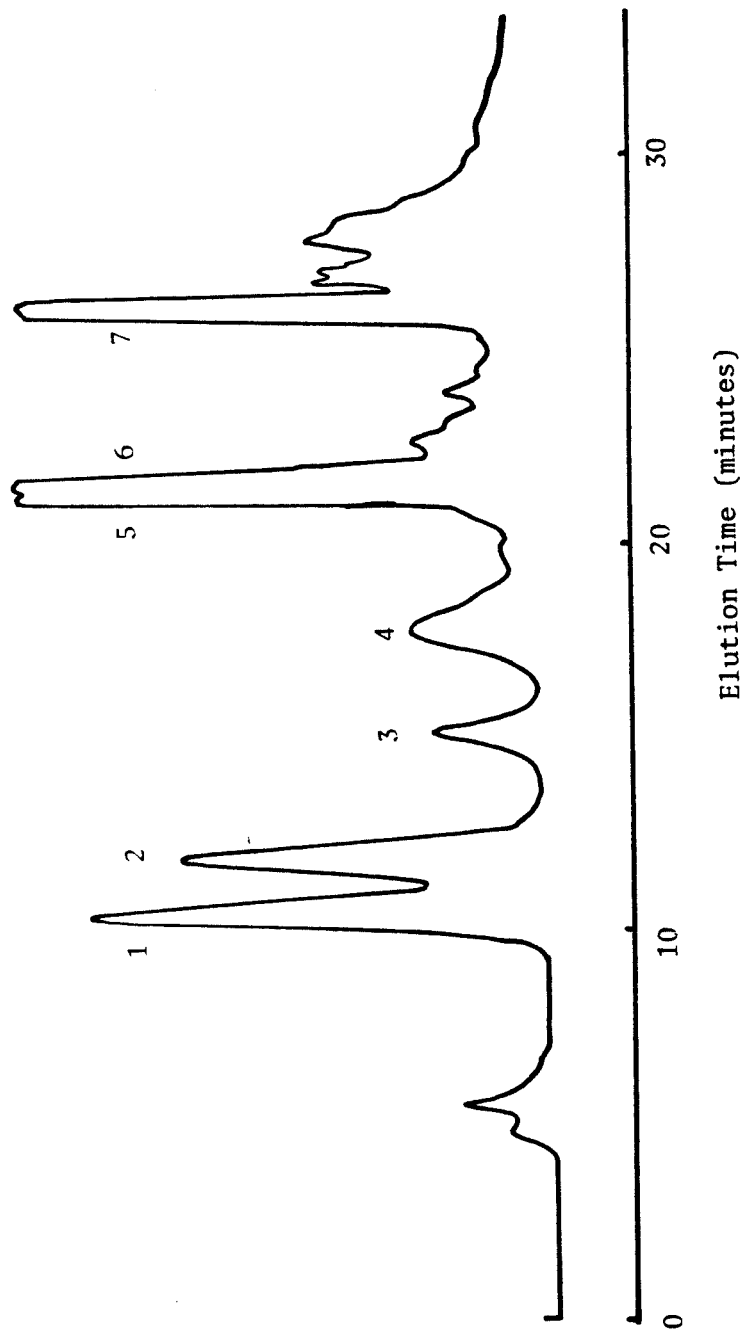


FIGURE 6.6
HPLC OF 1-NOH + MN THERMOLYSIS PRODUCTS
425°C, 15 MINUTES

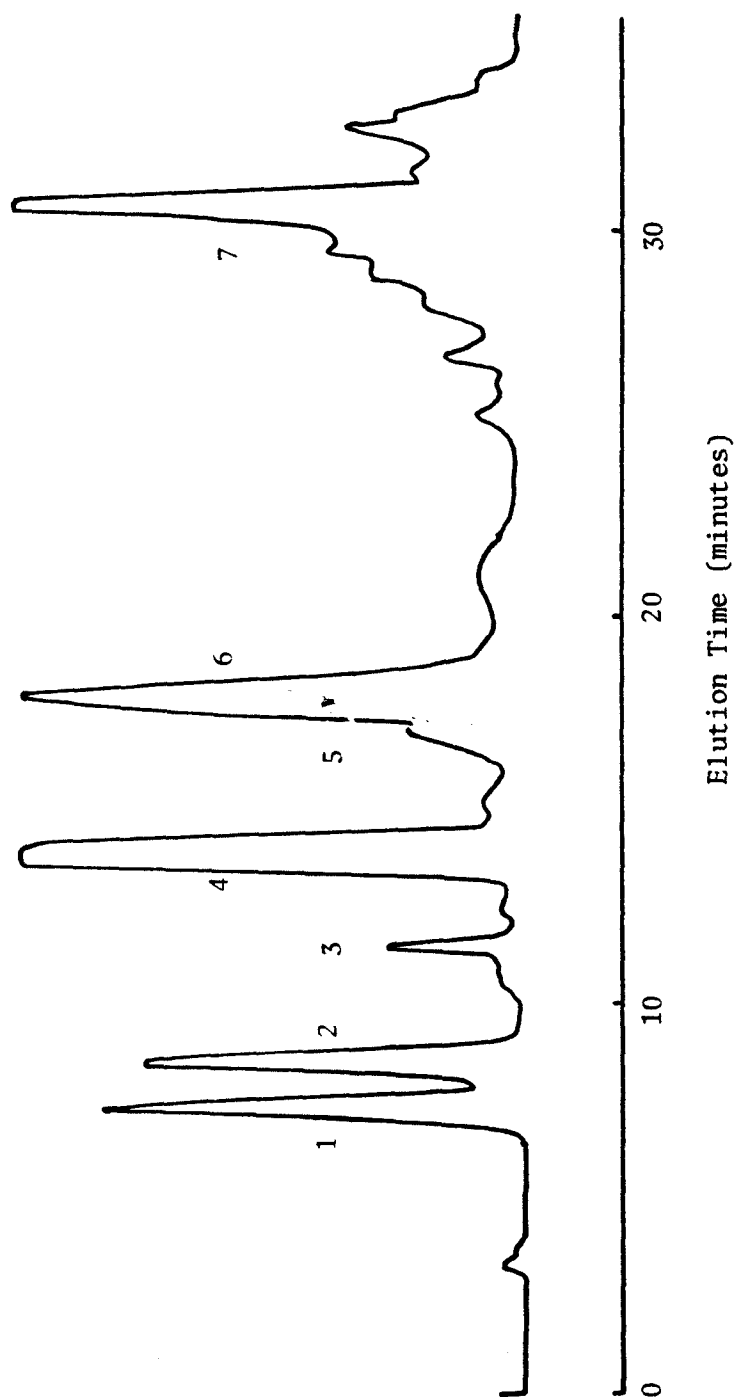
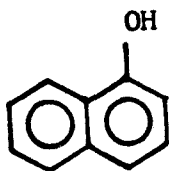


TABLE 6.1

REACTANT MIXTURES FOR THE RECOMBINATION EXPERIMENTS

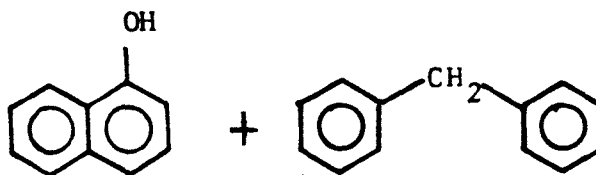
PART II 1-NAPHTHOL

1



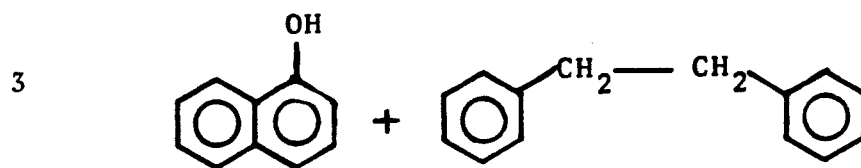
Temperature: 400-425°C
Reaction Time: 15 minutes

2



KINETIC EXPERIMENTS

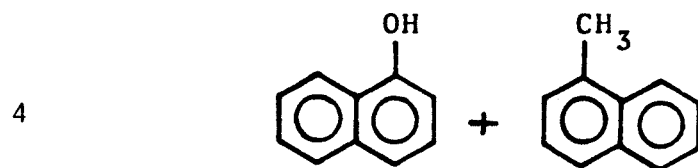
Mole Ratio: 1:0.4 to 1:10
Temperature: 425°C
Reaction Time: 15 minutes

TABLE 6.1 (cont'd)

Mole Ratio: 2:1

Temperature: 425-450°C

Reaction Time: 15 minutes



Mole Ratio: 1:2

Temperature: 425-450°C

Reaction Time: 15 minutes

TABLE 6.2

THERMOLYSIS MECHANISM FOR L-NAPHTHOL

NO.	REACTION	$\log_{10} A$	E_a
INITIATION			
1	$\text{NOH} + \text{NOH} \longrightarrow \text{NO}\cdot + \text{NOH}\cdot$	11	48.5
PROPAGATION			
2	$\text{NOH}\cdot + \longrightarrow \text{NE}\cdot + \text{H}_2\text{O}$	13	18.1
3	$\text{NE}\cdot + \text{NOH} \longrightarrow \text{NO}\cdot + \text{NE}$	5.9	13
4	$\text{NOH}\cdot + \text{NOH} \longrightarrow \text{NO}\cdot + \text{TEN}$	10	9
TERMINATION			
5	$\text{NO}\cdot + \text{NO}\cdot \longrightarrow \text{BN}$		0
6	$\text{BN} + \longrightarrow \text{DNF} + \text{H}_2\text{O}$		0
7	$\text{NO}\cdot + \text{NOH}\cdot \longrightarrow \text{NOH} + \text{NOH}$		0
8	$\text{NO}\cdot + \text{NE}\cdot \longrightarrow \text{P1}$		0
9	$\text{NOH}\cdot + \text{NOH}\cdot \longrightarrow \text{P2}$		0
10	$\text{NOH}\cdot + \text{NE}\cdot \longrightarrow \text{P3}$		0
11	$\text{NE}\cdot + \text{NE}\cdot \longrightarrow \text{P4}$		0

TABLE 6.2 (cont'd)

DEFINITION OF SYMBOLS

NOH	=	1-naphthol	NO \cdot	=	naphthoxy radical
NOH \cdot	=	radical C ₁₀ H ₉ O \cdot			(C ₁₀ H ₇ O \cdot)
NE	=	naphthalene	NE \cdot	=	naphthyl radical
H ₂ O	=	water			
TEN	=	tetralone			
BN	=	binaphthol			
DNF	=	dinaphthofuran			

P1 - p4 = recombination products

TABLE 6.3

MODEL RESULTS VS. POUTSMA'S EXPERIMENTAL DATA
THERMOLYSIS OF 1-NAPHTHOL AT 400°C

Reaction Time (minutes)	% 1-Naphthol Conversion	
	Model	Poutsma's Data
5	3.0	2.9
15	8.0	7.2
22.5	11.5	12.1
30	14.5	16.1
75	29.5	32.0
240	56.0	59.5

TABLE 6.4

THERMOLYSIS MECHANISM FOR 1-NOH + BB

NO.	REACTION	$\log_{10} A$	E_a
INITIATION			
1	$\text{NOH} + \text{NOH} \longrightarrow \text{NO}\cdot + \text{NOH}\cdot$	11	48.5
2	$\text{BB} \longrightarrow \text{TO}\cdot + \text{TO}\cdot$	16.9	63
3	$\text{BEN} \longrightarrow \text{NO}\cdot + \text{TO}\cdot$	11	45
PROPAGATION			
4	$\text{NOH}\cdot \longrightarrow \text{NE}\cdot + \text{H}_2\text{O}$	13	18.1
5	$\text{NE}\cdot + \text{NOH} \longrightarrow \text{NO}\cdot + \text{NE}$	5.9	13
6	$\text{NE}\cdot + \text{BB} \longrightarrow \text{BB}\cdot + \text{NE}$	7	9
7	$\text{NOH}\cdot + \text{NOH} \longrightarrow \text{NO}\cdot + \text{TEN}$	10	9
8	$\text{NOH}\cdot + \text{BB} \longrightarrow \text{BB}\cdot + \text{TEN}$	7	9
9	$\text{NO}\cdot + \text{BB} \longrightarrow \text{BB}\cdot + \text{NOH}$	7	9
10	$\text{TO}\cdot + \text{NOH} \longrightarrow \text{NO}\cdot + \text{TO}$	5.9	9
11	$\text{TO}\cdot + \text{BB} \longrightarrow \text{BB}\cdot + \text{TO}$	7	9
12	$\text{BB}\cdot + \text{NOH} \longrightarrow \text{NO}\cdot + \text{BB}$	5.9	12.5
RECOMBINATION			
13	$\text{NO}\cdot + \text{NO}\cdot \longrightarrow \text{BN}$		0
14	$\text{BN} \longrightarrow \text{DNF} + \text{H}_2\text{O}$		-
15	$\text{NO}\cdot + \text{NOH}\cdot \longrightarrow \text{NOH} + \text{NOH}$		0
16	$\text{NO}\cdot + \text{TO}\cdot \longrightarrow \text{BEN}$		0
17	$\text{NO}\cdot + \text{NE}\cdot \longrightarrow \text{P1}$		0
18	$\text{NO}\cdot + \text{BB}\cdot \longrightarrow \text{P2}$		0
19	$\text{NOH}\cdot + \text{NOH}\cdot \longrightarrow \text{P3}$		0
20	$\text{NOH}\cdot + \text{TO}\cdot \longrightarrow \text{P4}$		0
21	$\text{NOH}\cdot + \text{NB}\cdot \longrightarrow \text{P5}$		0
22	$\text{NOH} + \text{BB}\cdot \longrightarrow \text{P6}$		0
23	$\text{TO}\cdot + \text{TO}\cdot \longrightarrow \text{BB}$		0
24	$\text{TO}\cdot + \text{NB}\cdot \longrightarrow \text{P7}$		0
25	$\text{TO}\cdot + \text{BB}\cdot \longrightarrow \text{P8}$		0
26	$\text{NB}\cdot + \text{NB}\cdot \longrightarrow \text{P9}$		0
27	$\text{NB}\cdot + \text{BB}\cdot \longrightarrow \text{P10}$		0
28	$\text{BB}\cdot + \text{BB}\cdot \longrightarrow \text{P11}$		0

TABLE 6.4 (cont'd)

DEFINITION OF SYMBOLS

NOH	=	1-naphthol	NO \cdot	=	naphthoxy radical (C ₁₀ H ₇ O \cdot)
NOH \cdot	=	radical C ₁₀ H ₉ O \cdot			
BB	=	bibenzyl			
TO	=	toluene	TO \cdot	=	benzyl radical
BEN	=	benzyl naphthol			
NE	=	naphthalene	NE \cdot	=	naphthyl radical
H ₂ O	=	water			
TEN	=	tetralone			
BN	=	binaphthol			
DNF	=	dinaphthofuran			
P1 - p11	=	recombination products			

TABLE 6.5

MODEL RESULTS VS. EXPERIMENTAL DATA
 THERMOLYSIS OF 1-NOH + BB, 15 MINUTES

	Temperature (°C)			
	425		450	
	Model	Exptl.	Model	Exptl.
<u>Conversions (%)</u>				
Naphthol	12.3	10	12.6	14
Bibenzyl	40.8	43	38.8	40
<u>Yields</u> (% Naphthol consumed)				
Naphthalene	0.48	2	0.46	2
Tetralone	41.7	36	40.1	34
Binaphthol	10.4	9	1.6	3
Dinaphthofuran	37.9	36	50.0	45
Benzyl naphthol	1.1	3	0.94	2

TABLE 6.6

THERMOLYSIS MECHANISM FOR 1-NOH + 1-MN

NO.	REACTION	$\log_{10} A$	E_a
INITIATION			
1	$\text{NOH} + \text{NOH} \longrightarrow \text{NO}\cdot + \text{NOH}\cdot$	11	48.5
2	$\text{NNM} \longrightarrow \text{NO}\cdot + \text{MN}\cdot$	11	40
3	$\text{DNE} \longrightarrow \text{MN}\cdot + \text{MN}\cdot$	15.9	60
PROPAGATION			
4	$\text{NOH}\cdot \longrightarrow \text{NE}\cdot + \text{H}_2\text{O}$	13	18.1
5	$\text{NE}\cdot + \text{NOH} \longrightarrow \text{NO}\cdot + \text{NE}$	5.9	13
6	$\text{NE}\cdot + \text{MN} \longrightarrow \text{MN}\cdot + \text{NE}$	7	9
7	$\text{NOH}\cdot + \text{NOH} \longrightarrow \text{NO}\cdot + \text{TEN}$	10	9
8	$\text{NOH}\cdot + \text{MN} \longrightarrow \text{MN}\cdot + \text{TEN}$	7	9
9	$\text{NO}\cdot + \text{MN} \longrightarrow \text{MN}\cdot + \text{NOH}$	7	9
10	$\text{MN}\cdot + \text{NOH} \longrightarrow \text{NO}\cdot + \text{MN}$	5.9	9
RECOMBINATION			
11	$\text{NO}\cdot + \text{NO}\cdot \longrightarrow \text{BN}$		0
12	$\text{BN} \longrightarrow \text{DNF} + \text{H}_2\text{O}$		-
13	$\text{NO}\cdot + \text{NOH}\cdot \longrightarrow \text{NOH} + \text{NOH}$		0
14	$\text{NO}\cdot + \text{NE}\cdot \longrightarrow \text{P1}$		0
15	$\text{NO}\cdot + \text{MN}\cdot \longrightarrow \text{NNM}$		0
16	$\text{NOH}\cdot + \text{NOH}\cdot \longrightarrow \text{P2}$		0
17	$\text{NOH}\cdot + \text{NE}\cdot \longrightarrow \text{P3}$		0
18	$\text{NOH}\cdot + \text{MN}\cdot \longrightarrow \text{P4}$		0
19	$\text{NE}\cdot + \text{NE}\cdot \longrightarrow \text{P5}$		0
20	$\text{NE}\cdot + \text{MN}\cdot \longrightarrow \text{P6}$		0
21	$\text{MN}\cdot + \text{MN}\cdot \longrightarrow \text{DNE}$		0

TABLE 6.6 (cont'd)

DEFINITION OF SYMBOLS

NOH	=	1-naphthol	NO·	=	naphthoxy radical
NOH·	=	radical $C_{10}H_9O·$			$(C_{10}H_7O·)$
NNM	=	naphthoxy naphthyl methane			
MN	=	1-methylnaphthalene			
NE	=	naphthalene	NE·	=	naphthyl radical
H ₂ O	=	water			
TEN	=	tetralone			
BN	=	binaphthol			
DNF	=	dinaphthofuran			
DNE	=	dinaphthylethane			
P1 - p6	=	recombination products			

TABLE 6.7

MODEL RESULTS VS. EXPERIMENTAL DATA

THERMOLYSIS OF 1-NOH + MN, 15 MINUTES

	Temperature ($^{\circ}\text{C}$)			
	425		450	
	Model	Exptl.	Model	Exptl.
<u>Conversions (%)</u>				
Naphthol	6.4	5	11.2	11
Methylnaphthalene	5.0	6	7.5	9
<u>Yields</u> (% Naphthol consumed)				
Naphthalene	6.0	4	6.6	5
Tetralone	39.4	35	34.7	32
Binaphthol	1.8	5	0.79	3
Dinaphthofuran	47.2	43	49.9	46
Naphthoxy naphthyl methane	0.28	2	0.33	3
<u>Yields</u> (% Methylnaphthalene consumed)				
Dinaphthylethane	99.2	90	97.6	92

CHAPTER 7

CONCLUSIONS AND RECOMMENDATIONS
FOR FUTURE WORK

7.1 Conclusions

The following conclusions highlight the significant results of the model compound studies of phenoxy radicals under liquefaction conditions, as discussed in detail in Chapters 4, 5, and 6.

- [1] Phenoxy radicals were determined to be more reactive than carbon-centered radicals, rapidly undergoing hydrogen abstraction as soon as they were formed. Consequently, fewer phenoxy radicals were available for recombination when a good hydrogen donor was present. The majority of the products in that case resulted from recombination of the more stable carbon-centered radicals.
- [2] In the case where no good hydrogen donors were available, oxygen-oxygen radical recombination products were found to be more abundant than carbon-oxygen recombination products. This result did not necessarily imply preference of oxygen radicals to recombine with one another. Rather, the relatively low concentrations of the carbon-oxygen products were attributed to the thermal cleavage of the methylene bridge in a carbon-oxygen product via keto-enol tautomerization.
- [3] At liquefaction temperatures, 1-naphthol underwent noticeable thermoly-

sis whereas phenol was quite stable. A mechanistic scheme for 1-naphthol dissociation was proposed based on the extra stability of the condensed ring structure. This scheme accounted for the major reaction products and yielded product concentration profiles that matched experimental data. The scheme also demonstrated that a bimolecular, reverse disproportionation reaction was preferable in the case of naphthol dissociation, even though unimolecular bond dissociation reactions are generally believed to account for the majority of the chemical changes in the process of coal liquefaction. For example, unimolecular reactions accounted for the ethylene bridge dissociation in bibenzyl, and the ether bridge dissociation in benzyl phenyl ether, as evidenced by the model compound studies in Chapters 4 and 5. In the thermolysis of 1-naphthol, we also noticed dehydration reactions to form dinaphthofuran and naphthalene. Further, naphthalene formation may have resulted from a concerted reaction. These findings underscore the fact that several reaction pathways exist for thermolysis of coal-related materials.

- [4] Phenoxy and naphthoxy radicals appeared to follow similar recombination pathways. Biphenol and binaphthol were the products of phenoxy-phenoxy and naphthoxy-naphthoxy radical recombination, respectively. The structures of naphthoxy-benzyl and naphthoxy-methylnaphthalene radical recombination products were also analogous to the structure of phenoxy-benzyl recombination product. Binaphthol, however, underwent extensive dehydration to form dinaphthofuran, whereas biphenol apparently did not yield dibenzofuran.

- [5] Model compounds were assumed to undergo thermolysis via free-radical

pathways. Kinetic mechanisms were advanced for the model compound systems under study. These mechanisms were used in a computer program that simulated free radical interactions. The computer model successfully predicted the experimental data generated in this work as well as the data reported in the literature (3). Such results would tend to suggest that thermolysis of coal-derived materials consisting of similar functional groups would also follow free-radical paths, in agreement with the current views on coal liquefaction processes (4, 5, 6, 7). In the dissociation of 1-naphthol, however, the kinetic pathways for naphthalene formation was not clear-cut. Conceivably, a concerted reaction might have taken place. The use of free radical mechanisms to model naphthalene formation gave a satisfactory match with experimental data. This agreement tends to support the proposed mechanistic scheme, but it in no way rules out the possibility of a concerted reaction.

- [6] Thermochemical kinetics (1) was employed in conjunction with transition-state theory to successfully estimate the rate parameters for the reactions involving model compounds in the liquid phase. Allen (2) had demonstrated that the transition-state theory, originally developed for gas-phase reactions, were also valid for model compound systems consisting of dihydronaphthalene, tetrahydronaphthalene, as well as certain compounds containing methylene and ether bridges. In this work, this list of compounds was extended to include 1,2 diphenyl ethane (bibenzyl), which contains an ethylene bridge, benzyl phenyl ether which contains an ether bridge, and phenol and naphthol. Because these model compounds contain representative functional groups found in coal-derived products, rate parameter calcula-

tion via thermochemical estimates that yielded satisfactory results for these compounds should also apply to coal thermolysis processes. These estimates may not be applicable to high molecular weight compounds, heavily branched molecules, or very viscous liquids. Further, certain solvents may contribute to the stability of the transition state activated complex (2). Nevertheless, thermochemical estimates provide a quick way of obtaining approximate rate values, which can in turn be utilized in a mechanistic scheme to validate reaction pathways for coal liquefaction processes.

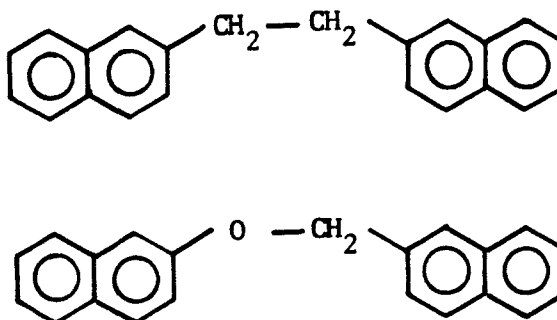
- [7] The diffusion-limited rates of recombination of free radicals appeared to be consistent with experimental data. In the reactions involving coal itself, this assumption would obviously ignore the transport limitation due to the coal's pore structure. Nonetheless, the diffusion-controlled rates of radical recombination reactions appeared satisfactory for liquid-phase reactions involving moderately viscous fluids, such as the systems under investigation.
- [8] Isotopically tagged species were employed for rate determination of hydrogen abstraction reactions involving the phenoxy radicals. The kinetic isotope effect associated with the O-D or C-D bond cleavage vs. O-H or C-H bond cleavage were ignored at the elevated temperatures such as in the cases discussed in Chapter 4. In general, however, the kinetic isotope effect must be considered before the effective rate parameters can be reported.
- [9] Determination of the products of radical recombinations was achieved by a combination of analytical tools, the most important of which are the high performance liquid chromatograph and the gas chromatograph-mass spectrometer. Reactant mixtures and/or reaction conditions could be chosen

so that certain recombination products were favored and others were inhibited. In the thermolysis of naphthol, for instance, the concentration of binaphthol and dinaphthofuran were inversely proportional. A short reaction time could be chosen if binaphthol was the preferred product, whereas a long reaction time would result in a high concentration of dinaphthofuran and very small amount of binaphthol. Binaphthol would be preferred over dinaphthofuran where separation of the acidic, or phenolic fraction (binaphthol) was easily achieved, for example. More importantly, the knowledge of the product structure often provides a clue as to the mechanistic pathways by which these products were formed. Elucidation of the kinetic mechanism associated with a thermolysis process is crucial to model compound studies.

- [10] Finally, the ability to apply model results for a simple system to predict results for a more complex reaction network cannot be overemphasized. In Chapters 4, 5, and 6, the rate parameters determined for selected model compound systems could be used in modeling certain other model compound mixtures. In Chapters 5 and 6, the structure of one unknown product containing the naphthoxy group was correctly predicted from the knowledge of the structure of an analogous recombination product containing the phenoxy group. The ability to extrapolate from one model compound mixture to another, more complex system will ultimately provide the connection between the reactions of model compounds and the interactions of coal-derived materials.

7.2 Recommendations for Future Work

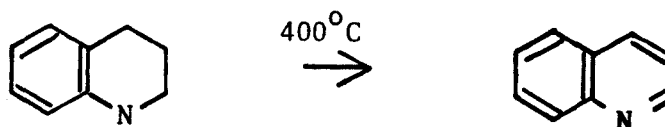
- [1] One goal of this thesis was to better comprehend the processes of free radical recombination. These recombination reactions in coal liquids are generally the opposite of the dissociation of large molecules into low molecular weight fragments. These fragments are eventually capped to produce light hydrocarbon products which are further refined to yield liquid fuels. As the mechanistic pathways for radical recombination are more clearly understood, efforts should be made to minimize these repolymerization reactions that lead to formation of undesirable coke or char residues.
- [2] A long term objective of this research is to develop a data bank of rate parameters for the most important elementary reactions of coal liquids and integrate these rate values into chemically sound kinetic models for coal liquefaction. Chapters 4 and 5 have investigated the hydrogen abstraction and recombination reactions in mixtures containing single-ring phenoxy and α radicals. Chapter 6 began the studies of thermolysis reactions involving condensed aromatic rings, namely 1-naphthol. Notable differences were observed between the reactions of naphthol and its single ring counterpart, phenol. Evidently, more research needs to be done on compounds such as



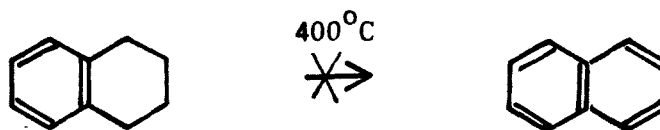
to study the comparative effects of double ring vs. single ring aromatics on free radical interactions under coal liquefaction conditions. Several of these compounds are not commercially available, and may have to be synthesized.

- [3] The success of the model compound studies in this work, whether in estimating rate parameters or in advancing a mechanistic scheme, was contingent upon the ability to postulate the chemical structures and accurately determine the concentrations of thermolysis products. Specifically, the high performance liquid chromatograph (HPLC) was not particularly well suited for operation in the preparative mode. Separation of certain compounds from a product mixture was not satisfactory when the concentrations of those fractions were lower than about 5 percent of total products. Identification even by high-resolution nuclear magnetic resonance spectroscopy (NMR) was in turn rendered ineffective. Analysis of the entire products by gas chromatograph-mass spectrometry (GCMS) could sometimes yield the masses of the major products and their relative concentrations. But the resolutions of the GCMS was even worse than the HPLC, and concentration determination in this manner was often impractical. Clearly, more efficient analytical tools are imperative for careful studies of compounds present in small concentrations. For example, larger columns specifically designed for preparative work for the HPLC can greatly enhance the capacity of fraction collection, and identification by NMR and GCMS will subsequently be much more accurate. Further, elemental analysis, yielding information on the relative abundance of oxygen to carbon, for instance, can provide additional information useful for structure identification.

- [4] Another problem associated with concentration determination stems from the unavailability of authentic samples with which to calibrate the integration data. In several instances in this study, only relative concentrations were attainable, and even those were only approximate data. Access to authentic samples such as dinaphthofuran would certainly allow more accurate information on product concentration. Organic synthesis of several of these compounds that are likely to occur as recombination products would provide researchers with a convenient data bank of reference compounds.
- [5] Another important class of compounds found in coal-derived materials consists of nitrogen-containing molecules. The presence of nitrogen in certain compounds can radically alter their behavior under liquefaction conditions. For example, thermolysis at 400°C has shown that tetrahydroquinoline (THQ) was found to yield quinoline



whereas tetrahydronaphthalene (tetralin) was relatively stable and did not yield naphthalene



Instead of reacting via a free-radical mechanism, THQ might undergo a concerted reaction to yield quinoline and molecular hydrogen. Elucidating the mechanistic pathways for THQ thermolysis can contribute to the understanding of the excellent solvent property of THQ in particular, and the effect of nitrogen substitution in general.

- [6] Since free radical exchange reactions occur much more rapidly than dissociation reactions, the concentrations of free radicals can be assumed to reach an equilibrium level during thermolysis. As Allen and Gavalas have demonstrated in thermolysis studies of dihydronaphthalene (8) and several compounds containing ether and methylene bridges (9), steady-state approximation and in some cases long-chain approximation should be useful in developing mechanistic models for thermal reactions of complex mixtures.

REFERENCES

- [1] Benson, S. W., 'Thermochemical Kinetics: Methods for the Estimation of Thermochemical Data and Rate Parameters,' John Wiley & Sons, New York, Second Edition, 1976
- [2] Allen, D. T., 'Modeling the Reactions of Coal Liquids,' Ph.D. Thesis, Department of Chemical Engineering, California Institute of Technology, Pasadena, California, 1983
- [3] Poutsma, M. L. and Dyer, C. W., *J. Org. Chem.*, 1982, **47**(18), 3367
- [4] Whitehurst, D. D., Mitchell, T. O., and Farcasiu, M., 'Coal Liquefaction. The Chemistry and Technology of Thermal Processes,' Academic Press, New York, 1980
- [5] Curran, G. P., Struck, R. T., and Gorin, E., *Ind. Eng. Chem. Proc. Des. Dev.*, 1967, **6**, 166
- [6] Wiser, W. H., *Fuel*, 1968, **47**, 475
- [7] Neavel, R. C., *Fuel*, 1976, **55**, 237
- [8] Allen, D. T. and Gavalas, G. R., *Int. J. Chem. Kinetics*, 1983, **15**, 219
- [9] Allen, D. T. and Gavalas, G. R., *Fuel*, 1984, **63**(5), 589